FINNISH METEOROLOGICAL INSTITUTE
CONTRIBUTIONS

NO. 52

A CHEMISTRY-TRANSPORT MODEL SIMULATION OF THE STRATOSPHERIC OZONE FOR 1980 TO 2019

JUHANI DAMSKI

DIVISION OF ATMOSPHERIC SCIENCES
DEPARTMENT OF PHYSICAL SCIENCES
FACULTY OF SCIENCE
UNIVERSITY OF HELSINKI
HELSINKI, FINLAND

ACADEMIC DISSERTATION IN APPLIED METEOROLOGY

To be presented, with the permission of the Faculty of Science of the University of Helsinki, for public critisism in Auditorium Physicum E204 (Gustaf Hällströmin katu 2) on November 18th, 2005, at 2 p.m.

Finnish Meteorological Institute
Helsinki, 2005

ISBN 951-697-617-4 (paperback)
ISBN 952-10-2723-1 (pdf)
ISSN 0782-6117

Yliopistopaino
Helsinki, 2005

FINNISH METEOROLOGICAL INSTITUTE

Published by Finnish Meteorological Institute
Erik Palménin aukio 1, P.O. Box 503
FIN-00101 Helsinki, Finland

Series title, number and report code of publication
Contributions 52, FMI-CONT-52

Date
October 2005

Author
Juhani Damski

Name of project

Commissioned by

Title
A CHEMISTRY-TRANSPORT MODEL SIMULATION OF THE STRATOSPHERIC OZONE FOR 1980 TO 2019

Abstract

In this study the results from a global 40-year middle atmospheric simulation are shown and discussed. The simulation has been done using an off-line FinROSE-chemistry-transport model (FinROSE) coupled with winds and temperatures from a chemistry-coupled general circulation model, UMETRAC. The performed simulation covers a time period from 1980 to the end of 2019.

The FinROSE model includes numerical scheme for stratospheric chemistry with parameterizations for heterogeneous processing on polar stratospheric clouds (PSC), and on liquid binary aerosols, together with a mechanism for the growth of the nitric acid trihydrate particles (NAT), and PSC sedimentation. The total number of trace species in the model is around 40, and the total number of gas-phase reactions, photodissociation processes, and heterogeneous reactions is around 150. The completed simulation was performed in a 5.00° × 11.25° (Lat-Lon), and with vertical resolution of around 3km up to around 0.15hPa. For the past period (1980-1999), the UMETRAC winds and temperatures were based on the use of observation-based sea surface temperatures, sea ice amounts, greenhouse gas loadings, and halogen concentrations while during the future period (2000-2019), the concentrations of greenhouse gases and halogens followed commonly agreed emission scenarios.

In general, during the past period, FinROSE results show a good or moderate comparison with the measured total ozone. The timing, the depth, and the deepening of the Antarctic ozone hole were captured well in the simulation. The simulated decadal total ozone trend estimates from the past period (1980-1999) were in close agreement (i.e. within few percents) with the corresponding trend estimates, calculated from the satellite total ozone measurements. The model trend estimates gave also the same level of statistical significance as those achieved from TOMS ozone analyses. Over the Antarctic areas, the effect of heterogeneous processing was well exhibited in the FinROSE results. The chlorine activations and the denitrifications were complete, especially during the latter part of the past period (i.e. 1990's). Over the Arctic regions the effect of chlorine activation was simulated by the model during the coldest winter-spring months. However, since the stratospheric temperatures were typically well above the ice formation thresholds, no massive-scale denitrifications were reproduced, and the levels of ozone destructions stayed much less profound than in the high southern latitudes.

During the future period (2000-2019), the trend estimates did not reveal any significant signs of turn over of the ozone trends. The estimated decadal total ozone trend was more likely levelling off, over the high southern latitudes, and no significant increases or decreases over the northern high latitudes total ozone were seen. Over the Antarctica, the period until the end of 2019 was rather similar to the past period (1980-1999). This rather expected result was due to the fact that enough inorganic chlorine was available for massive Antarctic ozone destruction also in the near future, and the deep denitrifications, caused by the PSC sedimentations took place on annual basis. Over the Arctic high latitudes the expected cooling of the stratosphere due to the global change, in turn, exhibited no signs of any massive-scale denitrifications. However, the effect of grown NAT particles was clear, and caused occasional denitrifications up to 75% at some atmospheric levels. The results of this study are suggesting that the increases in the GHG-concentrations will not lead to the enhanced northern stratospheric ozone destruction during the next two decades.

Publishing unit
Finnish Meteorological Institute, Research and Development, Meteorological Research Unit

Classification (UDC)
551.510.534

Keywords
chemistry-transport model, ozone depletion, climate-change, trends

ISSN and series title
0782-6117 Finnish Meteorological Institute Contributions

ISBN
951-697-617-3 (paperback), 952-10-2723-1 (pdf)

Language
English

Sold by
Finnish Meteorological Institute / Library
P.O.Box 503, FIN-00101 Helsinki
Finland

Pages
147

Price

Note

ILMATIETEEN LAITOS

Julkaisun sarja, numero ja raporttikoodi
Contributions 52, FMI-CONT-52

Julkaisija Ilmatieteen laitos, Erik Palménin aukio 1
PL 503, 00101 Helsinki

Julkaisuaika
Lokakuu 2005

Tekijä(t)
Juhani Damski

Projektin nimi

Toimeksiantaja

Nimeke
STRATOSFÄÄRIOTSONIN SIMULAATIO KEMIA-KULJETUS MALLILLA VUOSILLE 1980–2000

Tiivistelmä

Tässä työssä on tutkittu otsonikadon lähihistoriaa ja lähitulevaisuutta kolmiulotteisen kemia-kuljetusmallin avulla. Työssä käytetyllä mallilla on toteutettu 40 vuoden globaali simulaatio, vastaten vuosia 1980–2019. Mallin tarvitsemina syöttötietoina, eli ilmakehän kolmiulotteisena tuuli- ja lämpötilarakenteena, on käytetty kemiakytketyn ilmastomallin tuloksia. Syöttötiedot huomioivat ilmaston-muutokseen liittyvien kasvihuonekaasujen ja otsonikatoa aiheuttavien kaasujen pitoisuuksien muutokset päästöskenaarioiden avulla.

Työssä käytetty kemia-kuljetusmalli sisältää stratosfäärin kemian simulointiin suunnitellun numeerisen ratkaisuskeeman, joka huomioi mm. polaaristratosfääripilviin ja ilmakehän aerosoleihin liittyvän heterogeenisen kemian, sekä polaaristratosfääripilvien pilvipisaroiden kasvun ja sedimentaation (eli laskeutumisen). Työssä käytetty malli ottaa huomioon yhteensä noin 40 eri yhdisteen käyttäytymisen noin 150 erilaisen kemiallisen prosessin avulla. Työssä esitelty stratosfäärisimulaatio on toteutettu laskentahilassa, jonka tarkkuus leveyspiirien suunnassa on 5° ja pituuspiirien suunnassa 11.25°. Mallin pystysuuntaisen laskentahilan tarkkuus on noin kolme kilometriä, ulottuen maan pinnalta n. 60 km korkeudelle.

Kemia-kuljetusmallin tulokset vastaavat hyvin lähimenneisyydessä havaittuja otsonimuutoksia. Etelämantereen otsonikadon kehittyminen viimeisten vuosikymmenien aikana on sekä ajoittumisensa että suuruusluokkansa puolesta hyvin simuloitu. Laskenta-tuloksista määritetyt trendit osoittavat myös, että käytetyllä kemia-kuljetusmallilla saadaan havaintoja vastaavat polaarialueiden otsonimuutokset simuloitua hyvin. Etelämantereen otsonikadon perimmäinen syy on polaaristratosfääripilvien esiintymisen yhteydessä tapahtuva heterogeeninen kemia. Koska polaaristratosfääripilviä esiintyy yleisesti Etelämantereen talven ja kevään aikana, tapahtuu pilvipisaroissa tai niiden pinnalla otsonikatoa aiheuttavien klooriyhdisteiden muuntuminen ns. aktiiviseen muotoon. Näissä pintareaktioissa pilvipisaroihin sitoutuva typpi poistuu, eli ilmamassa de-nitrifikoituu, pilvipisaroiden sedimentaation kautta. Tällöin otsonikerrokselle vaarattomien, tyypillisesti klooria sisältävien, varastoyhdisteiden uudelleenmuodostuminen estyy ja laaja-alainen otsonikato tulee mahdolliseksi. Mallin tuloksien mukaan käytännössä kaikki Etelämantereen yläpuolisen stratosfäärin kloori muuntuu otsonikadolle otolliseen muotoon, ja lähes kaikki typpi poistuu ilmakehästä lähes vuosittain. Pohjoisen pallonpuoliskon talvisessa ja keväisessä stratosfäärissä lämpötilat pysyvät Etelämannerta lämpimämpinä. Tästä johtuen laaja-alaista otsonikatoa ei pääse muodostumaan, vaikka kloorin asteittainen aktivoituminen mallisimulaation mukaan tapahtuukin lähes vuosittain. Typen poistuminen pohjoisilla napa-alueilla estyy, koska alhaisia lämpötiloja ei tavata riittävän pitkäkestoisina ajanjaksoina. Typpihappoa sisältävien ns. tyypin I polaaripilvien kasvu tai jääkiteistä koostuvien tyypin II polaaripilvien puuttuminen ei siten johda laaja-alaisen otsonikadon muodostumiselle keskeiseen tehokkaaseen de-nitrifikaatioon.

Kemiakuljetusmallin simuloiman tulevaisuuden (2000–2019) aikana ei nähdä selkeitä merkkejä otsonikerroksen paranemisesta. Mallitulosten pohjalta lasketut trendit osoittavat, että talvi- ja kevätjaksoina esiintyvät otsonikatojaksot pysyvät nykyisen kaltaisina vuoden 2019 loppuun. Koska vuoteen 2019 mennessä otsonikatoa aiheuttavien yhdisteiden pitoisuuksien odotetaan vähenevän vain hiukan, on tämä tulos odotusten mukainen. Kasvihuoneilmiön voimistumisesta seuraava stratosfäärin viileneminen ei malli-laskelmien mukaan johda nykyistä laaja-alaisempaan polaaristratosfääripilvien esiintymiseen, ja siten pohjoisen otsonikadon pahenemiseen. Mallitulosten mukaan on kuitenkin mahdollista, että vuoteen 2019 mennessä ajoittaisia otsonikatovuosia esiintyy pohjoisilla napa-alueilla lähitulevaisuudessa, johtuen lähinnä tyypin I polaaripilvien aiheuttamasta de-nitrifikaatiosta.

Julkaisijayksikkö
Meteorologinen tutkimus

Luokitus (UDK)
551.510.534

Asiasanat
kemia-kuljetusmalli, otsonikato, ilmastonmuutos, kemia-ilmasto vuorovaikutukset

ISSN ja avainnimike
0782-6117 Finnish Meteorological Institute Contributions

ISBN
951-697-617-4 (paperback), 952-10-2723-1 (pdf)

Kieli
englanti

Myynti
Ilmatieteen laitos / Kirjasto
PL 503, 00101 Helsinki

Sivumäärä
147

Hinta

Lisätietoja

This work is dedicated to Eetu, Aake and Sanna

Preface

The original idea for this work was developed by Prof. Petteri Taalas, General Director of the Finnish Meteorological Institute, and Prof. Guy Brasseur Director of the Max Planck Institute for Meteorology to whom I'm first and foremost indebted. During the course of this work, they have both been not only my advisors, but mentors as well.

I'm most grateful to my supervisors Prof. Markku Kulmala, of University of Helsinki and Prof. Yrjö Viisanen of FMI, whose trust in my work, and enthusiasm towards science is admirable. I'm also most thankful for their great optimism and their ability to push me. This pushing was essential for me to finish my thesis.

I want to express my sincere thanks to Prof. Veli-Matti Kerminen of FMI and Docent Jouni Räisänen of University of Helsinki for the well-aimed and encouraging review of my thesis and for the most valuable comments. I also wish to express my gratitude to my advisor Prof. Kari Lehtinen of FMI for his invaluable support and help.

Warm thanks especially go to Dr. Jussi Kaurola of FMI for your unflagging friendship, support and guidance during these years. Jussi is also acknowledged for helping me with the statistical analysis and numerous scientific and technical matters.

I wish to thank Prof. Esko Kyrö Director of the FMI-ARC for his never-failing, invaluable support and positive attitude to my work. You have been a great companion and I truly appreciate your friendship.

I am truly thankful to M.Sc. Leif Backman and M.Sc. Laura Thölix. It has been a great pleasure to work with such wonderful persons as you, and share everyday challenges of the modelling business with all its ups and downs. My sincere thanks go also to the experts and friends in the former Ozone and UV research group of FMI for pleasant collaboration, and for all those enjoyable moments I have been able to share with you. I wish you all a great future.

I also wish to express my gratitude to Dr. John Austin of UKMO, and his team for providing the UMETRAC data, and for their help in numerous matters concerning the use and applicability of the UMETRAC fields. Dr. Arve Kylling is warmly thanked for making the PHODIS radiative transfer programme available, and for fruitful discussions on its usage.

I have been blessed with absolutely magnificent family. I owe a great amount of gratitude to my dear wife, Sanna, for her support, love, and moments of happiness together, and to my sons, Aake and Eetu for their unconditional love. Whole-hearted thanks also to my mother and my father for their support and love. I also wish to thank my brothers, all my grandparents and my mother-in-law and my father-in-law for their support and interest towards my work. I am also most thankful to all my relatives, in-laws, friends and colleagues. You have

always been there for me.

The main financial support for this study was granted by EC through EuroSPICE-project (EVK2-CT-1999-00014) in the fifth EC framework programme. The financial support from the EU/EC projects CANDIDOZ (EVK2-CT-2001-00133), QUOBI (EVK2-CT-2001-00129), and RETRO (EVK2-CT-2002-00170), as well as from the Academy of Finland, (namely FIGARE/LOUVRE and FAUVOR-I & II) is also acknowledged. I also wish to thank the TOMS team for putting the data available for the scientific community

Vantaa, October 2005

Juhani Damski

Contents

1 Introduction

The Antarctic springtime ozone depletion, caused primarily by human-produced gases like chlorofluorocarbons (CFCs) and halons, so far, has been probably one of the most dramatic environmental disasters that mankind has ever caused (e.g. WMO, 1985, 1992, 1994, 1999, and 2003). The concern about the possible stratospheric ozone destruction due to the emissions of chlorofluorocarbons and nitrogen compounds was already raised during the 1970's by Crutzen (1971) and Stolarski and Cicerone (1974), as well as Molina and Rowland (1974). Around mid 1980's the "ozone hole" was for the first time reported to exist. In 1982, the Japanese station at Antarctica, Syowa, was the first one to report about the low total ozone values (reported at Ozone Commission meeting in Halkidiki, Greece in September 1984 by Shigeru Chubachi), while the British scientists at Halley, Antarctica were finally the first to report the chemically driven ozone depletion (Farman et al. 1985).

Since 1980's the springtime ozone depletion over Antarctica has increased in depth and size, as ozone depleting gases have accumulated in the atmosphere (e.g. WMO, 2003). During the last decade the records were broken year by year, as reported by WMO (see press releases available at http://www.wmo.ch). Recently, the size and depth of the phenomenon have stayed at very high level. Typically the depleted area has covered a surface area over the South Pole equivalent to two and a half times the size of Europe (more than 25 million square-km). During the most dramatic years, more than 85% of the total ozone has been destroyed in the lower stratosphere over a surface area of more than 10 million square-km (e.g. WMO, 2003, and press releases available at http://www.wmo.ch). The record breaking year over Antarctica, so far, has been the year 2000 when the size of the Antarctic ozone hole reached almost 30 million square-km. Another major ozone hole year was during the late September of 2003 when the size of the ozone hole was almost 29 million square-km. The only exception to this observed pattern of annual major ozone holes above Antarctica was the austral spring of 2002, when an extremely rare southern sudden stratospheric warming event took place over the Antarctic latitudes, causing the split of the vortex, and ending the ozone destruction period already during late September (see Shepherd et al., 2005; Special issue of J. Atmos. Sci., and papers therein).

The northern polar areas have also been exposed to ozone depletion. During the coldest winters about 30% loss of the total column ozone has been reported due to the ozone depletion chemistry (e.g. WMO, 2003). The latest Arctic winter-spring (2004-2005, prior to this study), has been one of the most dramatic (together with the winter of 1999-2000), so far, as the conditions favourable for ozone depletion lasted more than three months, and the consequent ozone losses at around 18km were over 50% (press releases available at http://www.ozone-

sec.ch.cam.ac.uk/scout_o3 and at http://www.wmo.ch).

The balance between the production and destruction of atmospheric ozone, as well as the complex interactions between dynamics, radiation and chemistry determine the concentration of ozone in the atmosphere (e.g. Brasseur and Solomon, 1984). While the atmospheric circulation determines the transport of the species, the atmospheric temperature and the radiation flux together with the amount of species themselves determine the chemical reaction characteristics. Typical timescales of these different processes vary from just nanoseconds to several months, and therefore the evolution of the ozone layer is taking place in various temporal and spatial scales, and depends on a rather large number of different parameters (see e.g. Brasseur and Solomon, 1984; NASA, 2000; WMO, 2003).

Recently the understanding of the causes behind the past polar stratospheric ozone changes has increased significantly, as this area has been under substantial scientific interest (see e.g. WMO, 2003 for an extensive review). After the discovery of the Antarctic springtime ozone depletion, the impact of the polar stratospheric clouds forming under low polar wintertime stratospheric temperatures was recognized as the reason behind the high levels of active chlorine, and low levels of atmospheric nitrogen (e.g. Crutzen and Arnold, 1986; Solomon et al., 1986; Brasseur et al., 1990; Fahey et al., 1990). At present, the connections between the springtime ozone destruction, the amount of chlorine and other active halogen species, and polar stratospheric clouds are well known (e.g. Solomon, 1999; WMO, 2003). The assessment of the processes associated with the ozone depletion relies typically on both measurements and model studies. Due to the large number of parameters that one should measure simultaneously, and also taking into account the needed measurement frequency, it is difficult (or even impossible) to take a global 'snapshot' of the atmosphere where all significant parameters are simultaneously measured. The use of numerical models provides one way for these kinds of studies.

During the last decade, the production of many halocarbons has been regulated by the Montreal protocol (UNEP, 2000). The common understanding at the moment is that the abundances of ozone-depleting substances in the atmosphere have peaked and are now declining (e.g. WMO, 2003). Therefore the possible ozone layer recovery has been raised into discussions. Another hot topic, recently, has been the effect of enhanced greenhouse effect on the stratospheric ozone, as important links between climate change and ozone depletion exist (WMO, 2003, and references therein). The enhanced greenhouse effect, caused by the increasing amounts of the so–called greenhouse gases (hereafter GHGs) like carbon dioxide, methane, nitrous oxide, ozone, and stratospheric water vapour, is expected to cause cooling in the stratosphere (e.g. NASA, 2000; WMO, 2003, Shine et al. 2003). This potential cooling may have dramatic effects on ozone layer, particularly over the high northern latitudes (Austin et al., 1992; Shindell et al., 1998). The observed global annual mean cooling of the stratosphere that has taken place

over the past two decades is also coupled with the ozone depletion, as there is less ozone in the stratosphere to absorb solar radiation (e.g. WMO, 2003).

In this work a modelling approach will be utilized for the study of both the past and future behaviour of the stratospheric ozone layer. For this purpose a chemical-transport model of the middle atmosphere is used. The aim of this work is to drive an off-line chemistry-transport model (i.e. CTM) with a chemistry-coupled general circulation model (i.e. Chemistry Climate Model, CCM), and to address questions concerning the near past and near future stratospheric ozone concentration changes. Several CTM-type simulations using observation-based meteorological fields have been published during the recent years. These studies include e.g. those by Brasseur et al. (1997a), Carslaw et al. (2002), Chipperfield (1999, 2003), Chipperfield and Jones (1999), Chipperfield and Pyle (1998), Chipperfield et al. (1993, 2005), Egorova et al. (2001), Granier and Brasseur (1991), Gauss et al. (2003), Grooß et al. (2005), Hadjinicolaou et al. (2002), Horowitz et al. (2003), Khosravi et al. (1998), Lefèvre et al. (1994), Levelt et al. (1998), Massie et al.(2000), Rasch et al. (1995), Riese et al. (1999), Rummukainen et al. (1999), Tie et al. (1996, 1997) (for more extensive listing, see WMO, 1999, and 2003). A number of CCM-type simulations have also been published. These include the works by Austin (2002), Austin and Butchart (2003), Austin et al. (1992, 2001, 2003a, 2003b), Hein et al. (2001), Manzini et al. (2003), Nagashima et al. (2002), Shindell et al (1998), Steil et al. (2003), and Tian and Chipperfield (2005). However, studies where the CTM-approach has been used with the meteorological forcings from CCM integration are relatively rare. Such a study is e.g. the work by Brasseur et al. (1997a).

The focus of this work is not in specific processes studies, or in case studies, but in the general climate-scale (or climatological scale) features that the model should be able to reproduce. The main results of this study are based on a 40-year simulation of the ozone layer. The actual simulation has been designed mainly during 2002, and executed during early 2003. Therefore, the results should be considered mainly from that perspective (e.g. the Ozone Assessment 2002, by WMO (2003) and chemical data of Sander et al. (2003) were not available during the design-phase of the simulation).

In this study, I will show comparisons of the different processes affecting the high-latitude ozone layer during the near past and near future, and discuss the changes in the ozone behaviour. The discussions on the possible influences of the enhanced greenhouse effect on stratospheric ozone and analyses of the possible recovery of the ozone layer due to reduced halogen emissions are also given. The analysis of the model results is focused on the high northern and southern latitudes. The major goals and objectives of this thesis can be listed as follows:

1) To demonstrate the general applicability of the CTM-approach in the case

where chemistry-coupled climate model's winds and temperatures have been used to drive the chemical transport model (CTM).

2) To document, analyse, and discuss the results of a 40-year chemical transport simulation of near past and near future high-latitude ozone behaviour from the climatological perspective.

3) To compare the measured total ozone trends with the modelled trends for the past period (1980-1999) and future period (2000-2019), as well as determine the likely causes, and precursors of the past trends. Focus is at the high-latitude winter-spring stratosphere.

4) To intercompare the effects of different atmospheric processes on the high-latitude stratospheric ozone in near past and in near future.

5) To discuss, and gain understanding on the possible effects of emission reductions due to the international regulations and effects of global climate change on the stratospheric ozone behaviour (i.e. ozone recovery and enhancement of ozone depletion).

This thesis has the following structure: Chapter 2 gives a short thematic introduction about the polar stratospheric ozone characteristics, and processes, in Chapter 3, a generalized description about the FinROSE-CTM model is given. Chapter 4 is devoted to the model simulation with result assessments and discussions against the set objectives, and finally in Chapter 6 all the goals set for this thesis are assessed, and concluded. The acronyms and abbreviations used in this thesis are listed in the Appendix.

2 Ozone Depletion

Polar wintertime and springtime ozone behaviour and distribution are regulated by processes associated with atmospheric transport and chemistry. The 1987 Montreal Protocol (UNEP, 2000) regulating the use and trade of the ozone depleting substances also promotes the value of science in fighting the ozone depletion, and in fact, the scientific understanding of the ozone depletion phenomenon has increased significantly after the ratification of the Montreal Protocol (e.g. WMO, 2003). As one may assume, the destruction of the ozone layer has many consequences since the ozone layer is, by large, protecting the Earth's biosphere against unhealthy levels of solar UV-radiation. The decreases in stratospheric ozone are directly increasing the UV radiation at the ground. The UV radiation levels depend also on the cloud cover, aerosol amounts, and surface albedo which all may change due to the changes in climate (e.g. NASA, 2000; WMO, 2003).

The purpose of this chapter is to give a brief summary on those major factors that control the natural and perturbed behaviour of polar stratospheric ozone (from the perspectives of this study, listed as objectives in the previous chapter). The scope of this study lies within the ozone layer, and in the near past, and near future behaviour of high latitude winter-spring ozone depletion, and its numerical modelling. More detailed discussion of the middle atmospheric processes may be found for example from Brasseur and Solomon (1984), Andrews et al. (1987), and Brasseur (1997). An excellent electronic textbook on stratospheric ozone, composed by a number of renowned scientists in the field, has been put available at http://www.ccpo.odu.edu/SEES/index.html (hereafter NASA, 2000). The atmospheric modelling aspects have been discussed in detail by Trenberth (1992), and the chemistry-transport type modelling by Brasseur and Madronich (1992) as well as by Brasseur et al. (1997b). The most recent published "Scientific Assessment of Ozone Depletion" prior to this study is the 2002 Assessment, published by WMO (2003). The WMO-2002 assessment has an exclusive discussion on various aspects about the stratospheric ozone, while IPCC reports include detailed discussions on the issues connected to climate change (IPCC, 1990, 1992, 1996, and 2001).

2.1 Natural Ozone

The atmospheric chemistry is a composition of chemical reactions, the effect of temperature on chemistry, the effect of dynamics on chemistry, the effect of solar radiation on chemistry (due photolysis processes) and atmospheric heating. While the absolute concentrations of trace species are low compared to the molecular nitrogen and molecular oxygen, their influence in the atmosphere is large. Middle atmospheric ozone is known to be the main contributor to the strato-

spheric radiative-dynamical drive determined by the dynamical warming caused by the wave-driven mean meridional circulation and by ozone absorption of solar radiation (e.g. Brasseur, 1997, NASA, 2000). Solar radiation is capable of breaking chemical bonds through photolysis (e.g. Brasseur and Solomon, 1984). This phenomenon usually produces very reactive radicals that can affect all the atmospheric chemistry. While the photodissociation of the bulk atmospheric gas, namely the molecular nitrogen, has a negligible effect on atmospheric chemistry due to the very weak absorption, the second most abundant gas, namely the molecular oxygen has a key role in the middle atmospheric chemistry (e.g. Brasseur and Solomon, 1984). The photodissociation of the molecular oxygen leads to the formation of oxygen atoms which in turn give rise to the production of ozone. From the biospheric viewpoint, this formation of ozone is probably the most significant effect of the radiation since it causes the formation of the 'life-protecting' ozone layer (e.g. WMO, 2003). The purpose of this section is to explain briefly, how the observed ozone distribution forms and what those main processes are that control the natural production and destruction of stratospheric ozone.

In an unperturbed atmosphere the production of ozone takes place in the tropics and midlatitudes by photodissociation of oxygen since over these latitudes the required ultraviolet radiation, with wavelength less than 242nm is readily available in the stratosphere. This basic ozone production, as well as ozone's natural loss is known as the Chapman-cycle (Chapman, 1930):

$$O_2 + h\nu \longrightarrow O + O \tag{2.1}$$

$$O + O_2 + M \longrightarrow O_3 + M \tag{2.2}$$

$$O_3 + h\nu \longrightarrow O + O_2 \tag{2.3}$$

$$O + O_3 \longrightarrow O_2 + O_2 \tag{2.4}$$

The photodissociation of molecular oxygen is a relatively slow process with a time scale of weeks near the altitude of 30km over the tropics. The photodissociation of the molecular oxygen, in equation 2.1 is mainly caused by the absorption within the Herzberg continuum (around 200 - 220 nm) and in the Schuman-Runge band (around 185-200nm). Due to the oxygen absorption at higher atmospheric levels, the magnitude of UV radiation with wavelength shorter than 242nm falling down the atmosphere, decreases significantly with decreasing altitude, and the photodissociation of molecular oxygen becomes relatively slow in the lower and middle stratosphere (e.g. Brasseur and Solomon, 1984).

The produced oxygen atoms (in equation 2.1) are highly reactive, and the natural production of ozone (in equation 2.2) takes place quickly, since the typical stratospheric lifetime of atomic oxygen is substantially less than one second (e.g. Brasseur, 1997). The absorption by ozone molecules (in equation 2.3) is the main source of middle atmospheric heating. This absorption of solar radiation

by ozone in the Huggins and Hartley bands (242 - 310nm, and 310 - 400nm, respectively) converts the energy of photons into thermal energy (e.g. Brasseur, 1997). This heating is highly dependent of the concentration of the ozone. The interaction between the atmospheric dynamics and chemistry is therefore mainly a product of the radiative coupling between ozone and temperature. A decrease in the stratospheric ozone would therefore lead to a decrease in the stratospheric temperatures (e.g. NASA, 2000).

The natural loss of ozone (in equation 2.4) is a relatively slow process (around three times slower than the production in reaction 2.2), and this natural ozone destruction depends also on the amount of ozone itself. Since the production of ozone depends mainly on the molecular oxygen which in turn is the second most abundant atmospheric constituent, the production itself is therefore a function of the solar radiation at given place and season (i.e. the altitude and solar zenith angle; SZA). In the atmospheric chemistry models it is often convenient to take advantage of this direct coupling between the oxygen atoms and ozone molecules, as well as of the differences in the chemical kinetics, by forming a chemical family; odd oxygen (O_x), consisting of the atomic oxygen and ozone. Since the O_x -production (equation 2.1), and the O_x -loss (equation 2.4) are both relatively slow processes, the lifetime of O_x is relatively long, and, in fact longer than those of atomic oxygen or ozone (e.g. Brasseur, 1997).

Figure 2.1 (reproduced from NASA, 2000) shows a typical stratospheric latitude-altitude ozone concentrations derived from the SBUV satellite measurements (Nimbus-7, Solar Backscatter UltraViolet instrument) from 1980-1989, for northern hemispheric winter (i.e. January). An overall inspection of this figure shows clearly how the majority of the ozone, in fact more than 90%, is located in the stratosphere. The maximum values over the poles are around $5 \cdot 10^{18} \#/m^3$ near 22km (i.e. more than 14mPa in terms of partial pressure). The ozone concentrations shown in Figure 2.1 are somewhat controversial, since the largest absolute amounts of ozone are found clearly away from the tropical source regions, and actually over the winter pole which is not sunlit, and therefore not fitted for O_x production. This means that there have to be other dynamical and/or chemical reasons behind the observed ozone distribution.

From the odd-oxygen perspective, the production and loss of O_x are taking place on weekly or monthly scale, depending on the stratospheric altitude while the individual members are constantly formed and destroyed (i.e. O and O_3) on much shorter timescales. Due to the differences in chemical kinetics between the natural production and loss of ozone (i.e. equations 2.2, and 2.4 respectively), the bulk of the O_x in stratosphere is in the form of ozone (i.e. $[O_3\,] \approx [O_x\,]$). In Figure 2.1 the photochemical replacement times (PRT) for ozone are also illustrated. As can be seen, the time needed to produce the observed ozone concentrations depend on altitude and latitude, as well as on the availability of the solar radiation. In the lower stratosphere the time for producing the observed ozone distribution is long

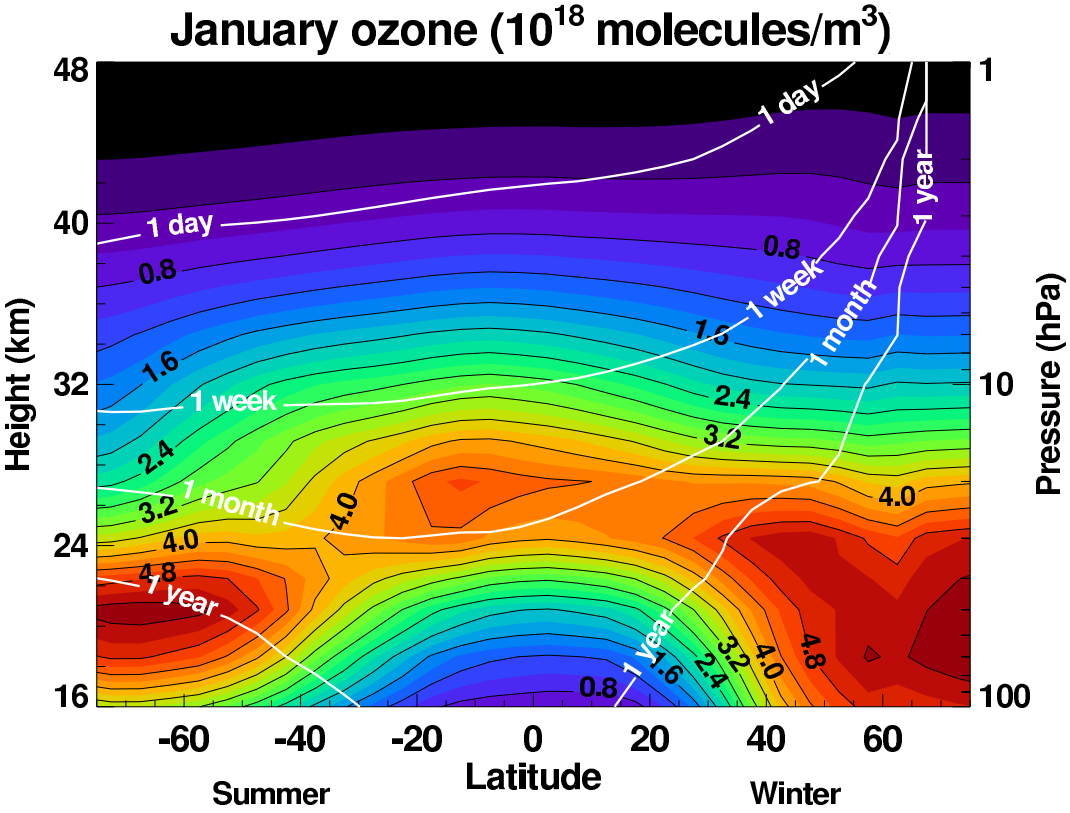

FIGURE 2.1. Altitude-latitude distribution of the ozone concentration with the typical photochemical replacement times for ozone. The ozone concentrations are based on the measurements by the Nimbus-7 Solar Backscatter UltraViolet instrument (SBUV) from 1980-1989. (Reproduced from NASA, 2000)

(i.e. more than one month). Basically the winter hemispheric replacement times increase towards the poles, having values over one year throughout the whole stratosphere. At higher levels, above 10hPa, over the sunlit areas, the stronger solar radiation causes the photochemical replacement times to be less than a week, while the lower level values are more than a month due to the ultraviolet radiation absorbed at higher levels. The connection between the maximum values of replacement times and maximum ozone concentrations is the transport of ozone. The transport of ozone from the tropical production areas towards the polar lower stratosphere is known as the Brewer-Dobson circulation (e.g. NASA, 2000; WMO, 2003). From the global modelling perspective, this means that in order to address questions related to high-latitude stratospheric ozone, the ozone production areas (e.g. tropics) also need to be carefully taken care of. The next section will discuss the transport processes.

2.2 Role of Transport

The general dynamical behaviour of the stratosphere is quite different from the troposphere. The presence of ozone drives in large the radiative characteristics of the whole middle atmosphere (i.e. stratosphere and mesosphere) and its thermal structure (e.g. NASA, 2000). A well known fact of the middle atmosphere is that the radiatively derived temperature fields are totally different from the observed temperatures (e.g. Brasseur, 1997). Due to the earth-sun geometry the net radiative heating (as provided mainly by the UV-absorption of ozone and molecular oxygen) of the middle atmosphere has its maximum over the summer hemisphere, and its minimum over the winter hemispheric high latitudes. Should the middle atmosphere be in the radiative equilibrium, the temperature distribution would have its maximum over the summer hemisphere in the vicinity of the stratopause. However, the observed temperature distribution exhibits rather different behaviour: The mesosphere has a cold summer pole, and a warm winter pole, while stratosphere has a cold winter pole and a warm summer pole. The reason for this imbalance can be found from the general circulation. In the troposphere the circulation system is sometimes described as thermally driven heat engine. In the middle atmosphere, temperatures departing from the radiative equilibrium are balanced by the meridional circulation over longer time scales, and therefore the middle atmosphere is radiative/dynamically driven (e.g. Brasseur, 1997). The induced winterpoleward circulation is called the Brewer-Dobson circulation (e.g. NASA 2000). A review article on the stratospheric dynamics has been recently given by Haynes (2005).

The pole to pole temperature gradient causes the increase in easterlies with height in the summer hemisphere and increase in westerlies in the winter hemisphere through the thermal wind balance (e.g. Brasseur, 1997). In the area where the meridional temperature gradient reverses, the zonal winds decrease. The jet stream around the wintertime polar areas isolates the polar area, or the polar vortex. The orographic forcings from the surface and the non-homogeneous heating of the land and sea generate upward propagating planetary waves that slow down the stratospheric polar night jet. Planetary waves are far less prevailing over the southern hemispheric high latitudes which are surrounded by the ocean, and therefore the Antarctic polar vortex becomes more stable, and much colder than northern polar vortex (e.g. NASA, 2000; WMO, 2003). Over the northern high latitudes the stronger wave activity means stronger wintertime Brewer-Dobson circulation, and more mixing between the mid-latitudes and high-latitudes over the northern hemisphere. These hemispheric differences in wave induced mixing properties are also affecting the lifespans of the two vortices: Over the southern polar areas less mixing means more persistent vortex, while over the north the opposite is true (e.g. NASA, 2000). Therefore it can be concluded that the net effect of the Brewer-Dobson circulation on the transport of long-lived tracers like

ozone is different over the two hemispheres, and the realized tracer distributions are also different (e.g. NASA, 2000).

The starting point for the global circulation of ozone is the tropics where most of the ozone is produced, and where the air is lifted from the troposphere to the stratosphere. The air entering the tropical levels of strong solar radiation will gain a high ozone concentration which is then transported towards the winter pole. The descending takes place over the mid-latitudes and high-latitudes causing the observed patterns of ozone (see Figure 2.1). Since the atmospheric transport processes are the primary sources for the observed variability of trace constituents, the different timescales of atmospheric motions can be used for understanding the observed behaviour of species like ozone (e.g. NASA, 2000). The effect of atmospheric transport on densities of different constituents is of primary importance since some trace species have long enough life time to be transported. In general, the constituents can be classified using their chemical lifetime versus the typical timescale of atmospheric transport. Those species that have much shorter lifetime than the transport timescale are typically in photochemical equilibrium, and the effects of transport are negligible. Those constituents that are well mixed throughout the middle atmosphere have a life time much longer than the transport timescale (e.g. molecular oxygen, or odd-oxygen). A third class would be those species that have life time comparable to the transport timescale. For these species both dynamical and chemical processes are of interest (e.g. Brasseur, 1997; NASA, 2000). The transport of different long-lived trace species along the Brewer-Dobson circulation is due to the advection by mean meridional circulation, and by the effects of wave activity which in turn is a product of wave drag and inhomogeneous heating due to the seasonal variations and land-sea contrasts. In WMO (2003) this effect is called the planetary wave drive (PWD).

The Brewer-Dobson circulation is relatively slow and its timescales can be estimated using an idealized transport tracer, known as the age of air (e.g. Plumb, 2002; Waugh and Hall, 2002). The age of air is often expressed as the average amount of time it takes for air parcels initiated from surface to reach a certain location in the atmosphere. Figure 2.2 (reproduced from NASA, 2000) shows a typical northern hemispheric wintertime distribution of a modelled age of air with a schematic illustration of the Brewer-Dobson circulation. As can be seen, the well-mixed troposphere exhibits relatively low values (i.e. less than a year) while towards the winter pole, the age of air gradually grows to over five years above the polar areas around 40hPa. The schematic Brewer-Dobson circulation in Figure 2.2 shows how this age distribution forms: The air enters from the tropics, crossing the tropopause, and travels towards the winter pole. The age of air distribution is therefore displaced upwards above tropics and downward over the winter pole. Similar characteristics were also seen in Figure 2.1 in case of ozone. The ascending up to the lower mesosphere takes more than four years, and the descent back to the lower wintertime mid and high-latitude stratosphere around one year more.

From this figure it is quite straightforward to conclude that trace species having long stratospheric or mesospheric lifetimes will have rather different atmospheric distributions over the tropics compared to extratropics. Such compounds are e.g. some CFCs which will be further discussed in the next section. It should also be remembered that the timescale for cycling the majority of the tropospheric air around a full Brewer-Dobson circulation pattern is several decades (e.g. NASA, 2000). While middle atmospheric models typically underestimate the age of air (e.g. Waugh and Hall, 2002), the modelled values exhibited in Figure 2.2 are in general agreement with the commonly known values of the age of air (see e.g. discussion given by Tian and Chipperfield, 2005).

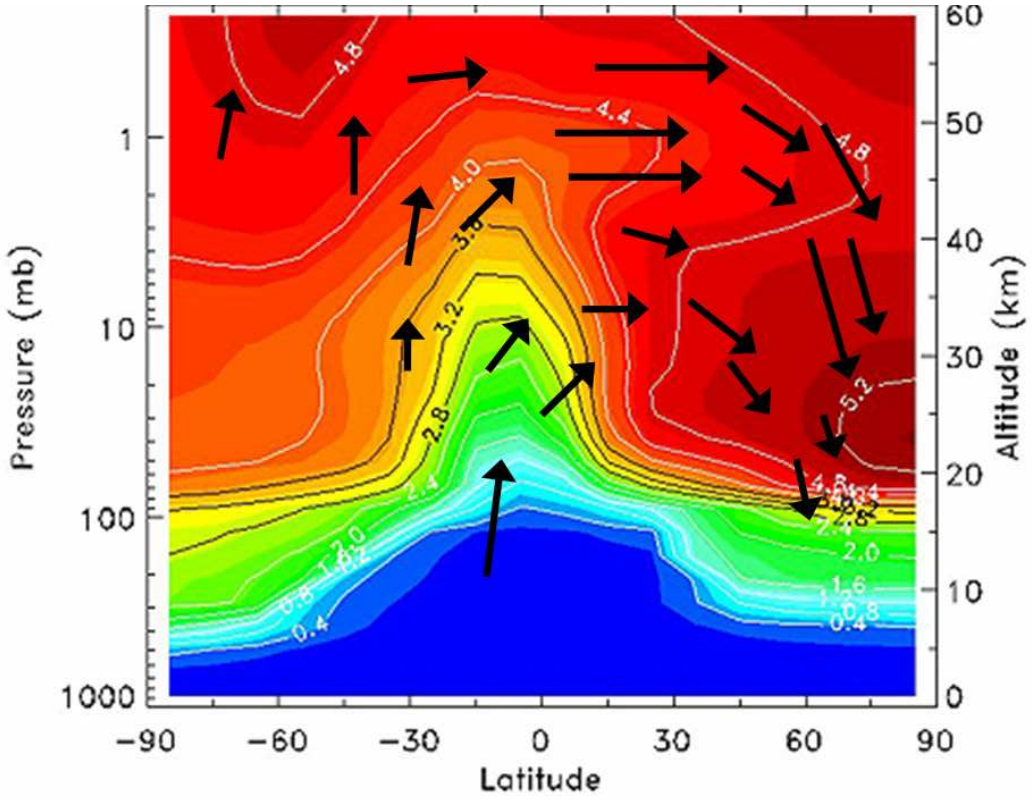

FIGURE 2.2. Typical northern hemispheric wintertime altitude-latitude distribution of the zonal-mean age of air and schematic illustration of Brewer-Dobson circulation (black arrows). (Reproduced from NASA, 2000)

The wintertime polar areas are not sunlit, and these areas are therefore cooled. From the wintertime polar vortex perspective the effect of Brewer-Dobson circulation is in the diabatic descent within the vortex, the magnitude of which depends on the magnitude of the circulation. The weaker wave activity over the southern hemisphere leads to weaker Brewer-Dobson circulation (e.g. Randel and Newman, 1999), and more symmetric, and stronger vortex. The southern polar vortex therefore also gains less transported wintertime ozone since the diabatic

descent is less profound (e.g. NASA, 2000).

The year-to-year differences in the Brewer-Dobson circulation is also affected by periodic wave-interactions, like the QBO (Quasi-Biennial Oscillation) which affects the interannual variability of the wave activity. Since the scope of this study is not on these periodic effects, the interested readers are referred e.g. to Andrews et al. (1987) for a detailed discussion, and WMO (2003) for a review from the stratospheric ozone perspective. In Chapter 4 the age of air type diagnostics will be used for the evaluation of the transport characteristics of a chemistry-transport model (CTM).

2.3 Ozone Depletion Mechanism

One conclusion from the Chapman-cycle, previously discussed, is the constant natural production and destruction of ozone, and the effect of Brewer-Dobson circulation. In order to have an ozone depleting effect on this natural behaviour, the basic production of ozone should be reduced, or the produced ozone molecules should be lost somewhere else. Since the production from molecular oxygen (available at "bulk magnitudes" in the atmosphere) due to the photolysis is a prevailing feature in the atmosphere, only the latter process is relevant in practice. The ozone loss due to the ozone chemistry with chlorine, bromine, nitrogen, and hydrogen containing species is now quite well understood (e.g. Solomon, 1999; WMO, 2003). The purpose of this section is to describe these processes briefly.

Those compounds that are contributing to the stratospheric ozone depletion (ie. perturbing the natural behaviour) are called ozone-depleting substances (ODS). ODS include CFCs, HCFCs, bromine containing halons, bromocarbons (like methyl bromide, CH_3Br), and chlorocarbons (e.g. carbon tetrachloride, CCl_4 or methyl chloroform, CH_3CCl_3) (e.g. WMO, 2003). A common feature for all ODSs is their stability in the troposphere. These compounds typically decompose only under strong radiation (available in the middle atmosphere) through photolysis (e.g. Brasseur, 1997). The photolysis of ODSs releases chlorine or bromine atoms, which then cause ozone destruction. A measure of ODSs potential for ozone depletion is called ozone depletion potential (ODP). The ODP is the ratio of the impact on ozone of a chemical compared to the impact of a similar mass of CFC-11 (ie. the ODP of CFC-11 is 1.0). CFCs and HCFCs have ODPs that range from 0.01 to 1.0. The halons have ODPs ranging up to 10. Carbon tetrachloride has an ODP of 1.2, and the ODP of methyl chloroform is 0.11. Hydrofluorocarbons (HFCs) have zero ODP because they do not contain chlorine or bromine.

Chlorofluorocarbons (CFCs) are compounds consisting of chlorine, fluorine, and carbon. CFCs are very stable in the troposphere, but in the stratosphere they can be broken down by strong ultraviolet radiation, and release chlorine which

is very effective for destroying ozone molecules. CFCs are used as refrigerants, solvents, and foam blowing agents. The most common CFCs are CFC-11, CFC-12, CFC-113, CFC-114, and CFC-115 with ODPs 1, 1, 0.8, 1, and 0.6 respectively. The CFCs are also effective greenhouse gases. For example the CFC-12 has a global warming potential (GWP) of 8500, while CFC-11 has a GWP of 5000. (The GWP is the ratio of the radiative forcing caused by a substance to the radiative forcing caused by a similar mass of carbon dioxide as averaged over a 100-year period following the emission) (see e.g. IPCC, 2001).

Halons are compounds that consist of bromine, fluorine, and carbon. The halons are used typically as fire extinguishing agents. The use of halons causes ozone depletion because they contain bromine which is much more effective at destroying ozone than chlorine with ODPs up to ten and more. The use of ODSs is internationally controlled by the Montreal Protocol (UNEP, 2000). The Montreal Protocol is an international treaty governing the protection of stratospheric ozone. The "Montreal Protocol on Substances That Deplete the Ozone Layer" and its amendments control the phase-out of ODS production and use. Under the Montreal Protocol, several international organizations report on the science of ozone depletion, implement projects to help move away from ODSs, and provide a forum for policy discussions. From the ozone science perspective the Scientific Assessments of Ozone Depletion are the best known reviews on this theme (WMO, 1985, 1992, 1994, 1999, and 2003). The most recent assessment, prior to this study has been published by WMO (2003).

Usually, the ODSs direct reaction with ozone or atomic oxygen is very slow (due to the stable nature of CFCs), and the photolysis of CFCs takes place with wavelengths typically lower than 240nm. Because of the fact that the majority of radiation below 240nm is absorbed by the ozone or molecular oxygen, the chlorine releases from CFCs have to take place at high altitudes. From the Brewer-Dobson circulation perspective, this means that it takes several years, decades, or even longer for CFCs to release all the chlorine available, as these compounds travel along the Brewer-Dobson circulation in and out the stratospheric domain. However, the decomposition of ODSs (or nitrous oxides) leads to the release of species that can have significant effect on ozone. For example in the case of CFC-11 a free chlorine atom is released through photolysis:

$$CFCl_3 + h\nu \longrightarrow CFCl_2 + Cl. \tag{2.5}$$

The released free chlorine atom initiates a catalytic ozone depletion cycle:

$$Cl + O_3 \longrightarrow ClO + O_2 \tag{2.6}$$

$$ClO + O \longrightarrow Cl + O_2 \tag{2.7}$$

, where the net effect is that one ozone molecule and one ozone atom are recombined into two oxygen molecules while the chlorine species remain untouched. The removal of the Cl or ClO typically takes place in reactions with methane or with nitrogen dioxide to form long-lived, non-ozone depleting chlorine reservoirs of hydrochloric acid (HCl), and chlorine nitrate ($ClONO_2$) respectively. From odd-oxygen perspective the effect of these cycles means, therefore that two odd-oxygens are converted into two molecules of diatomic oxygen. Since the above cycle needs free oxygen which is typically not commonly available in the lower stratosphere, this particular catalytic cycle is mainly important in the upper stratosphere (e.g. NASA, 2000).

The current understanding, as stated by WMO (2003), of the main chemical destruction mechanisms of high latitude stratospheric ozone during winter and spring is that the ozone depletion is primarily due to two gas-phase catalytic cycles, namely:

Cycle 1

$$ClO + ClO + M \longrightarrow Cl_2O_2 + M \tag{2.8}$$

$$Cl_2O_2 + h\nu \longrightarrow 2Cl + O_2 \tag{2.9}$$

$$2(Cl + O_3 \longrightarrow ClO + O_2) \tag{2.10}$$

$$Net: \quad 2O_3 \longrightarrow 3O_2 \tag{2.11}$$

and

Cycle 2

$$BrO + ClO \longrightarrow \begin{cases} Br + Cl + O_2 \\ BrCl + O2 \end{cases} \tag{2.12}$$

$$BrCl + h\nu \longrightarrow Br + Cl \tag{2.13}$$

$$Br + O_3 \longrightarrow BrO + O_2 \tag{2.14}$$

$$Cl + O_3 \longrightarrow ClO + O_2 \tag{2.15}$$

$$Net: \quad 2O_3 \longrightarrow 3O_2 \tag{2.16}$$

Since the above cycles do not require free atomic oxygen, these two mechanisms can destroy ozone also in lower stratosphere. However, it should be noted that these cycles also need solar radiation since both the photodissociation of Cl_2O_2 (i.e. the ClO dimer), and $BrCl$ are radiation driven, though the needed solar fluxes, and wavelengths are generally not as demanding as in the case of molecular oxygen photolysis (e.g. NASA, 2000).

A central aspect of the winter-spring ozone depletion in the high-latitude stratosphere is the fact that even these two most important cycles, shown above, are relatively unimportant since reactive nitrogen typically forms inactive chlorine reservoirs that rule out the possibilities for Antarctic type ozone depletion; as far

as reactive nitrogen (e.g. NO_x) is available, the available active chlorine stays low, and the ozone depletion does not become effective. However, as it was observed over Antarctica during mid 1980's, the levels of active chlorine were very high (Solomon et al., 1986), and these high abundances were found to be due to the heterogeneous processing provided by the polar stratospheric clouds (PSC; for a review see e.g. Solomon, 1999). The heterogeneous processes occurring on the surface or in the solutions of atmospheric particles are responsible for the devastating phenomena of Antarctic ozone depletion, since the heterogeneous conversions are much faster in the liquid/solid phase than in the gas phase (e.g. Brasseur, 1997; NASA, 2000). Therefore the polar stratospheric clouds (PSCs) catalyze the conversion of relatively inactive reservoir species (such as $ClONO_2$) to active-form chlorine (e.g. Cl or ClO) which in turn is needed for catalytical ozone destruction. The particles that are involved in this processing are polar stratospheric cloud particles, but also background sulfate aerosols play a role (e.g. WMO, 2003).

Under cold atmospheric conditions, typical in the wintertime stratosphere, the formation of PSCs becomes possible. The PSCs are often classified into two groups; PSCs type-I, and type-II. The type-I PSCs, again, are often divided into two subclasses; Ia, and Ib. The type-II PSCs are basically ice-form cloud particles that form below the frostpoint of ice. The frostpoint under typical stratospheric pressures is around 189K. The formed ice particles are relatively large (i.e. around 10μm), and therefore after their formation they undergo gravitational settling, or in other term, sedimentation. The type-I PSCs are believed to be either in a form of frozen, or partly frozen nitric acid trihydrate (NAT; Type-Ia), or in a form of supercooled liquid ternary solution of HNO_3 , H_2SO_4, and water (STS; Type-Ib). The type-I PSC particles are generally smaller than the ice-form particles (around 1μm), and the type-I PSCs form at temperatures higher than the ice frost point, typically around 195K. Due to the smaller size their settling velocities are also smaller than those of type-II (see e.g. NASA, 2000; WMO, 2003).

Only large PSC particles may sediment effectively to cause a mechanical removal of the PSC retentioned species, like HNO_3 or H_2O by fast enough gravitational settling causing mechanical denitrification or dehydration at the given level (e.g. WMO, 2003). From the Antarctic perspective, as the temperatures below the frostpoint are observed on annual basis during winter, the process of PSC sedimentation is relatively straightforward. However, as shown by Fahey et al. (2001), and further studied by Carslaw et al. (2002), under persistent conditions the NAT-type PSCs may also grow as large as 10-20μm, and therefore cause significant denitrifications due to the sedimentation. This possibility, while important also in the Antarctic wintertime stratosphere, is of great importance in the wintertime northern polar stratosphere where temperatures below ice frostpoint are rare.

Generally speaking, the stratosphere contains various types of particles on/in which an adsorption or absorption of a gas-phase constituent may take place. In

the stratosphere, the most common are the sub-micron sized sulphate aerosols. These aerosols are typically either of volcanic origin, or originated from the troposphere as a result of the transport by Brewer-Dobson circulation. Atmospheric aerosols also provide the needed surfaces for the reservoir conversion. Since the aerosols are in general small droplets or particles suspended in the atmosphere, typically containing sulfur, the available surfaces are smaller than in the case of the PSC particles. Since the size of these background aerosols is typically less than 1 μm, their abundance, and removal from the stratosphere, over the high latitudes is dependent on the Brewer-Dobson circulation (e.g. NASA, 2000).

In order to have substantial ozone loss due to the catalytic cycles, the very basic requirement is to have enough active radicals available (i.e. Cl and/or ClO). While the general levels of inorganic chlorine abundances in the atmosphere are high enough for the production of Antarctic-type ozone depletion, the chlorine activation is required. The conversion from the long-lived reservoirs, like HCl and $ClONO_2$, towards the active forms initiates in heterogeneous reactions like:

$$ClONO_2(g) + HCl(s) \longrightarrow Cl_2(g) + HNO_3(s) \tag{2.17}$$

or

$$ClONO_2(g) + H_2O(s) \longrightarrow HOCl(g) + HNO_3(s) \tag{2.18}$$

where the molecules that are relatively inactive in the gas phase become highly active in the liquid/solid phase (i.e. $ClONO_2$ and HCl), and result in desorption of gas-phase molecules like Cl_2 or $HOCl$. In these two examples the nitrogen from gas-phase $ClONO_2$ is converted into HNO_3 which remains in the liquid/solid form, and undergoes sedimentation if the absorbing/adsorbing particle is large enough. Under typical stratospheric conditions, these heterogeneous reactions are very slow in the gas phase, and thus the needed massive chlorine activation (e.g. for those catalytic ozone depletion cycles previously shown) cannot take place. The effectiveness of the heterogeneous processing on the PSC particles is based on the fact that the particles provide the needed surfaces where the thermodynamic barrier is lower and condensation of reactants can take place, making relatively inactive species highly active (e.g. NASA, 2000). This heterogeneous conversion takes place also in the dark as no solar radiation is needed for heterogeneous processing. The gas-phase products of these heterogeneous reactions (like Cl_2 and $HOCl$) are typically relatively unstable and are photolyzed even in visible range to form active ClO_x (see e.g. NASA, 2000). As long as the PSCs persist, the removal of gas-phase nitrogen to the solid/liquid phase continues. In the case of PSC evaporation, the entrapped HNO_3 is released to the gas-phase, and a process called renitrification may take place. However, due to the sedimentation of the PSCs this renitrification is typically displaced to a lower level. If the PSC sizes are greater (i.e. of order 10μm) then an irreversible deeper denitrification will take place, as the vertical displacement deeper down causes the renitrifica-

tion take place at altitudes where it has lesser effect on the ozone chemistry. At the level of ozone maxima, the main catalytic cycles, discussed above, become, therefore extremely effective for ozone destruction. The formation of the ice-form PSCs is also converting water vapour away from the gas phase, and therefore also a process called dehydration may become possible together with the rehydration process similar to renitrification. The actual heterogeneous chemistry scheme used in this study will be explained in the next Chapter.

The importance of PSCs is two-fold: they both make the conversion of chlorine reservoirs towards active, ozone depleting forms possible, and they remove the gas-phase nitrogen from the stratospheric chemistry system, allowing for more ClO_x catalyzed ozone depletion chemistry (e.g. Solomon, 1999, and WMO, 2003 for a recent review). This means that while the PSCs exist, the conversion from reservoirs is possible, but if the PSCs are evaporated without sedimentation, renitrification will become possible. The return of the solar radiation after winter will result in an increase of vortex temperatures to levels where PSC formation is no longer possible. Therefore, if no sedimentation is occurring, ozone depletion stays small (e.g. WMO, 2003). However, in case of large PSCs, the sedimentation is relatively effective, and therefore the process of PSC sedimentation may cause deep irreversible denitrification of the stratosphere. In these conditions the return of the sunlight during local spring has no immediate effect, in absence of nitrogen (NO_y), and the ozone depletion chemistry will continue until the vortex breaks, and mixing due Brewer-Dobson circulation replaces the absent NO_y . It should also be remembered that the formation temperatures for PSCs are typically lower than the evaporation threshold due to the hysteresis effect. Basically this means that after their formation, the PSC-events will last longer than the actual forming temperature persists. Therefore, whenever the stratospheric temperatures are low enough, PSCs start to form, and make the production of nitric acid (HNO_3), due to the heterogeneous processing possible, which in turn effectively removes reactive nitrogen from the system, and gives way for the ozone depletion chemistry. From the modelling perspective this effect is an important aspect, and it means that the advection of the PSCs should also be somehow taken into account, and that PSC treatment based on the pure thermodynamical equilibrium consideration may not reproduce reasonable results. These issues have been recently discussed in detail by e.g. Carslaw et al. (2002), Mann et al. (2002a, 2002b), and Tabazadeh et al. (2002).

A clear conclusion from the two main ozone destruction cycles, previously shown, is that the chlorine monoxide (ClO) is needed in both cases. Therefore, the course of the ozone depletion season is strongly dependent on the availability of ClO_x , either in the form of pure ClO , or in the form of ClO dimer (Cl_2O_2 , i.e. $ClOOCl$). The processing on the PSC surfaces both activates, and maintains the levels of active chlorine, and the dissipation of the PSCs during spring gives way for the deactivation of active chlorine, as the reservoirs are again formed. Un-

der the typical Antarctic wintertime and springtime conditions the temperatures between altitudes of 14 and 24km remains very low allowing for the large scale PSC type-II formation, and for nearly complete ozone destruction between these levels. If the chlorine loading is high, this destruction phenomenon is relatively insensitive to the chemical loss rates themselves (WMO, 1999).

In case of bromine species that generally have ODP far greater than chlorine species, the reservoirs like bromine nitrate ($BrONO_2$) are easily photolyzed, and therefore the reservoirs are long-lived only during dark. During day, basically all the bromine is in a form that has the potential for ozone depletion (e.g. NASA, 2000). Therefore, PSC processing is not necessarily needed for bromine activation. However, the bromine mixing ratios are typically low (i.e. in ppt_v scale) while the mixing ratios of inorganic chlorine are relatively high (in ppb_v scale). As discussed above, the catalytic Cycle 2 ($BrO + ClO$) is also an important contributor to the polar stratospheric ozone depletion. As already stated, this cycle is controlled by the abundance of active chlorine. The current understanding of the bromine abundances and chemistry is still somewhat controversial, as stated by WMO (2003). However, due to the regulations, the abundances of bromine species in the atmosphere are expected to rise longer than those of chlorine species, and the contribution of bromine induced ozone depletion may have increased faster than the chlorine induced ozone destruction (WMO, 2003). As shown by a model study of Chipperfield and Pyle (1998) this could be important in the case of the Arctic, as the catalytic cycles involving BrO may cause as much as 60% of the ozone depletion. Over the Antarctic where the low temperatures lead to large-scale denitrification on annual basis the effect of bromine is expected to be somewhat less significant. On the longer perspective, as the bromine-ozone interactions are strongly dependent on the availability of ClO , the regulation-driven decrease of total inorganic chlorine loading will eventually lead to the recovery of the ozone layer regardless of the future abundance of atmospheric bromine loading (Chipperfield and Pyle, 1998). The active-form chlorine (i.e. $ClO_x = Cl + ClO$), as needed above, forms due to the reactions of inactive chlorine reservoir species on polar stratospheric clouds (PSCs). The needed levels of BrO , however, are not strongly dependent on the existence of PSCs since most of the available inorganic bromine is in the form of active reservoirs (e.g. bromine nitrate, $BrONO_2$, or hydrogen bromide, HBr) which are readily photolyzed. According to WMO (2003), bromine monoxide (BrO) could contribute as much as 50%-60% of the total chemical loss of polar stratospheric ozone.

The effect of denitrification caused by the formation of large NAT particles has been recognized as one possibility for the Arctic ozone depletion (WMO, 2003). According to the observations, during the coldest Arctic stratospheric winters some areas have lost more than 50% of the total nitrogen around 20km altitude (e.g. WMO, 2003). It has been shown by Tabazadeh et al. (2000) that large-scale deep denitrification of more than 10km in vertical depth takes place

in the Antarctic when the duration of a PSC exposure is about 2 weeks. Such long periods of PSC events in the wintertime Arctic stratosphere occur extremely seldom (e.g. WMO, 2003). A number of recent studies on the Arctic denitrification and on the impact of PSCs on polar stratospheric ozone exist. These include the works by Carslaw et al. (2002), Chipperfield and Pyle (1998), Davies et al. (2002, 2005), Dessler et al. (1999), Fahey et al. (2001), Grooß et al. (2005), Hintsa et al. (1998), Jensen et al. (2002), Kleinböhl et al. (2002), Kondo et al. (1999, 2000), Mann et al. (2002a, 2002b), Northway et al. (2002), Rex et al. (1997), Santee et al. (1999, 2000), Tabazadeh et al. (2001), and Waibel et al. (1999). Since the current understanding states that denitrification due to sedimenting ice particles is not common in the Arctic, the models simulating these processes should include parameterizations for the growth of the large NAT particles. Such studies have been recently published by e.g. van den Broek et al. (2004), Chipperfield et al. (2005), and Fueglistaler et al. (2002). During the Arctic winter the possible ozone loss depends more critically upon the details of chlorine activation. WMO (2003) also states that high levels of ClO are measured typically throughout the polar vortex. Recent measurements of chlorine species indicate that over the Arctic there is more year-to-year variability in active chlorine, and that the overall levels of activated chlorine are higher over the Antarctica.

Since PSCs form in extremely low temperatures, the general problem, stratospheric ozone destruction, will be of primary importance also in the future, because of the long lifetimes of CFCs combined with the possible cooling of the stratosphere (e.g. WMO, 2003). In a colder stratosphere the PSCs may become more abundant, and significant ozone destruction may take place also over the high Arctic latitudes. This process may also have significant effect on the recovery of the ozone layer which is eventually expected to take place due to the regulations of Montreal Protocol (UNEP, 2000). These aspects will be addressed in the next Section. It should also be remembered that while the mechanisms behind the ozone depletion are relatively well understood, the understanding of the PSCs is still not complete (WMO, 2003).

With respect to the explanations and discussion above, the basic principles, and requirements of the ozone depletion can be identified as follows: 1) The abundance of atmospheric inorganic chlorine is high enough, 2) There exist low enough temperatures for the formation of PSCs which make the activation of chlorine possible, 3) The low temperatures are low enough for type-II PSC formation or persist long enough for large NAT-type PSCs to form, 4) These PSCs last long enough to cause deep denitrification that removes the possibility for chlorine inactivation, and finally 5) Solar radiation to drive the catalytic cycles of ozone depletion.

In Chapter 4, I will show results of a 40-year global chemistry-transport model for the near past and near future behaviour of polar ozone with respect to these requirements from a climate-scale perspective.

2.4 Climate Coupling

The role of atmospheric chemistry is of key importance with respect to possible climate perturbations, as chemistry controls the behaviour of various important climate forcing species (e.g. Brasseur et al., 1999; Brasseur et al., 2000; NASA, 2000; WMO, 2003). These species include stratospheric water vapour and stratospheric ozone. Since the focus of this study is in the near past, and near future behaviour of high-latitude stratospheric ozone, the climate-chemistry interactions need to be identified. Changes in stratospheric ozone and the phenomenon of climate change are closely connected, and coupled. Changes in the stratospheric ozone concentrations are among those factors that control the global mean radiative forcing (IPCC, 2001), together with the effects caused by increased GHG loadings, and with e.g. the effects of atmospheric aerosols. While processes related to stratospheric aerosols are also of importance with respect to this study, this study is not focusing on the behaviour of past and future aerosols, but rather tries to include the effect caused by typical stratospheric background aerosol content. Detailed discussions on the aerosol-climate aspects can be found from Miles et al. (2004), and from IPCC (2001). The effect of future volcanic eruptions on the stratospheric ozone depletion has been discussed by Tabazadeh et al. (2002).

Climate change may have an effect on the atmospheric ozone since ozone itself is a greenhouse gas. The stratospheric stratification derives from the warming caused by the ozone absorption of both solar ultraviolet radiation and the upwelling infrared radiation (e.g. NASA, 2000). In the case of enhanced greenhouse effect more of that infrared radiation, radiated from the Earth's surface is being trapped in the troposphere due to the increased absorption of carbon dioxide and other greenhouse gases, and therefore less radiative upwelling takes place up to the levels of ozone layer. Together with increased emissivity due to the increased stratospheric CO_2 loading, this means that less infrared radiation is being absorbed by the ozone in the stratosphere, and consequently the stratospheric temperatures will decrease. On the other hand, the possible wintertime and springtime ozone depletion would also reduce absorption of the incoming solar radiation (as well as the upwelling infrared radiation) which would cause cooling. Therefore, as a result of these two mechanisms the chemistry of the ozone depletion and the process of climate change due to the increased loadings of greenhouse gases are very much coupled, and furthermore, this coupling seems to form a positive feedback loop (e.g. NASA, 2000). The complexity of these climate-chemistry interactions is further increased since the ozone depletion chemistry itself is very sensitive to low temperatures. As stated earlier in this chapter, low temperatures are needed for the formation of polar stratospheric clouds (PSCs) which in turn make the ozone depletion chemistry possible through the processes of chlorine activation and denitrification. Carbon dioxide, and some other greenhouse gases, is relatively well mixed throughout the whole atmosphere, and they are often

addressed by WMGHG acronym. This means that these well-mixed greenhouse gases accumulate also above the tropopause. In the middle atmosphere these gases are causing cooling as they radiate more energy to space.

It can now be concluded that an enhanced greenhouse-effect, while causing warming in the troposphere, causes cooling in the stratosphere, which in turn may result in an increased ozone depletion. The effects of ozone on the annual-mean stratospheric temperature trends have been discussed by e.g. Ramaswamy and Schwarzkopf (2002), as well as by WMO (2003). Recently, a number of model studies have been made in order to investigate the complex ozone-climate couplings (see the list in the previous chapter). These studies have already shown that ozone depletions and increases in WMGHGs have already had an effect on the stratospheric temperatures (WMO, 2003). Due to the circulation characteristics, the Antarctic polar vortex and the adjacent polar night jet cause the low temperatures to exist on annual basis. As these low temperatures are needed for the formation of the PSCs and subsequent large-scale ozone depletion, it can be stated that if the stratosphere is cooling due to the enhanced greenhouse effect, this cooling would cause perhaps a prolonged existence of low temperatures, and consequent prolonging of the ozone depletion season. The same mechanism would also enlarge the areal coverage of the depleted ozone.

In the northern polar wintertime stratosphere the temperatures usually do not drop below the needed PSC-formation levels, at least not on a yearly basis (WMO, 2003). Therefore, if the northern wintertime stratosphere is getting colder, more chances for the PSC-formation will appear, and larger ozone depletion becomes possible. The complexity of these climate couplings is further increased since the ozone depleting substances themselves are also greenhouse gases (e.g. CFCs). Another key aspect of the future derives from the Montreal Protocol, as the regulations for ozone depleting substances should decrease the atmospheric contents of e.g. total inorganic chlorine. These decreases should in turn make the ozone layer recovery possible. The behaviour of these ozone depleting species in the future is of key importance since the enhanced greenhouse effect has a potential for delaying the recovery of the ozone layer (e.g. WMO, 2003).

The climate change may also have other connections with stratospheric ozone. These interactions include the possible effect of climate change on the strength of the Brewer-Dobson circulation, the changes in solar activity, and the effects of future volcanic activity. All these factors may affect both climate and stratospheric ozone. However, these connections as well as the connections between the possible changes in stratosphere-troposphere interactions have been left out from this study. More detailed discussions on climate coupling and interactions can be found from IPCC reports (e.g. IPCC, 2001) and WMO's ozone assessments (e.g. WMO, 2003) where the causes behind the possible stratospheric temperature trends have been discussed in detail. Furthermore, Roscoe et al. (2004) have discussed the long-term changes in stratospheric circulation, and the possi-

ble changes in the strength of the Brewer-Dobson residual stratospheric circulation based on the Antarctic column ozone measurements. In this study I will address these climate-chemistry interactions mainly from the chlorine loading perspective, and from the climate change perspective using a chemistry transport model (i.e. CTM) designed for stratospheric studies. The next Chapter will give a description about the model employed in this study, and the results gained from the model integration will be shown and discussed in Chapter 4.

3 FinROSE; Model Overview

Chemical transport model or chemistry transport model is typically an off-line model. Off-line means that the needed meteorological input, typically winds, temperatures, and sometimes also surface pressures are taken from a model that solves atmospheric dynamics by itself. Off-line refers especially to the condition where the changes in chemistry are not affecting the modelled atmospheric dynamics or thermodynamics. The opposite for the off-line treatment would be a coupled-chemistry model where the changes in atmospheric composition have an effect on the heating and cooling rates through e.g. absorption and scattering processes. This coupling is sometimes called as radiative back-coupling, meaning that a coupled model has to have a scheme that solves the heating and cooling rates in the atmosphere using some radiation transfer algorithm.

In this work my aim is to use a global three-dimensional chemical transport model for examination of the high-latitude ozone changes during the near past (1980-1999), and during the near future (2000-2019) using a version of the ROSE model developed by Rose and Brasseur (1989). Originally the ROSE model was developed for mechanistic general circulation and atmospheric composition studies. The dynamical part of the model was originally developed by Rose (1983), and the chemistry was included by Rose and Brasseur (1989). The original model was based on the solution of primitive equations in a grid. During the time of this work (since late 1990's) the model has been re-designed for the chemistry-transport-type of studies. Since early 1990's ROSE has been used in a number of middle atmospheric studies by several scientists and research groups and the model has developed from its original form, especially in the field of chemistry. Several scientific studies have used and implemented the ROSE model for their specific needs, and therefore there is no 'Master-ROSE-version'. For this reason and for the simple distinction between different ROSE versions the model used, and further developed at the Finnish Meteorological Institute has been given an acronym, FinROSE. A number of publications about the ROSE exist, and they reveal the evolution of the model in detail. The scope of this study is not to give a historical review on the use of ROSE. The readers are instead encouraged to take a look at least to the following publications: Granier and Brasseur (1991, 1992), Lefèvre (1994), Smith (1995a, 1995b), Tie and Brasseur (1996), Tie et al. (1996, 1997), Brasseur et al. (1997a), Khoshravi et al. (1998), Levelt et al. (1998), Riese et al. (1999), and Massie et al. (2000). The model development has also been done in many institutions, including NCAR (USA), Max Planck Institute for Meteorology (MPI-M; Germany), DLR (Germany), and CNRS (France).

During the course of my work, since late 1990's, a number of experiments on FinROSE's chemistry scheme, and transport scheme have been done in order to improve the model's performance and understand the model's basic and general

features. These experiments include e.g. the usage of different meteorological driver fields, transport algorithms (with respect to vertical velocities, and tracer mass conservation), chemical kinetics, and photodissociation coefficients. These developments have been focused on the model's performance in studies of the evolution and composition of the stratospheric ozone and its precursors. While significant number of working hours has been put into these experiments, the scope of this work has been chosen to show and analyze the results from the climate perspective. Therefore, in this Chapter, I will give the model's description from the perspective of this study. This means that I will shortly explain the current model configuration that has been chosen. The basic references for the FinROSE model are the works by Rose and Brasseur (1989) and Brasseur et al. (1997a). The chemical-transport model FinROSE was improved and developed in several ways from its original version adopted. These improvements include the replacements for the advection scheme (Lin and Rood, 1996), the replacement for the photodissociation calculation scheme (Kylling, 1992, Kylling et al. 1997, Mayer et al., 1998), the updates for the chemical kinetics (e.g. Sander, 2000), the improvements for the heterogeneous processing, and updates for the chemical mechanism of the model. The chemistry scheme, as well as the transport scheme and other model features are discussed only briefly, and the emphasis is on those model features that are relevant and important with respect to the results shown and discussed in Chapter 4.

Since the discovery of the Antarctic ozone hole, a number of model studies on polar stratospheric ozone have been performed. A recent review of these studies can be found from Scientific Assessments of the Ozone Depletion (e.g. WMO, 2003, and references therein). Prior to this study, no peer-reviewed publications of the FinROSE exist. However, there has been a number of other publications on the use and applicability of the FinROSE model. The most recent such studies include: Austin et al. (2003a), Backman et al. (2004), Damski et al. (2003), Hassinen et al. (2004), and Post et al. (2004).

3.1 Gas-Phase Chemistry Scheme

FinROSE's original gas-phase chemistry scheme was based on the family-concept as formulated by Rose and Brasseur (1989). This concept is based on the grouping of the fast reacting species, like atomic oxygen, into chemical families. These families in turn have chemical lifetimes longer than the typical transport timescales. The basic idea of the family-approach is to use quasi-steady state relations to solve the mixing ratios of the individual family members, since they typically establish photochemical equilibrium (PCE) with each other almost immediately in the sunlit stratosphere. The FinROSE's chemistry scheme has been designed mainly for stratospheric and mesospheric studies. Tropospheric-specific chemistry, like or-

Table 3.1 Chemical families in FinROSE

Family Name	**Symbol**	**Members**
Odd oxygen	O_x	$O(^3P), O_3, O(^1D)$
Odd hydrogen	HO_x	H, OH, HO_2
Oxides of nitrogen	NO_x	NO, NO_2
Reactive chlorine	ClO_x	Cl, ClO, Cl_2O_2
Reactive bromine	BrO_x	$Br, BrO, BrCl$
Total inorganic bromine	Br_x	$BrO_x, HOBr, HBr, BrONO_2$
Total inorganic chlorine	Cl_x	$ClO_x, OClO, HCl, ClONO_2, HOCl, Cl_2$ $ClNO_2, BrCl$
Total nitrogen	NO_y	$NO_x, HNO_3, N_2O_5, HO_2NO_2, ClONO_2$ $ClNO_2, BrONO_2, NO_3, N$

ganic chemistry, and processes coupled with clouds and rain, are not included in the model. Also the mesospheric chemistry, like ion-chemistry has been neglected. This means that the applicability of the model, in general, falls within the domain limited by the tropopause and the mesopause (i.e. around 10km and 80km respectively). The model does not have explicit treatment of the source gases like CFCs. Instead, in the current form, model needs described projections of the bulk long-lived tracers like total inorganic chlorine (Cl_x) or total bromine (Br_x). The purpose of this section is, to list the included processes rather than to discuss the effects of different chemical reactions. A detailed description of the middle atmospheric chemistry can be found from common literature (e.g. Brasseur and Solomon, 1984), and from the electronic textbook disseminated by NASA (NASA, 2000)

The definitions for the chemical model families in FinROSE are shown in Table 3.1. The three large families (Cl_x) (total inorganic chlorine), total inorganic bromine (Br_x), and total nitrogen (NO_y) are set up for the maintenance of mass conservation. Water vapour and methane are treated as individual species. The odd hydrogen family is short-lived, and therefore not transported. The FinROSE model consists of 28 transported tracers and 14 species in photochemical equilibrium (PCE). These are shown in Tables 3.2 and 3.3. Note that the list for the transported tracers also includes PSCs type-Ia and type-II. The treatment of these particulate-form species will be discussed in the next Section.

The actual chemistry scheme implemented in this work is presented in Table 3.4. This table is organised by the main families (i.e. chlorine reactions, nitrogen reactions, odd oxygen reactions, bromine reactions, hydrogen reactions, and hydrocarbon reactions). The photodissociation processes included in FinROSE's

Table 3.2 Transported species in FinROSE

Constituent	**Symbol**	**Family**
Nitrous oxide	N_2O	–
Methane	CH_4	–
Water vapour	H_2O	–
Odd nitrogen	NO_y	NO_y
Nitric acid	HNO_3	NO_y
Dinitrogen pentoxide	N_2O_5	NO_y
Total model chlorine	Cl_x	Cl_x
Total model bromine	Br_x	Br_x
Odd oxygen	O_x	O_x
Carbon monoxide	CO	–
Chlorine dioxide	$OClO$	Cl_x
PSC(type-Ia)-tracer	$PSC(I), NAT$	–
PSC(type-II)-tracer	$PSC(II), ice$	–
Hydrochloric acid	HCl	Cl_x
Chlorine nitrate	$ClONO_2$	Cl_x
Hypochlorous acid	$HOCl$	Cl_x
Chlorine molecule	Cl_2	Cl_x
Hydrogen peroxide	H_2O_2	–
Chlorine nitrite	$ClNO_2$	Cl_x
Hydrogen bromide	HBr	Br_x
Bromine nitrate	$BrONO_2$	Br_x
Oxides of nitrogen	NO_x	NO_x, NO_y
Peroxy nitric acid	HO_2NO_2	NO_y
Active chlorine	ClO_x	ClO_x, Cl_x
Active bromine	BrO_x	BrO_x, Br_x
Dichlorine peroxide (ClO-dimer)	Cl_2O_2	Cl_x
Hypobromous acid	$HOBr$	Br_x
Formaldehyde	CH_2O	–

Table 3.3 Short-lived species in FinROSE

Constituent	**Symbol**	**Family**
Exited state oxygen	$O(^1D)$	O_x
Hydroxyl radical	OH	–
Atomic chlorine	Cl	Cl_x
Ground state atomic oxygen	O i.e. $O(^3P)$	O_x
Ozone	O_3	O_x
Hydroperoxy radical	HO_2	–
Nitrogen dioxide	NO_2	NO_x, NO_y
Nitric oxide	NO	NO_x, NO_y
Atomic bromine	Br	BrO_x, Br_x
Atomic nitrogen	N	–
Chlorine monoxide	ClO	ClO_x, Cl_x
Bromine monoxide	BrO	BrO_x, Br_x
Nitrogen trioxide	NO_3	NO_y
Bromine monochloride	$BrCl$	Br_x

chemistry scheme are also listed in Table 3.4. Prior to the model integration presented in this study, the chemical kinetic data, reaction rate constants, and absorption cross-sections are based on the tabulations given by DeMore et al. (1997), Sander et al. (2000), and Bloss et al. (2001).

Table 3.4 Chemistry scheme of the FinROSE model.

Cl_x **Chemistry**		
Reaction	**Products**	**Ref.**
$Cl + O_3$	$ClO + O_2$	J00
$ClO + O$	$Cl + O_2$	J97
$ClO + NO$	$NO_2 + Cl$	J97
$Cl + CH_4$	$HCl + CH_3$	J00
$Cl + H_2$	$HCl + H$	J97
$Cl + HO_2$	$HCl + O_2$	J97
$ClO + OH$	$Cl + HO_2$	J00
$CH_2O + Cl$	$HCl + HCO$	J97
$OH + HCl$	$H_2O + Cl$	J97
$ClO + NO_2 + M$	$ClONO_2 + M$	J00
$O + ClONO_2$	$ClO + NO_3$	J97
$ClO + HO_2$	$HOCl + O_2$	J97
$OH + HOCl$	$H_2O + ClO$	J97
$O + HOCl$	$OH + ClO$	J97

Refs.: J97: DeMore et al. (1997); J00: Sander et al. (2000); B01: Bloss et al. (2001).

Table 3.4 – Chemistry scheme (continued)

Reaction	**Products**	**Ref.**
$Cl + NO_2 + M$	$ClNO_2 + M$	J97
$Cl + HOCl$	$OH + Cl_2$	J97
$ClO + OH$	$HCl + O_2$	J00
$ClO + ClO$	$Cl + OClO$	J97
$ClO + ClO$	$Cl_2 + O_2$	J97
$ClO + ClO + M$	$Cl_2O_2 + M$	J00
$Cl_2O_2 + M$	$ClO + ClO + M$	B01, J00
$OClO + OH$	$HOCl + O_2$	J97
$Cl + OClO$	$ClO + ClO$	J97
$OClO + O$	$ClO + O_2$	J97
$OClO + NO$	$NO_2 + ClO$	J97
$Cl_2 + O(^1D)$	$Cl + ClO$	J97
$Cl_2O_2 + Cl$	$Cl_2 + ClO_2$	J97
$NO_3 + Cl$	$ClO + NO_2$	J97
$ClO + NO_3$	$NO_2 + ClO_2$	J97
$HCl + O(^1D)$	$Cl + OH$	J97
$Cl_2 + OH$	$HOCl + Cl$	J97
$Cl + ClONO_2$	$NO_3 + Cl_2$	J97
$HO_2 + Cl$	$ClO + OH$	J97
$H_2O_2 + Cl$	$HCl + HO_2$	J97
$HCl + O$	$Cl + OH$	J97
$ClONO_2 + OH$	$HOCl + NO_3$	J97
NO_y **Chemistry**		
Reaction	**Products**	**Ref.**
$O + NO_2$	$NO + O_2$	J00
$O_3 + NO$	$NO_2 + O_2$	J00
$N + NO$	$N_2 + O$	J97
$N + O_2$	$NO + O$	J97
$O_3 + NO_2$	$NO_3 + O_2$	J97
$NO_2 + NO_3 + M$	$N_2O_5 + M$	J00
$N_2O_5 + M$	$NO_2 + NO_3 + M$	J00
$OH + NO_2 + M$	$HNO_3 + M$	J00
$HO_2 + NO_2 + M$	$HO_2NO_2 + M$	J97
$HO_2NO_2 + M$	$HO_2 + NO_2 + M$	J97
$HNO_3 + OH$	$H_2O + NO_3$	J00
$OH + HO_2NO_2$	$H_2O + NO_2 + O_2$	J97
$O(^1D) + N_2O$	$N_2 + O_2$	J97
$O(^1D) + N_2O$	$NO + NO$	J97
$O + NO_3$	$O_2 + NO_2$	J97

Refs.: J97: DeMore et al. (1997); J00: Sander et al. (2000); B01: Bloss et al. (2001).

Table 3.4 – Chemistry scheme (continued)

Reaction	**Products**	**Ref.**
$OH + NO_3$	$HO2 + NO_2$	J97
$HO_2 + NO_3$	$OH + NO_2 + O_2$	J97
$HO_2 + NO_3$	$HNO_3 + O$	J97
$O + NO_2 + M$	$NO_3 + M$	J97
$NO + O + M$	$NO_2 + M$	J97
$NO + NO_3$	$NO_2 + NO_2$	J97
O_x **Chemistry**		
Reaction	**Products**	**Ref.**
$O + O + M$	$O_2 + M$	J97
$O + O_2 + M$	$O_3 + M$	J00
$O + O_3$	$O_2 + O_2$	J97
$O(^1D) + N_2$	$O + N_2$	J97
$O(^1D) + O_2$	$O + O_2$	J97
$O(^1D) + O_3$	$2 \cdot O_2$	J97
$O(^1D) + N_2$	N_2O	J97
Odd bromine		
Reaction	**Products**	**Ref.**
$Br + O_3$	$BrO + O_2$	J97
$BrO + O$	$Br + O_2$	J97
$BrO + NO$	$NO_2 + Br$	J97
$BrO + ClO$	$OClO + Br$	J00
$BrO + ClO$	$Br + Cl + O_2$	J00
$BrO + ClO$	$BrCl + O_2$	J00
$BrO + BrO$	$2 \cdot Br + O_2$	J97
$Br + HO2$	$HBr + O_2$	J97
$Br + OClO$	$BrO + ClO$	J97
$Br + CH_2O$	$HBr + HCO$	J97
$OH + HBr$	$H_2O + Br$	J97
$BrO + NO_2 + M$	$BrONO_2 + M$	J00
$BrO + HO_2$	$HOBr + O_2$	J97
$HBr + O(^1D)$	$OH + Br$	J97
$OH + BrO$	$HO_2 + Br$	J97
$OH + BrO$	$HBr + products$	J97
$HBr + O$	$Br + OH$	J97
$HOBr + O$	$BrO + OH$	J97
HO_x **Chemistry**		
Reaction	**Products**	**Ref.**
$H + O_2 + M$	$HO_2 + M$	J97

Refs.: J97: DeMore et al. (1997); J00: Sander et al. (2000); B01: Bloss et al. (2001).

Table 3.4 – Chemistry scheme (continued)

Reaction	**Products**	**Ref.**
$O(^1D) + H_2O$	$OH + OH$	J97
$H + O_3$	$OH + O_2$	J97
$O(^1D) + H_2$	$OH + H$	J97
$O + OH$	$O_2 + H$	J97
$OH + O_3$	$HO_2 + O_2$	J97
$HO_2 + O_3$	$OH + 2O_2$	J97
$O + HO_2$	$OH + O_2$	J97
$OH + HO_2$	$H_2O + O_2$	J97
$OH + H_2$	$H_2O + H$	J97
$H + HO_2$	$OH + OH$	J97
$H + HO_2$	$H_2 + O_2$	J97
$H + HO_2$	$H_2O + O$	J97
$NO + HO_2$	$NO_2 + OH$	J97
$HO_2 + HO_2$	$H_2O_2 + O_2$	J97
$OH + H_2O_2$	$H_2O + HO_2$	J97
$OH + CO$	$CO_2 + H$	J97
$H_2O_2 + O$	$OH + HO_2$	J97
$OH + OH$	$O + H_2O$	J97
$OH + OH + M$	$H_2O_2 + M$	J97
Hydrocarbon Chemistry		
Reaction	**Products**	**Ref.**
$CH_4 + O(^1D)$	$CH_3 + OH$	J97
$CH_4 + OH$	$CH_3 + H_2O$	J97
$CH_2O + OH$	$CHO + H_2O$	J97
$CH_2O + O$	$CHO + OH$	J97
Photodissociation Processes		
Reaction	**Products**	**Ref.**
$O_2 + h\nu$	$O + O$	J97
$O_3 + h\nu$	$O + O_2$	J97
$H_2O + h\nu$	$H + OH$	J97
$N_2O + h\nu$	$N_2 + O(^1D)$	J97
$CH_4 + h\nu$	$H + CH_3$	J97
$NO_2 + h\nu$	$NO + O$	J97
$HNO_3 + h\nu$	$OH + NO_2$	J97
$HOCl + h\nu$	$OH + Cl$	J97
$HO_2NO_2 + h\nu$	$OH + NO_3$	J97
$HO_2NO_2 + h\nu$	$HO_2 + NO_2$	J97
$ClONO_2 + h\nu$	$Cl + NO_3$	J97

Refs.: J97: DeMore et al. (1997); J00: Sander et al. (2000); B01: Bloss et al. (2001).

Table 3.4 – Chemistry scheme (continued)

Reaction	**Products**	**Ref.**
$ClONO_2 + h\nu$	$ClO + NO_2$	J97
$N_2O_5 + h\nu$	$NO_2 + NO_3$	J97
$O_3 + h\nu$	$O(^1D) + O_2$	J97
$H_2O_2 + h\nu$	$OH + OH$	J97
$OClO + h\nu$	$O + OClO$	J97
$Cl_2O_2 + h\nu$	$Cl + ClO_2$	J97
$HCl + h\nu$	$H + Cl$	J97
$Cl_2 + h\nu$	$Cl + Cl$	J97
$CO_2 + h\nu$	$O + CO$	J97
$ClNO_2 + h\nu$	$Cl + NO_2$	J97
$BrONO_2 + h\nu$	$BrO + NO_2$	J97
$BrCl + h\nu$	$Br + Cl$	J97
$HOBr + h\nu$	$Br + OH$	J97
$BrO + h\nu$	$Br + O$	J97
$CH_2O + h\nu$	$H + CHO$	J97
$CH_2O + h\nu$	$H_2 + CO$	J97
$NO + h\nu$	$N + O$	J97
$NO_3 + h\nu$	$NO_2 + O$	J97
$NO_3 + h\nu$	$NO + O_2$	J97

Refs.: J97: DeMore et al. (1997); J00: Sander et al. (2000); B01: Bloss et al. (2001).

For this study, the photodissociation frequencies have been calculated using PHODIS–radiative transfer model (Kylling et al., 1997, Mayer et al., 1998). The PHODIS model version used in this study includes multiple scattering (up to eight orders), absorption by O_2 and O_3, and the effect of surface albedo. The wavelength range of the model is from about 116 nm to 735nm (ie. in the UV-visible-range). Since the explicit run-time solving of photodissociation coefficients in the FinROSE 3-D grid with typical time-step would be too expensive due to the CPU-intensive radiation transfer calculations, the photodissociation frequencies have been precalculated into lookup-tables. The tabulation of these tables is based on the altitude, solar zenith angle, ozone amounts, and surface albedo. The surface albedo, however, has been kept constant (i.e. 30%). The implemented solar zenith angle range is extended down to 92.9 °. Within FinROSE chemistry scheme, pre-calculated photolysis frequencies depending on e.g. local insolation and ozone column are interpolated for given timestep.

The purpose of this study is to use a coupled chemistry climate model as a driver for a multidecadal CTM simulation. Since the amounts of e.g. total model chlorine (Cl_x), total model bromine (Br_x), methane, and N_2O, are provided by

the driver model, the relatively weak production of these gases (e.g. Cl_x production from CFCs) has been neglected in this work, and the driver model concentrations are used as lateral boundary conditions instead. However, the formation and decomposition of odd-oxygen with relevant catalytic effects of HO_x, NO_x , Cl_x , and Br_x are explicitly solved, as shown by the previous tables.

3.2 Heterogeneous Chemistry Scheme

The PSCs play a very important role in the process of polar ozone depletion due to the heterogeneous chlorine activations taking place on or in the PSC surfaces, and due to the PSC sedimentation which may cause mechanical denitrification and dehydration at the level of PSC occurrence. Since the impact of PSCs on the stratospheric physics and chemistry is highly dependent on the temperature, and the typical formation temperatures for the PSC formation act as threshold barriers, the treatment of the PSCs in a model becomes a very demanding task. This means not only that the PSC schemes have to be well established, but also that the applied temperatures need to be accurate.

In the original ROSE model, the determination of the heterogeneous rate coefficients was based on the procedure of Chipperfield et al. (1993). In this study the original scheme has been significantly changed. The PSC treatment in FinROSE takes now into account the type-Ia particles, consisting of Nitric Acid Trihydrate (NAT), small spherical type-Ib particles consisting of ternary liquid solution (STS) of sulfuric and nitric acid, and water vapour, as well as type-II PSC particles composed of ice. Processes including sulfate aerosols are also taken into account. A simplified parameterisation for large NAT particles (sometimes called NAT rocks) is also included. The compositions of PSCs have been discussed in detail by e.g. Voigt et al. (2000), Toon et al. (1990), and Drdla et al. (1994).

The heterogeneous chemistry scheme in FinROSE is based on the calculation of i) the surface area densities and the composition of sulfate aerosols and PSCs, ii) the reaction rate coefficients for the heterogeneous reactions, in or on sulfate aerosols and polar stratospheric cloud (PSC) particles, iii) the partition between gas phase and condensed phase, and iv) the sedimentation of the PSC particles. The included hydrolysis processes, and reactions with mineral acids (i.e. HCl and HBr) are listed in Table 3.5.

The reaction rate coefficients for the heterogeneous processes are calculated for all types of particles (i.e. for sulfate aerosols, STS droplets, NAT particles, and for water ice) according to the recommendations given by DeMore et al. (1997), Sander et al. (2000) and Atkinson et al. (2000). The reaction rates for the heterogeneous reactions use the maximum kinetic mass flux approach and respective uptake coefficients. The uptake coefficients in turn take into account

Table 3.5 Heterogeneous reactions included in FinROSE's PSC scheme.

Reaction	**Products**
$ClONO_2(g) + H_2O(s)$	$HOCl(g) + HNO_3(s)$
$BrONO_2(g) + H_2O(s)$	$HOBr(g) + HNO_3(s)$
$N_2O_5(g) + H_2O(s)$	$2 \cdot HNO_3(s)$
$ClONO_2(g) + HCl(s)$	$Cl_2(g) + HNO_3(s)$
$HOCl(g) + HCl(s)$	$Cl_2(g) + H_2O(s)$
$BrONO_2(g) + HCl(s)$	$BrCl(g) + HNO_3(s)$
$HOBr(g) + HCl(s)$	$BrCl(g) + H_2O(s)$
$N_2O_5(g) + HCl(s)$	$ClNO_2(g) + HNO_3(s)$
$ClONO_2(g) + HBr(s)$	$BrCl(g) + HNO_3(s)$
$HOCl(g) + HBr(s)$	$BrCl(g) + H_2O(s)$

(s) – compound in solid-phase; (g) – compound in gas-phase

all processes controlling the mass transport (e.g. gas and liquid phase diffusion, mass accommodation, and chemical reactions).

In the PSC scheme, each PSC type is assigned with a number density while the sulfuric acid is taken from the model aerosol distributions. In order to take the effect of hysteresis due to the supersaturation requirements into account, the existence of NAT and ice is also transported, as time tracers. This means that at any grid location where NAT or ice has formed (or previously existed), the ice tracer or NAT tracer is assigned or added a value of one timestep. The age of the NAT tracer is also used for the formation of large and faster sedimenting NAT particles. The formation of NAT and ice is controlled by the supersaturation of HNO_3 and H_2O. The required supersaturation thresholds are 20.0 and 1.5, respectively.

The calculations associated with NAT ($3 \cdot H_2O \cdot HNO_3$) formation, persistence, growth, and sedimentation are taken into account, together with the required partition between the gas-phase HNO_3 and NAT. For the formation temperatures and vapour pressures of NAT particles, thermodynamic equilibrium approach is used (see Hanson and Mauersberger, 1988, and Marti and Mauersberger, 1993). However, a supersaturation requirement of 20 has been set for the NAT formation. The evaporation of the formed NAT particles is assumed to take place at the thermodynamic equilibrium (i.e. around 195K). The number density of the formed NAT particles is initially assumed to be $1\#/cm^3$ (e.g. Krämer et al, 2003). A scheme for the incorporation of large NAT particles is based on the use of transported PSC tracers, and the growing of the aged NAT particles is taken into account, using a simple parameterization based on the work by Fahey et al. (2001). The time requirement before the NAT particles are allowed to grow is set to 84 hours (i.e. the NAT should have existed continuously for three

and a half days). After that the number density of NAT particles is reduced to $0.002\#/cm^3$, and NAT particle radius is increased, and the volume of the NAT particles increased, accordingly. The NAT aging threshold and the decreased NAT number densities are based on the work of Fahey et al. (2001). The NAT radii are calculated using the assumption of spherical particles (e.g. Seinfeld and Pandis, 1997):

$$r_{NAT} = \sqrt[3]{\frac{3. \cdot (V/c_{NAT})}{4 \cdot \pi}} \tag{3.1}$$

where the V is the volume of NAT, and c_{NAT} is the number density of NAT particles.

The treatment of liquid binary aerosols (i.e. sulfate aerosols and STS droplets; $H_2SO_4 \cdot H_2O$; hereafter LBA) is based on a non-iterative method explained by Carslaw et al. (1995). The PSC scheme calculates both the composition and volume of these liquid aerosols, and assumes that there is no activation barrier for the formation of STS from aerosols. The LBAs are assumed within temperature range from 215K to 240K, and STSs are allowed below 215K, but not below the water ice formation point. The solubility of a gas phase component in an aerosol is calculated from its effective Henry's law constant. The number density of the sulfate aerosols is initially assumed to be $3.7\#/cm^3$ (e.g. Rosenfield et al., 1997), and the particle radii are calculated as in the case of NAT (see expression above). The required sulfate aerosol (H_2SO_4) loading is typically provided by the transport scheme.

The water ice surface area densities, temperature threshold for the ice formation, ice particle radii, as well as the partitions between H_2O and HNO_3 are calculated using the expressions of Marti and Mauersberger (1993), and Hanson and Mauersberger (1988) for the equilibrium pressures of H_2O and HNO_3 over ice. The formation of ice is controlled by the supersaturation of H_2O, for which a threshold value of 1.5 has been set. This means that the formation of ice particles takes place when the temperatures drop low enough to meet the supersaturation requirement at a given location, but the evaporation is assumed to take place at thermodynamic equilibrium. The formed ice number density is assumed to be $0.04\#/cm^3$ (e.g. Hu et al, 2002), and the ice particle radii are calculated similarly as in case of NAT.

The treatment of different types of particles divides into four branches: i) if temperature is below water ice formation threshold, only PSC type-II are assumed to exist, ii) LBA's are solved if temperatures are between the ice formation point (as stated by the supersaturation requirement for ice formation), and 240K, iii) if temperatures are below the NAT formation threshold, or if NAT particles were transported to the considered location and temperature is below the NAT evaporation temperature, then NAT particles are assumed to exist, and iv) otherwise the LBA scheme is used. This means that the coexistence of STS and NAT is

allowed, and the composition of STS is recalculated if NAT is found to exist, while the coexistence of NAT/STS and ice is forbidden.

The sedimentation of the condensed species on ice, NAT, or STS droplets is solved for H_2O , HNO_3 , and total nitrogen, NO_y , and the budgets of these species are adjusted accordingly to ensure exact mass conservation. Instantaneous mixing is assumed, and the sedimented fractions are added directly to the mixing ratios of HNO_3 , NO_y , and H_2O , at the corresponding level. The dissolved and/or adsorbed species (e.g. HCl or HBr) are not accounted for. The terminal velocities are based on the use of average particle radii for each PSC type as discussed above.

3.3 Transport Scheme

The basic idea of Chemistry-Transport-Models (CTMs) is the use of external analyses of winds and temperature fields. The transport is therefore driven with these fields, and temperatures are used for the chemistry. This off-line approach has proven to be very useful for the simulation of different atmospheric processes.

The transport of long-lived tracers in the FinROSE model was originally based on the semi-Lagrangian transport scheme (SLT) published by Smolarkiewitz and Rasch (1991). The idea of a SLT algorithm is to estimate the departure point of the air parcel that arrives at a particular grid location using the 3-D wind of this arriving location (see Smith, 1995a), and assign the value at the departure point to that gridpoint. In the FinROSE, the transport is done separately from the chemistry, and each transported tracer is solved individually. These transported tracers were listed in Table 3.2.

In this study the SLT method has been replaced by the so-called flux-form semi-Lagrangian scheme (FSLT), developed by Lin and Rood (1996). This scheme solves the three dimensional transport of volume mixing ratio fields, and has improved mass conserving characteristics over the original SLT scheme. The horizontal transport is solved using an un-constrained piece-wise parabolic method (PPM) together with a Zalesak-type multidimensional flux correction algorithm (Zalesak, 1979). This flux correction basically ensures the positivity of the subgrid tracer distributions. The PPM method itself is known to be nearly diffusion free. The vertical transport is based on the use of the Huynh/Van Leer/Lin full monotonicity constraint (for details see Lin et al., 1994, and Lin & Rood, 1996). The vertical velocities are solved internally as a residual by integrating the continuity equation from the top boundary to the lower boundary. The boundaries are set at half vertical gridlength away from the highest and lowest model levels.

The basic idea of the transport in FinROSE is to calculate the horizontal mass fluxes using the external horizontal winds and surface pressures, and solve the vertical fluxes internally. The basic requirement of the transport scheme is

the mass conservation. This means that the transport algorithm does not create or destroy any mass. The calculations of the mass-flux convergences do not necessarily yield to the same mass distributions as in the driver fields. Since the off-line meteorological fields (e.g. the surface pressures) are given at each time-step, and by definition known to the transport scheme, the reproduced mass-field and the given driver field may not be exactly consistent with each other. These possible inconsistencies are due to the fact that the horizontal wind fields, as well as the surface pressures typically need to be interpolated both in time and in space to match the needs of the CTM. This problem has been discussed e.g. by Prather et al. (1987), McLinden et al. (2000), and Jöckel et al. (2001). In the model, the inconsistency problem is solved using the pressure-fixer approach. The idea of this approach is to make adjustments to the horizontal mass-fluxes to ensure the consistency with the external surface pressure fields. While this adjustment has typically a minor effect on the model timestep timescale, it becomes important in longer simulations. This method has been widely used by e.g. in the MOZART model (see Brasseur et al, 1998 or Horowitz et al. 2003). The potential inconsistencies between the bulk chemical family mixing ratios and family members (e.g. Cl_x and members) are taken into account with a simple scaling scheme. After every timestep the mixing ratios of the family members are scaled to match the mixing ratio of the whole family.

3.4 Numerical Aspects

The model code (prior to this study; FORTRAN-77) has been made flexible to allow easy changes of the grid resolution. Therefore, the FinROSE model is capable of using driver input (e.g. winds and temperatures) from various sources. These sources include the data from general circulation models (as in this work) and meteorological analyses, such as those from the European Centre for Medium-Range Weather Forecasts (ECMWF). Due to this adaptability requirement the actual grid for individual simulations is typically fitted to match the configurations in the driver models. Originally, the model used horizontal resolution of $5.00° \cdot 11.25°$ (latitude-longitude), and the vertical resolution was around three kilometers. The number of vertical levels is typically 24 from surface up to middle or upper mesosphere (i.e. around 60-85km). In the meridional direction the model domain starts from latitude $90°S$, and extends to $90°N$.

The transport and chemistry of constituents having a life time longer than or similar to the typical atmospheric transport time scales is obtained by solving the continuity equation. During each timestep, the tracer transport is solved first based on the FSLT scheme described in the previous section. Using the intermediate mixing ratios solved by the FSLT scheme the forecast equation for the constituent n_i due to the chemistry can be written as

$$\frac{n_i(t+\Delta t) - n_i(t)}{\Delta t} = \frac{n_i^T - n_i(t)}{\Delta t} + \sum_i P_i - \sum_i L_i[n_i(t+\Delta t)] \tag{3.2}$$

where n_i^T denotes the intermediate result obtained by the FSLT transport scheme.

The set of stiff differential equations forming the chemistry scheme itself (see previous section about the FinROSE's chemistry scheme) are solved by a semi-implicit scheme. A simple backward-Euler method is used for the integration of gas-phase concentrations of species in time:

$$n_i(t+\Delta t) = \frac{n_i^T + \Delta t \sum_i P_i}{1 + \Delta t \sum_i L_i} \tag{3.3}$$

The loss frequencies $L_i[\, s^{-1}]$, and production rates $P_i[\, molecules/s]$ are solved in the chemistry scheme for each long-lived tracer using the temperatures from the driver model, and the mixing ratios for short-lived species are solved at every timestep through the photochemical equilibrium condition (PCE) between the family members:

$$n_i(t) = \frac{P_i}{L_i}. \tag{3.4}$$

In order to assure the photochemical equilibrium (i.e. PCE-condition) and stable partitioning, the chemistry procedure is iterated four times. Typically the transport and chemistry timestep is 5-30min.

The quality of the results with respect to transport or temperature dependent processes, as for example chemistry or denitrification in the polar winter stratosphere, depends very much on the quality of the meteorological analyses used. For example, if the analyses have shortcomings in the general circulation patterns the realized global distributions in model-simulated fields contain these signals. Therefore, one possible application of the CTMs is their measure of the quality of the driver analyses themselves, as the model results can be directly compared with the measured distribution of species like stratospheric ozone.

4 Results

In order to respond to the challenges of this study as set in Chapter 1, I will now present the results of a global 40-year middle atmospheric simulation from 1980 until the end of 2019. The simulation has been performed with the global chemistry-transport model, FinROSE, described in Chapter 3. For this study the FinROSE model has been driven with the winds and temperatures from a transient simulation of a chemistry-coupled climate model UKMO/UMETRAC, using specified concentrations of long-lived tracers such as well-mixed greenhouse gases. The basic features of the UMETRAC model integration as well as general simulation arrangements will be discussed in the next sections.

The focus of this study is in climatological scale features like regionally averaged seasonal ozone variations or year-to-year ozone variations in the high-latitude stratosphere. It is also worth noticing that the driver model, being a chemistry-coupled general circulation model, is intended to simulate typical climatological features, not any specific year. In order to validate and compare the results of this study, I will show how the average regional concentrations of stratospheric ozone, and ozone destruction have evolved during the past period (1980-1999), and how ozone is expected to evolve in the near future (2000-2019). The results will be shown as regionally averaged monthly or seasonal means, and zonal averages, compared with the respective quantities derived from measurements, or with the respective driver model results. The measurements used in this study are mainly from the Total Ozone Mapping Spectrometer (TOMS). The datasets used in this study are based on the version 8 algorithm (v8) (see Wellemeyer et al., 2004). The TOMS-instrument itself has been put on several satellite platforms. In this study I use the datasets provided by the NIMBUS-7 TOMS (measurements available for this study cover the period from 1980 up to early 1993) and by the EarthProbe TOMS (or EP-TOMS) which covers the period from late 1996 until early 2003. In the case of TOMS measurements, it is important to remember that while the measurements themselves are known to be of excellent quality (see e.g. WMO, 2003), the TOMS, being a spectrometer measuring the ratio between the Earth-atmosphere system's backscattered radiance, and the extraterrestrial solar irradiance, is not able to measure in dark. Since during the polar night the polar areas are not exposed to the solar radiation, the TOMS is not able to measure those areas during the winter. This basically means that for the global average the largest latitude range is between 60°N to 60°S which in turn covers around 87% of the whole globe.

The analysis of the modelled mean quantities in this chapter, derived from the FinROSE 40-year integration, has been divided into four main parts. First the model results will be compared against total ozone measurements and against the driver model results and the future period behaviour will be described. Secondly,

the stratospheric processes affecting the high latitude stratospheric ozone will be analyzed. Thirdly, trend analysis of the past and future periods will be shown and compared against the TOMS total ozone measurements and corresponding results from the UMETRAC integration. Finally, the effects of different ozone-controlling processes will be analyzed from the climate change perspective, and from the perspective of the possible recovery of the ozone layer.

4.1 Driver Model (UMETRAC) Integration

For this study the required meteorology, as explained in Chapter 3, comes from the UMETRAC (Unified Model with Eulerian Transport And Chemistry) model. UMETRAC is a chemistry-coupled general circulation model (a.k.a. chemistry-coupled climate model) based on the UK Met. Office's Unified Model (Cullen, 1993). The model has 64 levels from surface up to 0.01 hPa, and latitude-longitude resolution of 2.5° by 3.75°. In this study I use an UMETRAC model integration completed for the period from January 1975 to January 2020 (Austin and Butchart, 2003). This simulation is a so-called transient climate simulation using spectral gravity wave forcing scheme by Scaife et al. (2000) which by large eliminates the cold-bias problem typically exhibited by climate models (for details, see Austin and Butchart, 2003). The used integration is based on the usage of observation based sea surface temperatures and sea ice for the past period (1980-2000). For the future period (2000-2020) UMETRAC uses the results of coupled ocean-atmosphere version of the Hadley Centres climate model (Williams et al., 2001).

The concentrations of the long-lived tracers follow the projections defined by IPCC and WMO. In case of halogens the data from WMO (1999) have been adopted, and in case of well-mixed greenhouse gases the IPCC-projection IS92a has been adopted (IPCC, 1992; Leggett et al., 1992). The adopted "business-as-usual" type scenario (i.e. IS92a) has been widely used in climate studies. For the more recent IPCC assessment (i.e. IPCC, 2001) these IS92-type scenarios were replaced by the so–called SRES scenarios which in turn are comparable with the IS92 type scenarios with respect to this study, as the ranges of CO_2 emissions for both sets of scenarios are similar (see IPCC, 2001). The levels and the expected future evolutions of those long-lived species, relevant to this study are shown in Figure 4.1. As the figure shows, during the course of the simulation from 1980 to 2020, the level of carbon dioxide rises from $337 ppm_v$ up to $417 ppm_v$. The corresponding numbers for methane are from $1.6 ppm_v$ up to $2.14 ppm_v$, for N_2O from $302 ppb_v$ to $339 ppb_v$, and for total reactive nitrogen (NO_y) from $18.4 ppb_v$ up to $20.7 ppb_v$. In case of total atmospheric inorganic chlorine loading, the effect of regulations (i.e. Montreal protocol and its amendments) is seen as the mixing ratio grows during the first two decades (1980's and 1990's) from 1.64 ppb_v up to

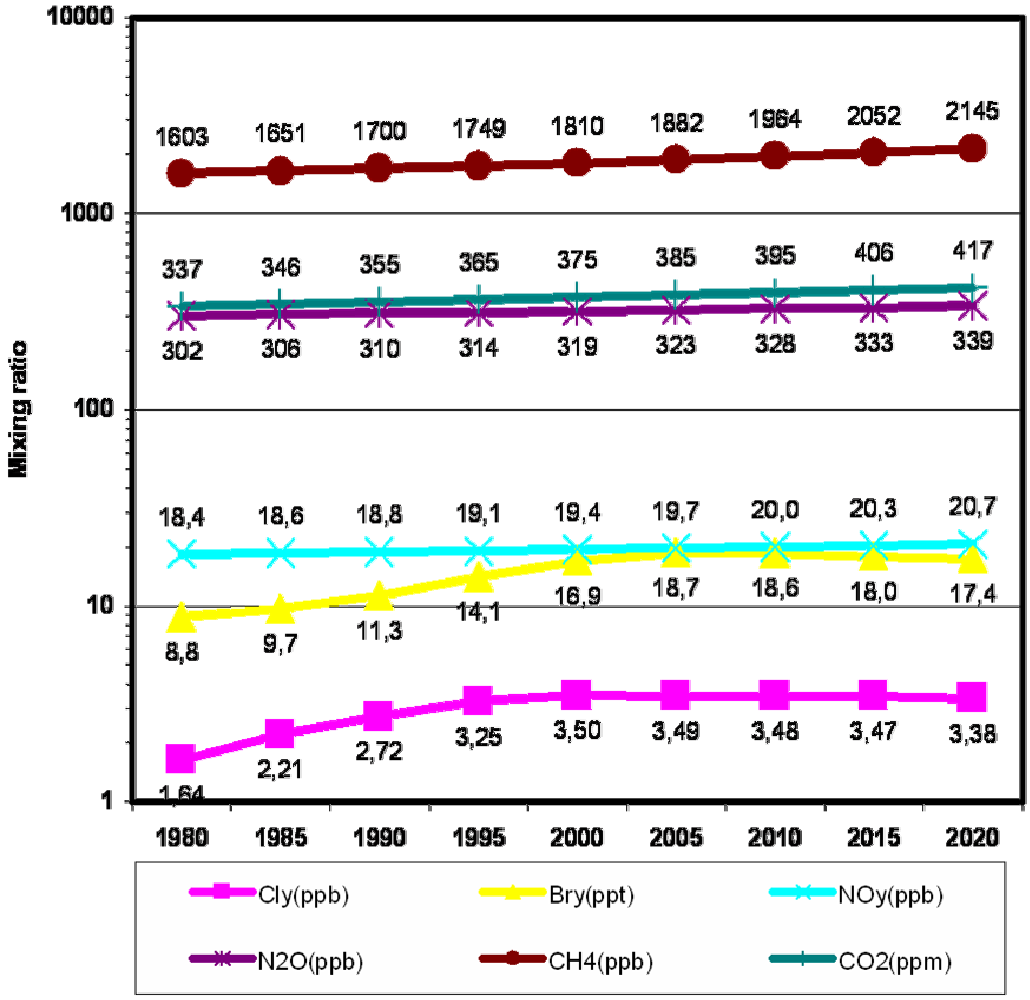

FIGURE 4.1. The implemented projections of long-lived tracers in the 40-year simulations. The projected evolutions are based on the IPCC-IS92a scenario by IPCC (1992) and tabulations by WMO (1999). See Austin and Butchart (2003) for more details.

3.5ppb_v , and the levels off gradually to 3.38ppb_v by the beginning of 2020. The total bromine loading follows the same pattern as total inorganic chlorine; The value for the beginning (1980) is 8.8ppt_v , peak value is seen around the year 2005 (i.e. somewhat later than in the case of inorganic chlorine), being 18.7ppt_v and the loading levels off to the value of 17.4ppt_v by 2020.

The chemistry scheme in the UMETRAC model has been coupled to the atmospheric dynamics solver of the UMETRAC through radiation transfer scheme. This ensures that the changes in the atmospheric composition due to the chemistry, or increased emissions of radiatively active gases have an effect on the diabatic heating and cooling characteristics of the atmosphere. This coupling makes it possible, for example, to see the effect of depleted ozone on the atmospheric temperatures, as ozone absorption causes significant heating in the stratosphere.

The UMETRAC chemistry scheme includes all the main stratospheric processes, and is therefore capable of simulating the typical stratospheric feedbacks between dynamics and chemistry. The scheme includes 12 transported long-lived species (O_3, HNO_3, N_2O_5, HO_2NO_2, HCl, $HOCl$, $ClONO_2$, $HOBr$, HBr, $BrONO_2$, H_2O_2, and H_2CO), and a specially formed tracer for the transport of H_2O, CH_4, Cl_y, Br_y, H_2SO_4, and NO_y. For more details see Austin and Butchart (2003) and references therein. The model also includes parameterizations for PSC-processing and PSC sedimentation. The chemical kinetics in the UMETRAC simulation are based on the tabulations given by DeMore et al. (1997) and Sander et al. (2000).

The main difference between the FinROSE's chemistry scheme and the UMETRAC's scheme is in the general representativeness of the stratospheric chemistry. In the FinROSE's chemistry solver all the main stratospheric chemistry has been included, and therefore the number of reactions is around 150 (see Table 3.4). The number of tracers is also greater, as the FinROSE has 28 individually transported tracers (see Table 3.2) and 14 short-lived species (see Table 3.3). The heterogeneous processing in the FinROSE is also different from the simplified scheme of UMETRAC. The PSC-aerosol scheme includes parameterizations for all the main surfaces, including liquid binary aerosols, PSCs type-Ib consisting of ternary solution, PSCs type-Ia consisting of nitric acid trihydrate (i.e. NAT), and ice-form PSCs (type-II). The heterogeneous processes involving chlorine, nitrogen, and bromine compounds were listed in Table 3.5. The formation mechanisms in the PSC-aerosol scheme are based on thermodynamics rather than specified temperature barriers. The transport-time growth of the NAT-particles including the effect of hysteresis due to the temperature changes has also been implemented to the FinROSE-model. This in turn allows the NAT-particles to grow to sizes where more rapid sedimentation is possible, and denitrification, in absence of ice-form PSCs, becomes more probable. Basically, this more detailed chemistry of the FinROSE model, should allow the model to simulate more realistically the diurnal patterns, seasonal variations, and in general, the amplitudes of temporal variation and absolute levels of various atmospheric constituents. It is, however, not expected that the more detailed chemistry of FinROSE over the driver model has an effect on the general multi-year behaviour of those dominating constituents like total reactive nitrogen, methane, water vapour, inorganic chlorine, or bromine, as they are to some degree driving the FinROSE's simulation (explanation given in the next Section), and since the UMETRAC has profound-enough chemistry from this perspective. Therefore, it is expected that while both FinROSE and UMETRAC should give similar results from general decadal perspective, the differences in chemistry scheme should lead to differences in average levels and variability of various atmospheric constituents as FinROSE reproduces the compositional inter-relations by different means. With respect to the tracer transport, similar behaviour of both models is expected, since winds from UMETRAC are used in FinROSE. The differences between the outcomes of the FinROSE and UMETRAC

integrations will be discussed later in this Chapter. For more information about the UMETRAC simulation the readers are guided to see the work by Austin and Butchart (2003), and references therein.

4.2 FinROSE Simulation Settings

As explained in the previous section, the 40-year integration with the FinROSE off-line chemistry-transport model has been done using the UMETRAC winds and temperatures for the transport and chemistry. A detailed discussion of the driver simulation can be found from the work of Austin and Butchart (2003). The purpose of this Section is to explain briefly the implementation of this particular FinROSE simulation and how it compares with the standard configuration described in Chapter 3.

The 40-year FinROSE integration used the standard 5.00° by 11.25° latitude-longitude grid with pole to pole latitudinal coverage. The vertical resolution of the simulation is around 2700 m at 24 pressure levels up to ∼0.15hPa (or ∼62km). The vertical grid is summarized in Table 4.1. The vertical grid of the model has been implemented to match exactly the one used by the UMETRAC driver simulation. For the horizontal grid, the needed values (i.e. horizontal winds and temperatures) are interpolated from the UMETRAC results using bilinear interpolation. While the FinROSE's own transport scheme solves the vertical winds from continuity by itself (see Chapter 3), for the horizontal winds as well as the temperatures an interpolation in time is also needed to get the values for each gridpoint at each timestep. For this purpose three-dimensional daily values from UMETRAC's horizontal winds and temperatures are used. As already explained in previous Section, the UMETRAC chemistry-coupled winds and temperatures are based on the use of observation-based SSTs, sea ice amounts, well-mixed GHG loadings, and halogen concentrations during the past period. For the future period (2000-2019) the winds and temperatures are based on the UMETRAC simulation where the evolvement of well-mixed GHGs and halogen concentrations follows the IPCC-IS92A-scenarios (IPCC, 1992) and WMO specifications (WMO, 1999) shown in Figure 4.1. The actual FinROSE integration starts at the 1st of January 1978 and the model was run continuously until the 15th of January 2020. The first two years are neglected from the analysis to avoid spin-up effects associated with the FinROSE's chemistry-transport scheme. The planning of the model integration documented in this study took place during 2002, and the continuous 40-year integration was executed during early 2003.

The initial distributions of chemical constituents were taken directly from the UMETRAC integration. Since FinROSE does not explicitly include surface parameterizations, the lateral boundary conditions have to be well established for the whole simulation period. The formulation of boundary conditions, both

at the upper and at the lower boundary, is quite straightforward. For the long-lived chemical families like total reactive nitrogen (NO_y), total inorganic chlorine (Cl_x), total inorganic bromine (Br_x), and for species like water vapour, methane, ozone (or odd-oxygen to be more precise), and N_2O , the monthly mean concentrations are readily available for the FinROSE from the driver simulation. The concentrations of these long-lived tracers are interpolated linearly in time to obtain values at the upper boundary and lower boundary. As the model solves itself the photochemical equilibrium for each short-lived species shown in Table 3.3 and inter-relations within the chemical families, or species used in UMETRAC simulation, no additional definitions for the boundary conditions are needed. For this study the data for chemical kinetics and for the absorption cross-sections required for the calculations of the photodissociation coefficients, follow the work by Sander et. al (2000), with amendments published by Bloss et al. (2001).

In this study, FinROSE's chemical scheme does not include parameterizations for the source gases (e.g. CFCs and their chemistry). Therefore it is necessary to take measures for the preservation of the projections used for the long-lived tracers. In this study the following procedure has been adopted for the correct mass-conservation of the NO_y , Cl_x , and Br_x families: i) Atmospheric concentrations of long-lived tracers (shown in Figure 4.1) are constrained at each timestep by relaxation towards monthly mean zonal averages given by the driver model, ii) In the case of a chemical family, the individual members of each family are then constrained with respect to their relative contributions, accordingly. Although this procedure somewhat reduces the models degrees-of-freedom, it insures that, if the transport has problems e.g. in forming the Brewer-Dobson circulation patterns, the typical and expected levels of these dominating compounds stay reasonable and in line with the driver model results. These issues will be discussed in more detail in the coming sections.

The advantages of using the off-line chemistry-transport-approach with more profound chemistry, with externally specified winds and temperatures, are abundantly cost-beneficial. Typically, chemistry-coupling for a climate model is expensive in terms of CPU costs, and therefore massive-scale computing is needed (e.g. supercomputers). This in turn means that there is a need to make compromises with the representativeness of the chemistry, as well as of the frequency and volume of model outputs. The CTMs, however, are not as expensive to run, as they do not solve the radiation transfer, or the dynamics of the atmosphere. As the typical semi-Lagrangian transport scheme is rather affordable to run, more effort can be put to the representativeness of the chemistry solvers and output diagnostics. Therefore the simulations can be designed to produce even rather exotic diagnostics if they are relevant for the objectives of the studies. The total control over the chemistry makes it possible to output, not only values of individual parameters, but also the behaviour of relevant processes can be recorded during the integration. In the case of climate models, as the simulations are ex-

Table 4.1 Vertical grid of the FinROSE model

Level	Z* (m)[1]	Pressure (hPa)	Level	Z* (m)[1]	Pressure (hPa)
1	90.4	1000.0000	13	32326.6	10.0000
2	2776.8	681.2921	14	35013.0	6.8129
3	5463.1	464.1589	15	37699.3	4.6416
4	8149.5	316.2278	16	40385.7	3.1623
5	10835.8	215.4435	17	43072.0	2.1544
6	13522.2	146.7799	18	45758.4	1.4678
7	16208.5	100.0000	19	48444.7	1.0000
8	18894.9	68.1292	20	51131.0	0.6813
9	21581.2	46.4159	21	53817.4	0.4642
10	24267.6	31.6228	22	56503.7	0.3162
11	26953.9	21.5443	23	59190.1	0.2154
12	29640.3	14.6780	24	61876.4	0.1468

[1)] Metric altitudes have been calculated using constant scale height (H) and constant surface pressure (p_0) using Z*= $-Hln(p/p_0)$ with H=7000m and p_0=1013hPa.

pensive, the repetition of a simulation just for obtaining additional diagnostics is often out of the question. Therefore, the CTMs provide a nice platform for the studies of individual atmospheric processes, and hopefully, add value to the chemistry coupled climate model (i.e. CCM-type) integrations. A study of this added value is one objective of this study.

4.3 High-Latitude Stratospheric Temperature Changes

As explained earlier in Chapter 2, the behaviour of stratospheric ozone over high latitudes is very sensitive to temperatures. In order to issue the questions both related to the possible recovery of the ozone layer due to the international regulations for the usage of halogenated compounds, and related to the possible cooling of the stratosphere, due to the enhancing greenhouse effect, and the impacts of this cooling on stratospheric ozone, I will now briefly discuss the temperature variations in the driver model integration. These features of the UMETRAC integration have been studied in detail by Austin and Butchart (2003), and Austin et al. (2003b). The evolutions of global ozone distributions of the UMETRAC model will be compared with the FinROSE results in later sections.

A possible trend in stratospheric temperatures could be caused by changes in concentrations of ozone, carbon dioxide and other well-mixed greenhouse gases, or stratospheric water vapour. In this study the focus is largely in the effect of temperature changes, and in the effect of changing halogen concentrations on ozone in general. Therefore I'm not trying to analyse the causes of the simulated

temperature changes. In a recent study by Shine et al. (2003) estimates of stratospheric temperature trends over the past two decades were analyzed using the results of a variety of models and the causes of the temperature changes were discussed in detail. In that study the following conclusions, among others, were made: i) Models are capable of simulating the average annual or global average temperature trends, although the magnitudes of these trend vary significantly between models, ii) The modeled stratospheric cooling, as seen by the trends in annual means and global means of temperatures, is in good or reasonable agreement with the measurements. The results from the driver integration, used in my study, are consistent with the results of Shine et al. (2003). Actually, the UMETRAC results applied in this study were included in the comparisons compiled by Shine et al. (2003).

In the work by Austin and Butchart (2003) the driver model trends were discussed in detail. A brief summary of those results goes as follows: 1) The cooling trend in the stratosphere, and the warming trend in the troposphere are both well exhibited, 2) The globally, and annually averaged cooling trend near 10hPa, is around 0.5 K/decade during both the past and the future periods, 3) The globally and annually averaged cooling trend near 50hPa is around 0.3 K/decade during the past period and disappears during the future period, 4) The globally and annually averaged cooling trend near 100hPa is around 0.2 K/decade during the past and the future trend disappears, 5) Annually averaged cooling trend over the high southern latitudes during the past period is more than 1.5 K/decade between the 200hPa and 30hPa levels, but levels off to a less than 1 K/decade, statistically non-significant cooling during the future period, 6) Annually averaged temperature trend over high northern latitudes during the past period exhibited slight, non-significant cooling at stratospheric altitudes, and finally 7) The UMETRAC simulation captures the main characteristics of the observed stratospheric temperature trends and also indicates continued cooling of the stratosphere in the near future. Furthermore, as stated by Austin and Butchart (2003), the past-time Antarctic cooling trend clearly suggests that a strong connection between the Antarctic ozone depletion and cooling of the stratosphere exists. The fact that no statistically significant cooling trend for the future period was simulated in turn suggests that the behaviour of winter-, spring-time stratospheric ozone would stay the same if affected by temperatures alone. Thus, changes in the ozone depleting substances during the near future are of primary importance.

As the focus of this study is in the winter- and springtime behaviour of polar stratospheric ozone, it is interesting to see how the actual evolution of high latitude stratospheric temperatures during the 40-year integration behaved with respect to temperatures required for typical PSC production. For this purpose I have created an analysis to Figure 4.2 using the driver model (i.e. UMETRAC) temperatures as they have been feeded into the FinROSE. In this figure the averages are calculated using all temperature values less than 195K at any model level

within the circumpolar areas enclosed by the 65°S and 70°N latitudes together with the monthly averages below 195K at the enclosing latitudes (i.e. at 65°S and 70°N; referred as lowest latitude). The lowest latitude in Figure 4.2 has been chosen as the farthermost latitude belt away from the pole, altogether exhibiting monthly mean temperatures less than 195K. Therefore, this Figure (4.2) shows how the extreme temperatures (favourable for PSC formation) are simulated by the UMETRAC model, and respectively used by the FinROSE model. Since the 195K temperature value is a good indicator for the possible creation of PSCs type-I, this figure gives an idea how chlorine activation and denitrification might affect ozone destruction in the 40-year simulation. The most direct conclusion from Figure 4.2 is the clear difference between the two poles. Over the southern polar areas, PSC-production temperatures occur, in practice, throughout the whole simulation period on annual basis. It is also clear that temperatures drop below the required limit for the ice cloud production (i.e. typically below 189K for PSCs type-II) almost every year. In the north, however, these occasions for possible PSC type-I production become somewhat more frequent after mid 1980's, but from this average perspective they never drop below the ice-forming levels (i.e. below 189K).

From this perspective the annual average cooling trend in the southern polar stratosphere, as discussed above, cannot be readily distinguished from Figure 4.2. However, it seems that the duration of these extreme events have been extended since the mid 1980's. It is also clear that no clear signs of any trend in the absolute minimum occur during the simulated 40-year period. Over the southern polar areas, it also seems that the occasions of the monthly mean incidents of temperatures lower than 195K increases areally during the simulation, as the low values become somewhat more frequent at the 65th southern latitude. In other words, the extreme temperatures are simulated to exist over the Antarctica during the near past and the near future periods by the UMETRAC model, and furthermore, the area of these extreme temperatures possibly increases in size with time. This result is most probably connected to the areal growth of the ozone hole. As the ozone gets depleted, less absorption of solar radiation takes place at the levels of typical ozone layer, and the respective layer becomes colder. As occasions of extreme temperatures at 65°S are very rare, no significant trend estimates can be made from the perspective of this study, and the possible increase in the frequencies of the extremely low temperatures at lower latitudes should be treated here as a signal of the inter-dependence between temperature and ozone.

In the case of northern high latitudes, the increase in the frequency of extreme temperatures is more clear than in the south. The extreme temperatures are simulated to become both more frequent, and the absolute minimum slightly colder since mid-1980's. Figure 4.2 also shows that from this average perspective the required temperatures for ice-cloud formation (PSC type-II) do not occur. This in turn suggests that during the course of the FinROSE (or UMETRAC) in-

tegration large-scale formations of type-II PSCs are not expected. However, this does not rule out the possibility of simulation of ice-clouds on daily basis in the model results. If no significant cooling trend exists in the northern polar stratosphere, this behaviour suggests that there should also be more frequent cases of warm polar vortices that compensate for these cold winters. This in turn would mean that the interannual variability has increased in the UMETRAC simulation (for more discussion, see Austin and Butchart, 2003). Over the northern polar areas the signal of the possible areal growth of the extreme temperature events is very weak as only a few events are revealed by this monthly columnal zonal average perspective. This means that more detailed analysis of these extreme temperature events is needed in the future. Furthermore, since the general circulation characteristics in the north are more complex than in the axisymmetrical south, this type of analysis is usually made using the frame-work of equivalent latitudes which take the asymmetrical nature of the arctic polar vortex into account. However, these studies are left outside the scope of this work, as my intention is to analyze climate-scale features which will be further discussed in the coming sections of this chapter. More information on the use of the equivalent latitudes can be found from Lary et al. (1995).

In WMO (2003), it has been stated that climate models typically exhibit annually averaged cooling in the Arctic stratosphere during the near past and the near future. It is also stated by WMO (2003) that most of the models find, in line with the satellite measurements, this cooling to be largest during March, April, and May. The modeled cooling is typically not as large as that seen in the measurements. However, as WMO (2003) states, the large natural variability over the wintertime high northern latitudes makes the assessment of the modeled temperature trends very difficult. Since the existence of low temperatures is of primary importance for the emergence of polar stratospheric clouds, the climate models capability for reproduction of realistic temperature trend estimates is very important. However, the understanding of the processes involved in the growth mechanisms of the PSCs is also of high importance. A number of different model studies on stratospheric temperature trends exist besides the studies cited above. These studies include the works by Graf et al. (1998), Waugh et al. (1999), Ramaswamy and Schwarzkopf (2002), and Langematz et al. (2003).

Finally an important clarification is needed as some unsteadiness exists in the results of the climate models in general; The so-called cold-pole problem. In the work of Austin and Butchart (2003), and Austin et al. (2003b) this problem has been assigned and discussed. Typically, climate models have a cold bias over high latitudes in the lower stratosphere due to the too weak residual circulation (Pawson et al., 2000) which in turn would lead to stronger polar night jet, and colder and more stable polar vortex. This is somewhat problematic for the simulation of PSCs and for the subsequent simulation of denitrification processes and therefore for the simulation of the ozone depletion in general. However, as explained by

Austin and Butchart (2003), and discussed in Austin et al. (2003b) this problem has been reduced considerably by the implementation of spectral gravity-wave forcing to the UMETRAC model. Keeping in mind the basic understanding of the processes leading to ozone depletion, which states that the key processes are both chlorine activation and denitrification which in turn are dependent on the formation of PSCs type-I and II, respectively, one may conclude that should this cold pole problem lead to a behaviour where the respective formation thresholds are by-passed more frequently than in reality, then this problem would cause too large ozone depletion. However, with respect to the results shown by Figure 4.2, this not the case for the driver model in this study, since the occurrences of extremely low temperatures is very much as expected, and in line with the measured frequencies found in literature. Therefore, it may be concluded that the UMETRAC model is capable for realistic temperature trend reproduction, and that one might expect that the effect of changing temperatures will be exhibited by the modelled ozone behaviour. The possible effect of this expected behaviour of stratospheric temperatures on future stratospheric ozone will be studied and discussed in later sections of this Chapter.

4.4 Transport Characteristics

The basic requirement for the CTM-type simulations is the model's ability to reproduce the observed atmospheric circulation patterns, including the seasonal cycle and interannual variability. In order to analyze the model's performance in reproduction of the observed atmospheric patterns, several aspects have to be evaluated. In this section I will discuss, in general terms, how the 40-year FinROSE simulation reproduces the Brewer-Dobson circulation of the stratosphere. In the next section I will then show, how the modelled ozone compares with measurements.

An estimate of a transport model's ability for reproduction of the stratospheric Brewer-Dobson circulation can be made using the "age of air" framework. In this concept the influence of the Brewer-Dobson circulation can be studied with the aid of an idealized mixing ratio type tracer entity, the value of which increases in time. Basically the age of air (hereafter also AOA) is defined as the average amount of time spent by the air parcels for the transportation from the source areas to any specific latitude and altitude in the stratosphere, or in model terms, from the lower model boundary in to the main model domain. In the case of FinROSE's 40-year simulation these tracers are used in the following way: I) For every model time-step the AOA-tracers are initialized at the lower boundary with model timestep, II) the AOA-tracer is transported within the model domain exactly the same way as all the other model trace constituents, III) during each time-step within the model domain the amount of time (ie. the duration of one

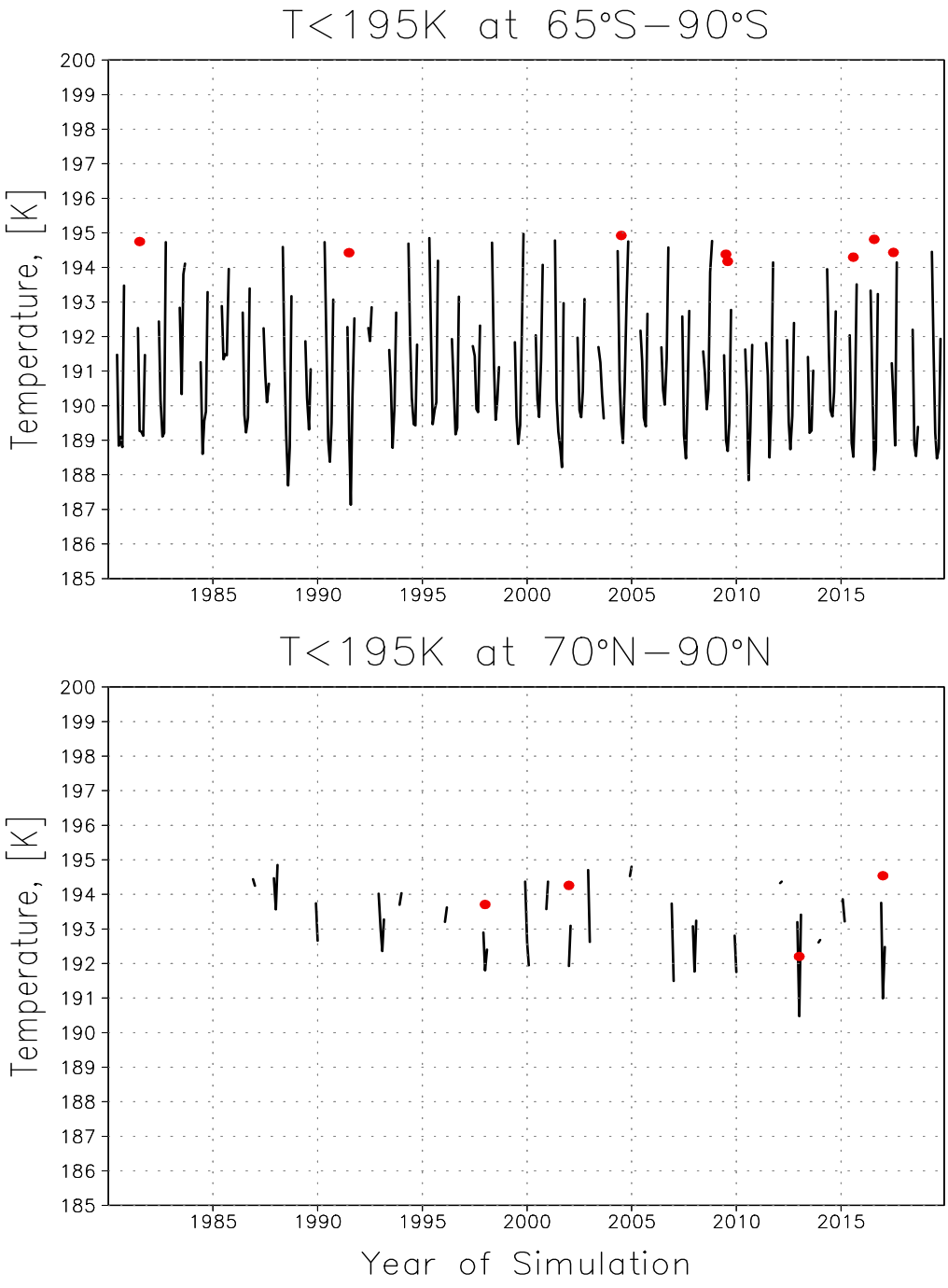

FIGURE 4.2. Periods with low temperatures over the high latitudes. Black lines show the areal monthly average evolution of temperatures less than 195K beween latitude ranges of 65°S and 90°S (top frame), and between 70°N and 90°N (bottom frame). The whole vertical model domain has been accounted for. The red dots show the cases when the monthly mean temperature values have broken the 195K threshold at the indicated lowest latitude (i.e. at 65°S or 70°N). Values are based on the UMETRAC results regridded to the FinROSE horizontal grid.

transport time-step; 30 minutes in this study) is added to the tracer value, and finally IV) every time the tracer falls down to touch the lower boundary it will be reinitialized. This type of a scheme therefore gives at any instant the time since the respective air-parcel has been in contact with the model's lower boundary, thus the age of air (AOA). In this study, the AOA-diagnostics is used to see how the transport drive, provided by the UMETRAC model, works in the case of FinROSE's transport scheme in comparison with the observed Brewer-Dobson circulation, and how the used lower boundary conditions are fed in to the model's interior. As stated by Hall et al. (1999), in most CTM-models the propagation of the annual atmospheric oscillations is too rapid in the vertical, and the CTM-models also underestimate the mean age of air throughout the stratosphere. Basically if the Brewer-Dobson circulation is too strong the age of the air becomes too small in the upper stratosphere. Since the age of air distributions are not directly affected by the effects of photodissociation, the age of air framework can be used for the analysis of the model transport scheme itself as well as for the analyses of the realized Brewer-Dobson circulation. For these reasons the age of air analysis has become a standard way for testing stratospheric transport models in general (see Waugh and Hall (2002) for a review).

Keeping the statements discussed above in mind, the zonally averaged cross-sections of transport timescales, as revealed by the age of air tracer, are shown in Figure 4.3. This figure shows the monthly mean distribution of the AOA-tracer after 20-years of simulation initialization during high latitude winters (ie. January-1998, and July-1998), and the evolutions of the monthly mean AOA-tracers at 10hPa above both poles. As the Figure 4.3 shows (by higher frames), the general patterns are qualitatively well reproduced by the model; The wintertime stratosphere (ie. the northern and southern high latitudes) exhibit higher values than the summertime stratosphere (ie. the air is older over the wintertime circumpolar areas). In the tropics, "new air" enters the stratosphere where the values of the AOA-tracer stay low due to the steady feed of young air from the troposphere. The transport towards the wintertime extratropical areas then ages the air as values over the winter poles are close to three years. As discussed in Chapter 2, in reality the age of air may exceed values more than five years. While the simulated general patterns are as expected from the observations, and theory, the absolute values are significantly lower than those given in Figure 2.2, and follow the conclusions stated by Hall et al. (1999). In Figure 4.3 (lower frames) the evolutions of the AOA-tracer at 10 hPa level over the North Pole and South Pole are shown. The evolution of the age-of-air tracer over the both poles is very similar. The interannual variability shows clearly the peaks during the wintertime periods, as expected, and lowest values during the summer. Over the South Pole the maximum values are around three years, and the minimum summer values just below two years. Over the North Pole, also as expected (see Chapter 2), the maximum values are less than three years, and the minimum typically around two years.

Basically this means that each tracer, found in the high-latitude stratosphere, has aged in the stratosphere for at least two years. It can also be concluded that the evolution of the AOA-tracers stays stable throughout the 40-year simulation period, but the model has faster-than-reality Brewer-Dobson circulation.

Despite the clear shortcomings in the FinROSE's performance in the reproduction of the Brewer-Dobson circulation, it is quite safe to say that the FinROSE's flux-form semi-Lagrangian transport scheme (i.e. FSLT-scheme) does not cause any unrealistic features, and the results of this model are in general terms similar to the model results discussed in Hall et al. (1999). While the age of air is clearly too young in the stratosphere, the situation stays stable during the whole 40-year simulation, and the interannual variations are well exhibited. Basically the too young age of air may be caused by the tracer advection scheme, or due to the incompatibility of FinROSE's chemistry scheme with the radiation coupling in the driver model. This, however, is a general problem for all CTM-type models. As explained in previous sections, in FinROSE's integration the mass-conservation of long-lived tracers, derived from the compilations by IPCC and WMO for the driver model integration, is ensured through zonal relaxation. With respect to these gases (i.e. NO_y , Cl_x , and Br_x , as presented in Figure 4.1), this procedure in turn forces FinROSE to imitate the results of UMETRAC. From the age of air perspective this means e.g. in the case of chlorine compounds that the observed/projected amount of chlorine species is not dependent of the stratospheric aging process and the consequent conversion of the CFCs to chlorine reservoirs (like $ClONO_2$ and HCl) during the aging process caused by the Brewer-Dobson circulation. Therefore the effect of this faster-than-nature Brewer-Dobson circulation may not realize as severe in the FinROSE's results as one may expect.

In order to understand the global distributions of tracers like ozone, the analysis based on the age of air alone omits one extremely important process, since the compositional tracers are also affected significantly by the atmospheric chemistry. However, based on the analysis of the age of air, it is safe to say that the used lower boundary conditions do not cause any extra unrealism for the model results, and for stratospheric simulations the most important thing is to make sure that realistic concentrations are used as a lower boundary conditions around the tropics. More generally, should there be problems over the tropical latitudes adjacent with either too fast or too slow Brewer-Dobson circulation; more problems will appear over the wintertime poles. So even if one wants to study the multi-year behaviour of polar processes, it is the tropics that need to be taken care of first.

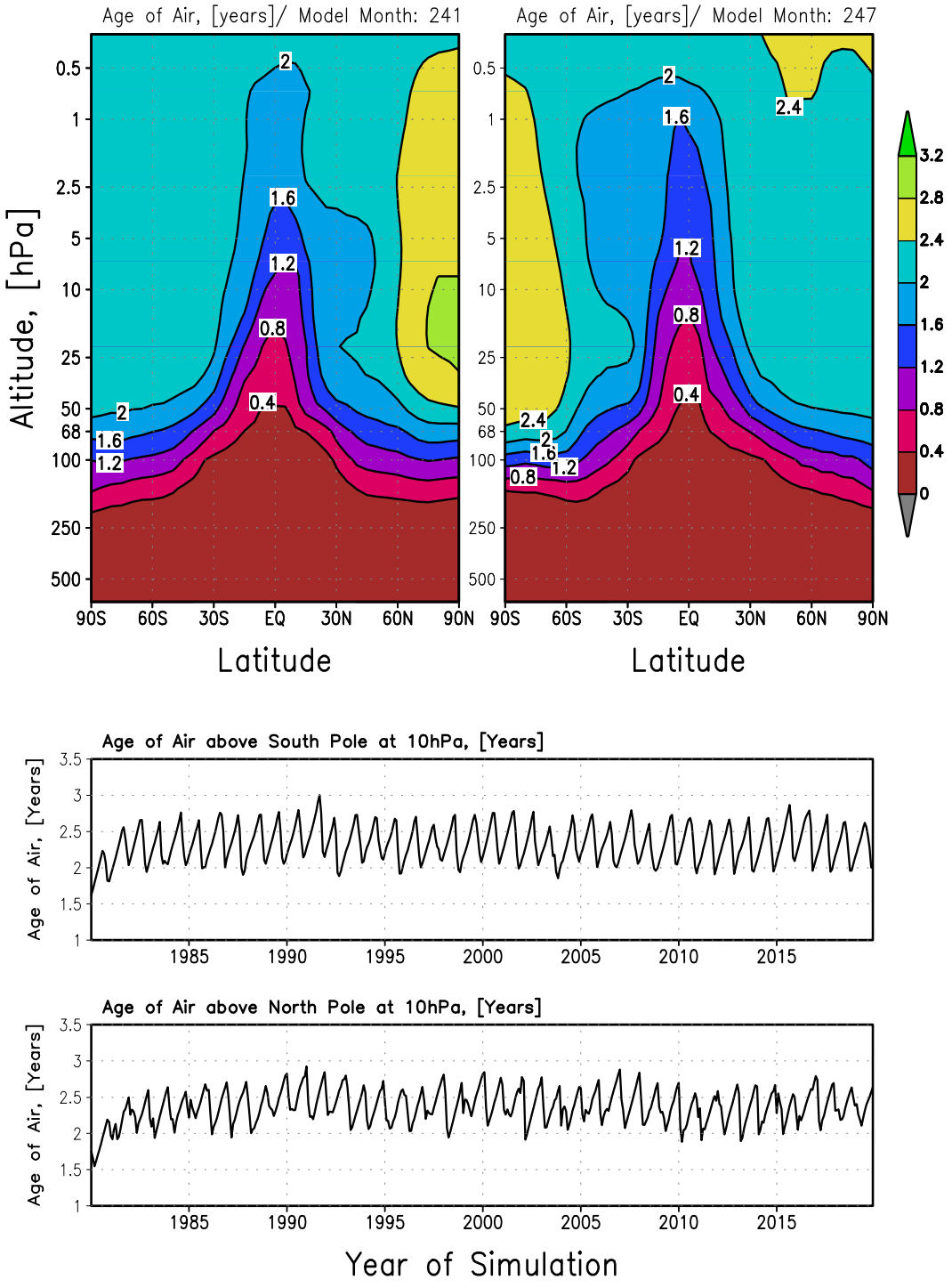

FIGURE 4.3. The modelled distributions of the age of air tracer (in years). Upper left frame shows the monthly mean altitude-latitude cross-sections after 20-years of simulation for January 1998, and upper right for July 1998, respectively. The lower frames show the evolution of the age of air tracer above the both poles at 10hPa during the 40-year FinROSE simulation.

4.5 Global Ozone Evolution

In case of a long simulation of the atmosphere, the very basic requirement for any model is the stable evolution of the atmospheric composition, without any loss or gain of atmospheric mass. In this study, this is extremely important, as I aim for trend analysis of the modelled ozone behaviour. In order to prove the stability of the model integration, I show the temporal evolution of the globally averaged total ozone column abundance in Figure 4.4, where the modelled globally averaged total ozone is compared against satellite measurements, and against the driver-model. As the TOMS measurements show, a typical global column of ozone contains around 280-300 DU depending on the season. This Figure (4.4) shows that, in general terms, the evolution of total ozone stays stable during the whole model integration period, while the absolute level differs from the measured global levels. In the case of the UMETRAC driver simulation the global mean total ozone is, on average, more than 90 DUs higher than the measured ozone. In the case of the FinROSE-simulation, the reproduced global average is less than 30 DUs lower than measured. These differences are clear indications of the different formulations of the chemistry in the two models. The overall evolution in both models, however, is acceptable, since the annual and seasonal evolutions follow nicely the measured evolutions.

The seasonal and interannual variations are also well reproduced by both models. FinROSE's interannual variations are slightly smaller than the measured variations, and in the UMETRAC case the opposite is true. The cause of the absolute difference between the measured column ozone values, and modelled values lies in the reproduced Brewer-Dobson circulation. At this point it is important to distinguish the inert age of air type diagnostics from the behaviour of photochemically active long-lived tracers, like ozone, as the atmospheric constituents exhibit different lifetimes for example due to the photodissociation. In the case of ozone, as well as other long-lived photochemically active tracers, the transport of too young air through areas of fast photochemistry (eg. tropics) ends up in different equilibrium state than the older air would. The concentrations of the tracers in the old air saturate well before the circulation removes the air from the stratosphere (see Waugh and Hall 2002 for detailed discussion). If the air is too young this saturation does not necessarily take place, and the resulting global average has its equilibrium at different level depending on the formulations in the models chemistry schemes. Basically this means that even though the Brewer-Dobson circulation is too fast in the combined UMETRAC-FinROSE-simulation, the behaviour of long-lived gases like ozone is still very much in line with the measured behaviour, and therefore the results could be used for studying the changes in the past and future behaviour of stratospheric ozone.

The zonally averaged evolution of the simulated monthly mean total ozone for the whole simulation period is shown in Figure 4.5. Figure 4.5 also shows

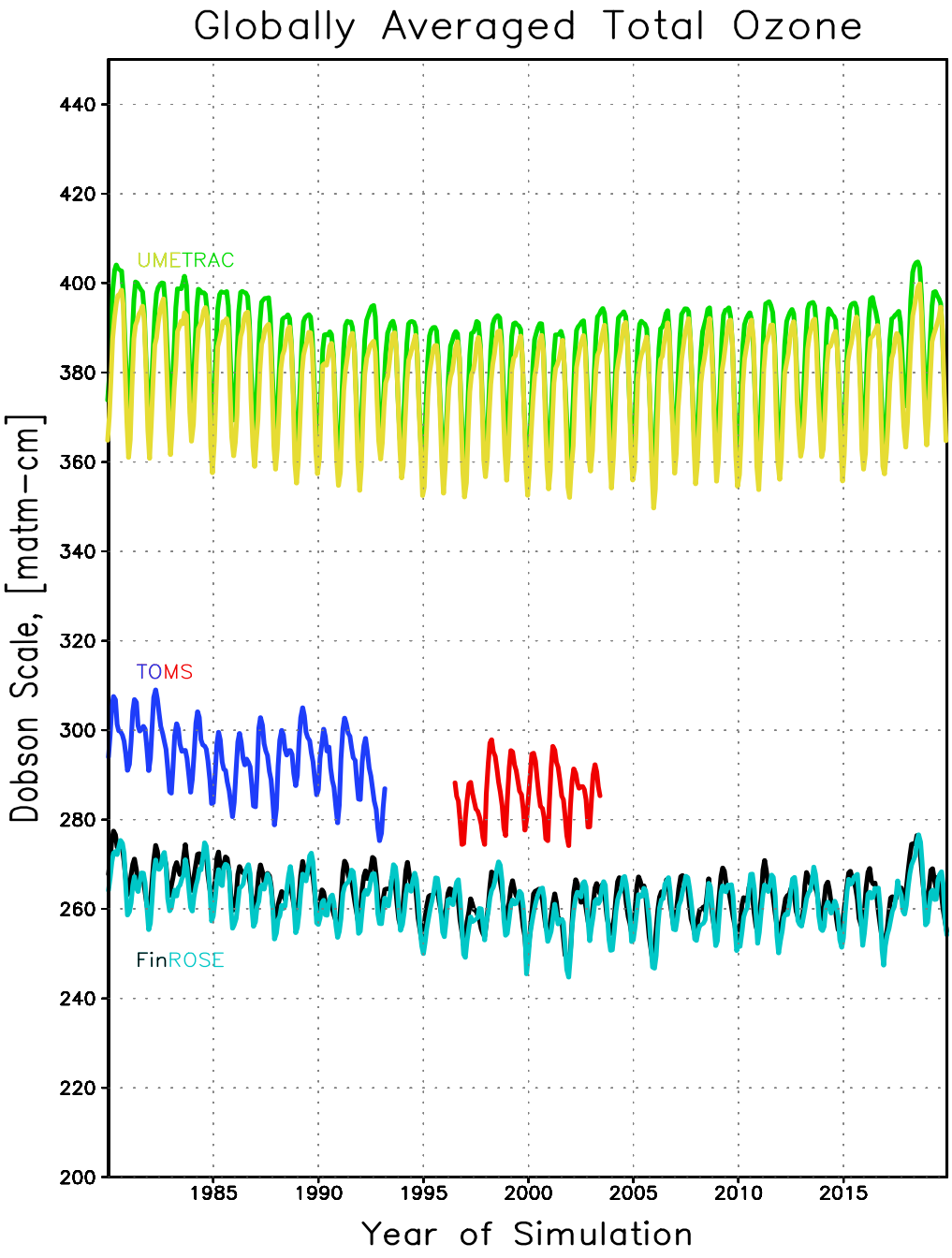

FIGURE 4.4. Temporal evolution of the globally averaged monthly mean total ozone. The black line shows the evolution of the global average FinROSE total ozone, the light blue shows the evolution of FinROSE total ozone between 60°N and 60°S, the green and yellow lines show the respective evolutions of the total ozone simulated by UMETRAC model. The blue and red lines are values based on the measured total ozone by the Nimbus-7/TOMS, and EP/TOMS instruments, respectively. The Dobson Unit is a measure of the total ozone column height at surface conditions (1 DU = 10^{-5}m, e.g. typical amount of 300 DU of ozone is equivalent to a pile of ozone molecules about 3 millimeters high).

the corresponding results from the UMETRAC-simulation, as well as the measured values by the satellite instrument TOMS. Although a direct year-to-year comparison of the CCM-driven FinROSE-results (or the UMETRAC results) is somewhat misleading, as the driver model is not expected to capture the details of interannual variability (i.e. specific years), a few conclusions from the comparison can be drawn. Firstly, it is clear that the model reproduces the observed latitude distribution as well as the seasonal behaviour of total ozone. The global mean result given in Figure 4.4 is also visible here: FinROSE gives somewhat lower values than measurements, while the UMETRAC-values are generally higher. Overall, the modelled ozone is around 10 to 15% lower in the FinROSE-model compared to the measurements. During the early 1980's the levels of inorganic chlorine in the atmosphere were still low compared to those of today. The resulting moderate (but still rather significant) ozone depletion over the high southern latitudes during the first half of the 1980's Septembers and Octobers is clearly captured by the model. Another clear feature of the model results is the deepening of the southern ozone depletion since early 1980's. Figure 4.5 also shows how the severity of the Antarctic ozone depletion has been increasing since the beginning of the simulation. Each year the area covered by low total ozone starts to spread in early August, and the lowest ozone values are typically seen in late September and early October (i.e. during the austral spring). The ozone-depletion season is typically over by early December. This result is especially encouraging since the resolution of the model is relatively coarse. The matters concerning the high-latitude ozone evolutions, and the effects of increased halon loadings in the atmosphere, will be discussed in more detail in the next sections.

Based on the results shown in Figures 4.4 and 4.5, one may directly conclude at least the following: i) The modelled patterns in the UMETRAC model and in the FinROSE model exhibit similar behaviour, and are comparable with the measurements, ii) The resulting Antarctic ozone depletion is less significant in UMETRAC, and iii) the overall total ozone levels of the UMETRAC model are higher than those exhibited by the FinROSE model. In other words, the differences in the chemistry-schemes seem to give somewhat more realistic results in the case of FinROSE. Another interesting feature in both models is the frequency of the no-ozone-depletion springs over the Antarctica. During the past and future cases there seem to be some occasions in both models when the ozone depletion over Antarctica stays moderate. These occasions will be discussed further in the next few sections. Finally, while the analysis of the ozone behaviour over the midlatitudes and tropics is outside the scope of this study, one may say that the patterns reproduced by both models are in general agreement with the measurements, and exhibit similar differences as in the case of high latitudes, though large absolute differences between the modelled values and measured values exists.

As already explained, the FinROSE results are achieved using the CCM-model as a driver. A reasonable comparison of the model results should be gained

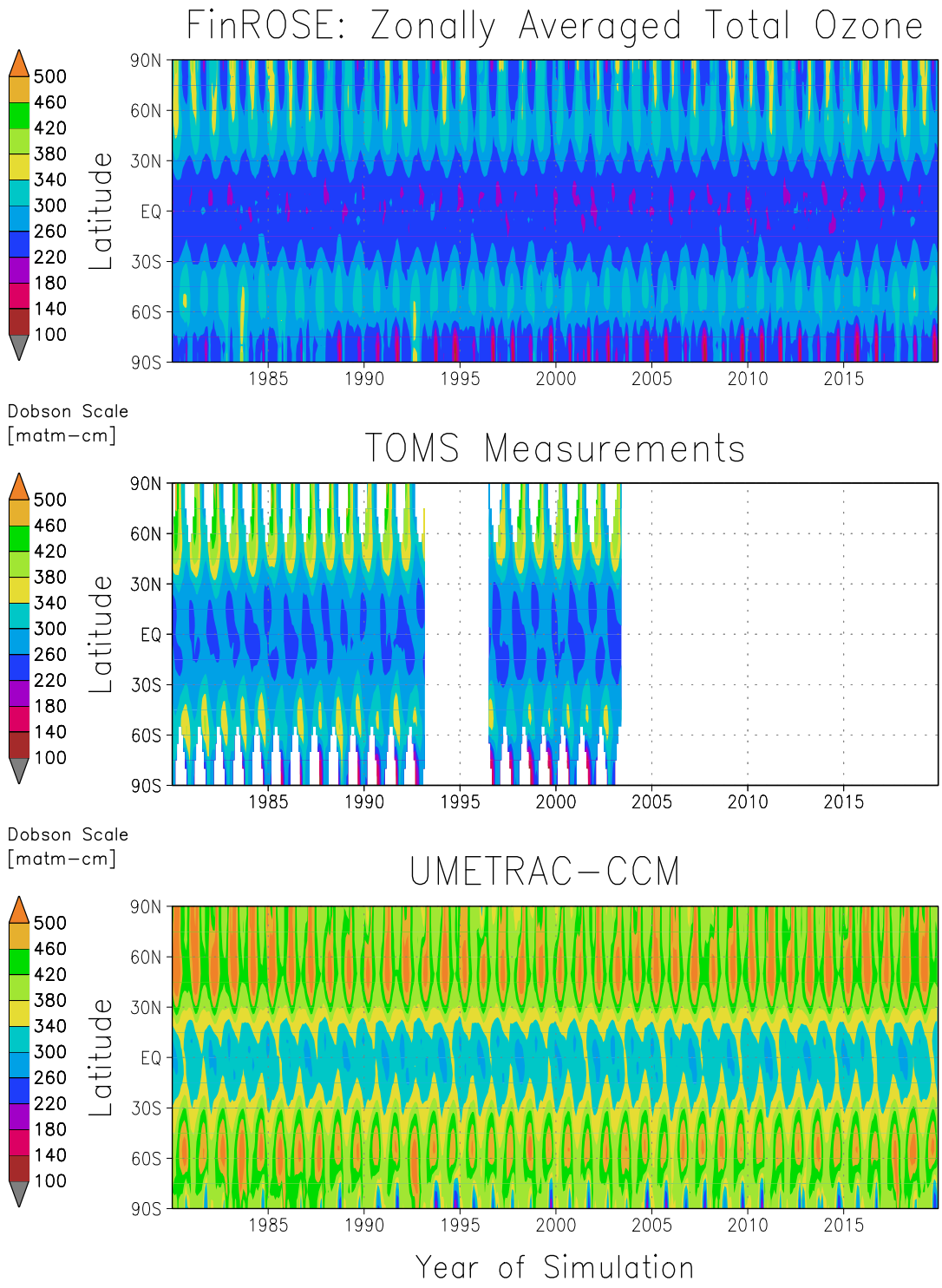

FIGURE 4.5. The evolution of zonally averaged monthly mean total ozone from 1980 to 2019, and the measured zonal average TOMS total ozone. The upper panel shows the FinROSE-results, the middle panel shows the TOMS total ozone measurements, and the lowermost panel is the UMETRAC result.

if the results are compared against available ozone climatology. Such comparisons are given in Figures 4.6, and 4.7. Figure 4.6 shows these comparisons from the mixing ratio perspective, and Figure 4.7 from the partial pressure perspective. The ozone climatology in question was compiled by Fortuin and Kelder (1998). This climatology is based on the ozonesonde measurements and satellite measurements of ozone, covering the period from 1980 to 1991. In the shown two figures (i.e. 4.6 and 4.7) the same period is used for averaging the model results. The comparison of both FinROSE results and UMETRAC results with the ozone climatologies shows that both models give reasonable and comparable results. The used climatology already includes the deepening of the Antarctic ozone depletion, and the FinROSE model climatology also nicely captures this phenomenon. However, there are discrepancies between the simulations and observations. These differences include: i) The modelled ozone mixing ratios are generally lower than observed in the case of FinROSE, and higher than observed in the case of UMETRAC, ii) The maximum, reproduced by both models, over the tropics is somewhat higher than in the measurements (in FinROSE somewhat less profound though), iii) The basic distribution pattern in FinROSE case seems to be located at a higher level than in the measurements, while in the case of UMETRAC-model the altitude matching seems to be better but the values generally higher than in the case of measurements. These differences are further emphasized in Figure 4.7 where the ozone partial pressures are shown. It is quite clear that FinROSE's tropical ozone maximum is too weak while in the case of UMETRAC the opposite is true. Over the high southern latitudes FinROSE's result is clearly in line with the measurements, since both the altitude and the magnitude compares nicely with the measurements. Over the high northern latitudes the result of FinROSE is clearly worse, as the partial pressure of ozone is too low while the level of the ozone maximum is reasonable. These differences give one explanation for the total ozone discrepancies shown in previous figures. Due to the Brewer-Dobson circulation, the FinROSE's higher altitude level distribution yields to lower column abundance of ozone over the poles, while in the case of UMETRAC model the higher mixing ratios at more correct altitude level give elevated ozone column abundances.

As a general conclusion from Figures 4.4 through 4.7 it is now fair to say that the FinROSE model reproduces the observed global patterns, seasonal variations, and year-to-year evolutions of stratospheric ozone quite well. The differences with the two shown model results, as well with the measurements, seem to be connected with limitations and imperfections in model tracer transport (or in the reproduction of the Brewer-Dobson circulation), and with the differences in the stratospheric chemistry formulations in these two models. However, while these discrepancies between the measurements and model results exist, the results given in this section show that the FinROSE-model is capable of simulating realistic behaviour of stratospheric ozone. In the next section the model results are further

analyzed from the high-latitude ozone point of view, and FinROSE's ability to simulate the processes leading to ozone destruction will be evaluated

4.6 High Latitude Ozone

In order to assess FinROSE's ability to simulate the processes affecting the polar ozone I will now show the results from the high-latitude point of view. These analyses are basically divided into two branches: i) Result analysis over the high southern latitudes, and ii) Result analysis over the high northern latitudes. As the scope of this study mainly lies within the processes involved in the high-latitude ozone destruction the analysis of the mid-latitude and tropical ozone is ignored.

4.6.1 Ozone Evolution over the Antarctic Areas

Before analysing the processes leading to the observed massive ozone destruction in the springtime Antarctic stratosphere, a more detailed overview of model ozone evolution over the high latitudes is needed. Figure 4.8 shows the average simulated total ozone enclosed by the 75th southern latitude during the 40-year simulation period and compares these results with available TOMS total ozone measurements. Results from both the FinROSE simulation and the UMETRAC simulation are shown. The year-by-year total ozone comparison shows that the performance of the FinROSE-model is satisfactory. The model clearly reproduces all the observed main features, and the FinROSE's ozone values are of the same magnitude as the TOMS measurements. Before and after the actual ozone destruction period (i.e. before August, and after November, respectively) it seems that the FinROSE-simulated values are somewhat lower than those measured by the TOMS-instruments. In all cases the "ozone-hole-season" starts, as expected, to grow during July-August, and the recovery is complete by the end of November or early December, meaning that the ozone depletion caught by the FinROSE model is well timed. Another well-reproduced element in Figure 4.8 is the gradual deepening of the Antarctic ozone depletion in both models. The UMETRAC simulation (i.e. the driver simulation) also follows the measured behaviour, though in the case of UMETRAC the total ozone levels are generally higher than the measured total ozone. The occasional non-existence of springtime ozone destruction seems to happen during the same years in FinROSE and UMETRAC. This similar time evolution and differences between the general total ozone levels basically confirm two things: i) The UMETRAC transport scheme and FinROSE transport scheme end up in a very similar result, and therefore the driver model mainly determines the relative year-to-year, and season-to-season variations, and ii) The differences between the FinROSE's absolute levels and the UMETRAC levels derive mainly from the differences in chemical formulations.

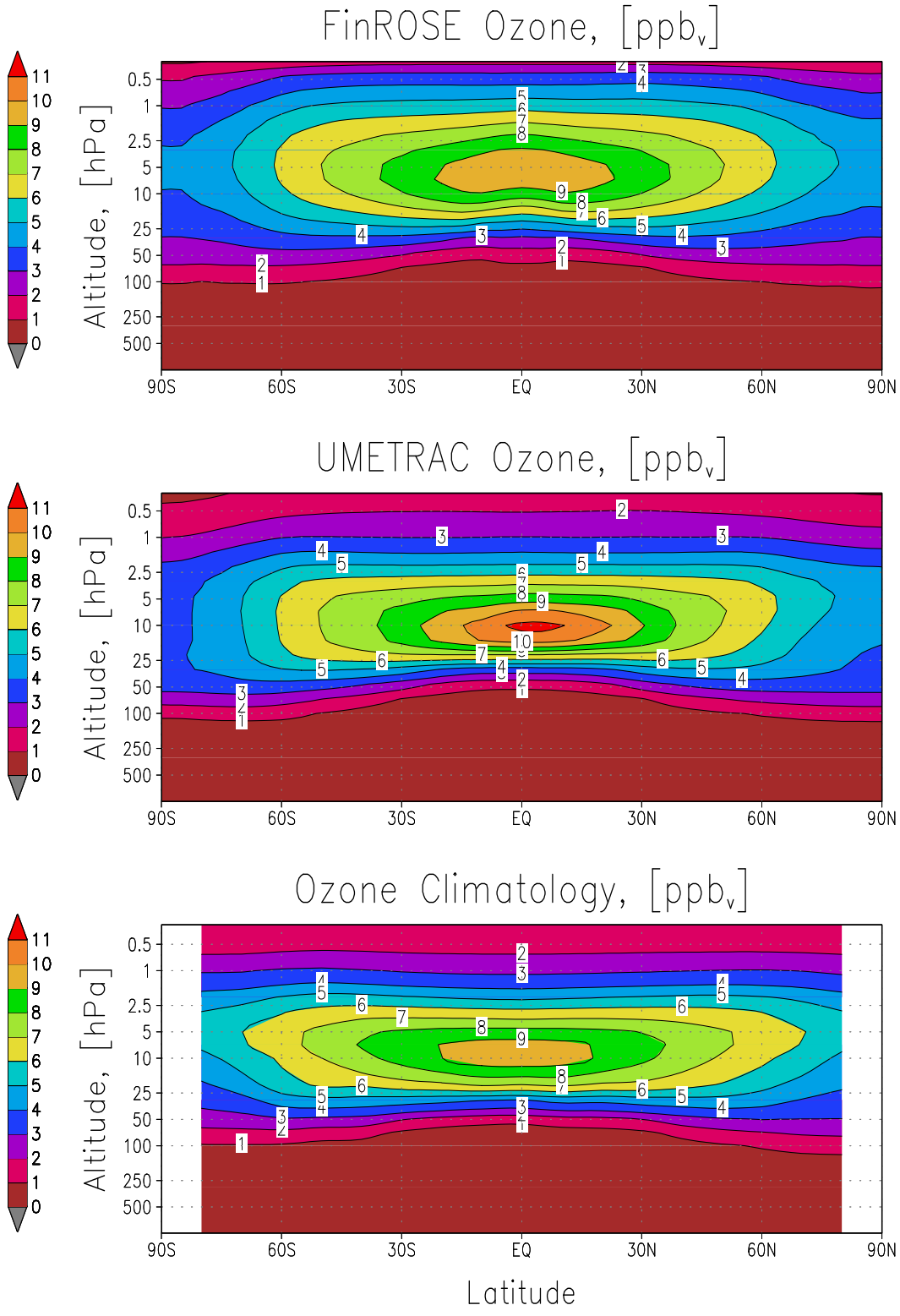

FIGURE 4.6. Calculated model ozone climatologies for the period from 1980 until 1991, and the measurement-based ozone climatology (Fortuin and Kelder 1998). Values are shown as mixing ratios.

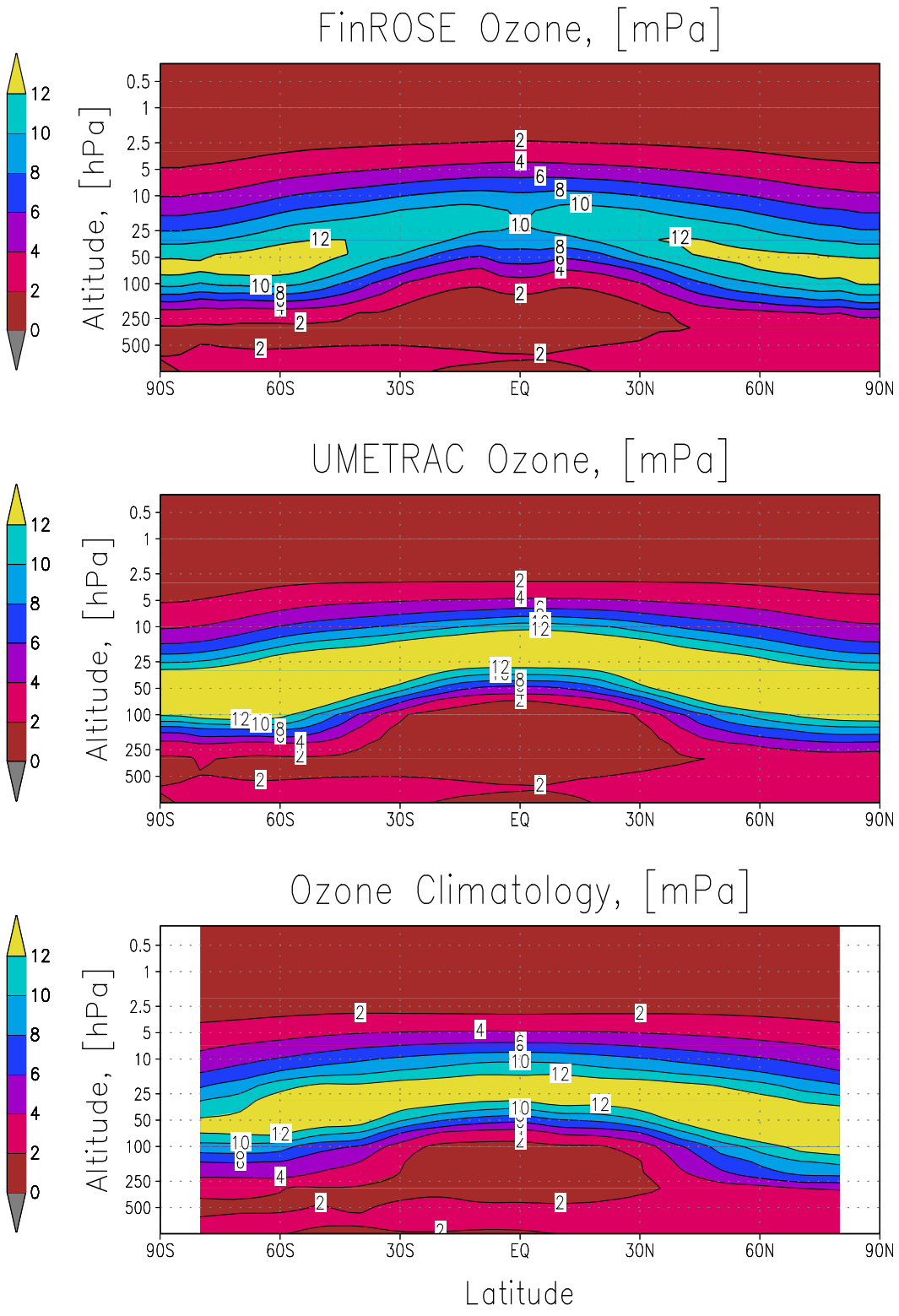

FIGURE 4.7. Same as Figure 4.6 except that the values are shown as ozone partial pressures.

During the future period of the simulation (in Figure 4.8) both models exhibit similar month-to-month ozone variations and overall evolution patterns, as they do during the past period. A comparison between the typical levels seen during the past years (i.e. 1980 to 1999) and during the near future (i.e. from 2000 to 2019) suggests that in the near future the ozone behaviour will be similar to that observed during the 1990's. The differences between the past behaviour and future behaviour will be further discussed in coming sections.

In conclusion of this sub-section, I may say that the FinROSE model results of the ozone evolution simulated in the 40-year run capture the deepening, levels and timings of the individual Antarctic ozone depletion seasons very well, and that the results are in good agreement with the measurements. Since the chemistry scheme of the FinROSE model is rather profound, and the main processes leading to large-scale ozone destruction are included (e.g. PSC-processing and sedimentation of the PSCs), further analysis of the reasons behind the phenomenon is justified. Such an analysis for the FinROSE-results will be done in the next Section.

4.6.2 Antarctic Ozone Destruction

As discussed in Chapter 2, the processes causing the ozone depletion, as seen especially over the Antarctica, require first of all the formation of polar stratospheric clouds (i.e. PSCs), enough inorganic chlorine (and possibly other halogens) to be converted to active form, low enough stratospheric temperatures to cause denitrification, and finally, solar radiation for driving the actual ozone loss processes. In this subsection these processes are further analyzed for the whole FinROSE 40-year time-series in case of high southern latitudes.

Following the basic requirements needed for stratospheric ozone destruction, one needs to study the evolution of the chlorine activation, total nitrogen, water vapour, and ozone at some representing level in the atmosphere. The evolution of ozone itself is dependent on both atmospheric transport and atmospheric chemistry. In order to have an approximate separation for these two main processes, one may use a concept of inert tracer. In this study I have formulated a passive ozone tracer, for which only the transport scheme of the model has been applied. The formulation of the tracer is as follows: I) The passive ozone tracer is initialized with the actual model ozone, II) This passive tracer is only transported (using the same boundary formulations as for the regular model ozone), and III) The passive ozone tracer is initialized twice every year, at 1st of June, and at 1st of December (i.e. well before the initiation of the springtime ozone chemistry season). This gives a measure of how the ozone would have behaved if there would have not been any chemical processing. The evolutions of total nitrogen (NO_y), water vapour (H_2O), chlorine activation (i.e. ClO_x /Cl_x), and the difference between the passive ozone tracer and regular model ozone (i.e. O_3 subtracted

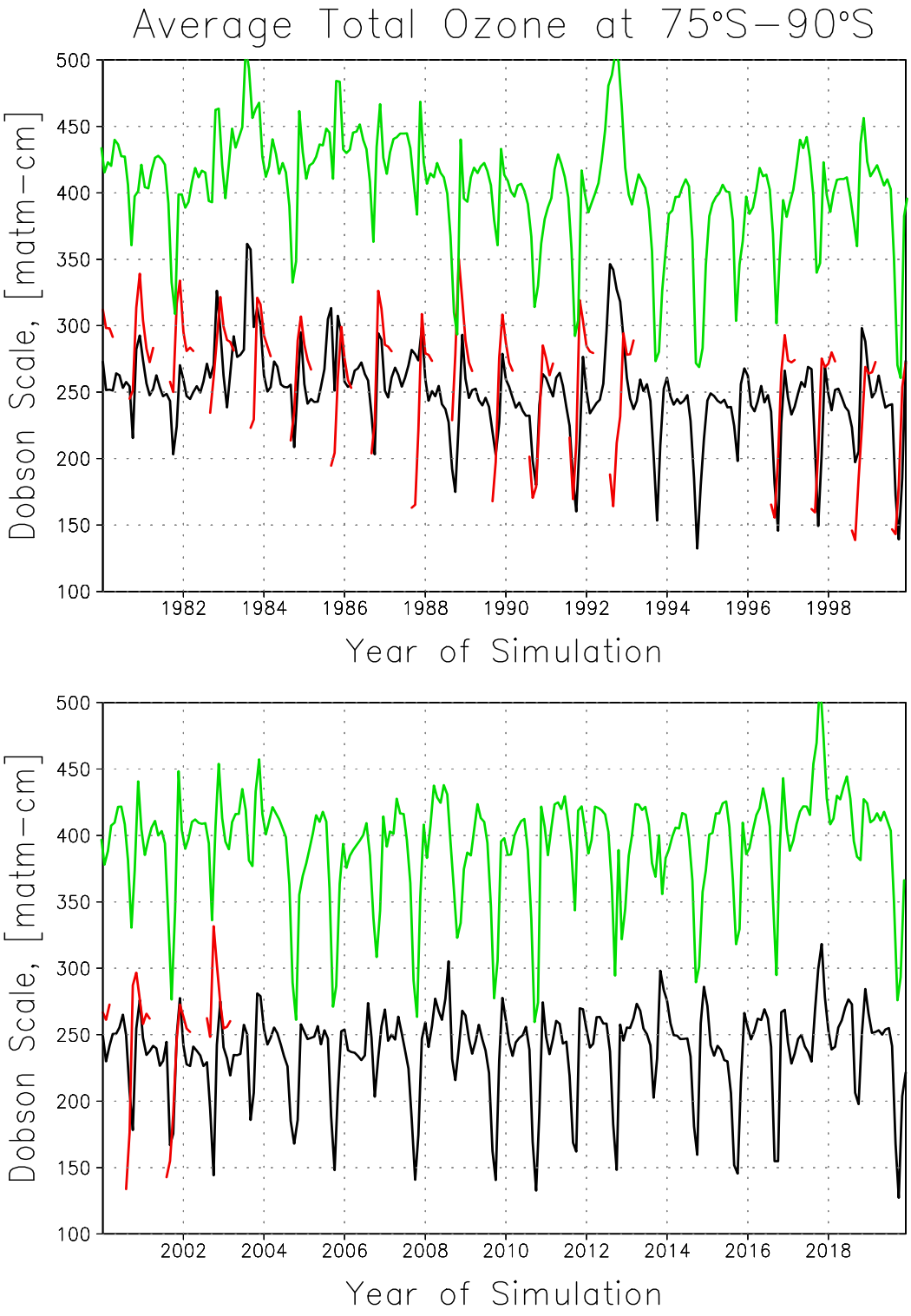

FIGURE 4.8. Comparison of the observed total ozone evolution with the modelled ozone evolution. Time-series are shown as average values within the 75°S-latitude circle. The FinROSE-model ozone values are presented by black lines, the UMETRAC-values as green lines, and the measurements by TOMS-satellite instruments by red lines.

from Tracer-O_3) are shown in Figures 4.9 through 4.11 for the whole 40-year timeseries together with the PSC exposure times (for types I and II). All values are shown as monthly mean values within 75°S – 90°S, averaged over the vertical column from 146hPa to 31hPa (i.e. between 14 and 24 km, including the core of the ozone layer).

Following the time-series extending from the early 1980's until the end of 2019, we see how the major processes are simulated in the model. The first thing to look for is the start of the chlorine activation soon after the initiation of the austral polar night (i.e. during June). The chlorine activation starts as the first signs of the PSCs type-I appear. At the same time the level of total nitrogen, as expressed by NO_y , starts to drop. This dropping of NO_y is further accelerated, or the rate of denitrification is increased, when the temperatures drop below the water freezing point, and the large PSC-type-II particles start to form and fall. This is further manifested by the evolution of the water vapour which also exhibits a clear drop like in the case of NO_y . This phenomenon, often called dehydration, is connected with the sedimentation of ice-form PSCs (i.e. type-II PSCs). The impacts of the stratospheric water vapour changes on the PSC formation and stratospheric ozone have been studied by e.g. Stenke and Grewe (2005, and references therein), and Evans et al. (1998). The disappearance of PSCs has a clear connection with the ozone depletion. As the temperatures gradually increase during the spring and the vortex is dissolved, the PSCs evaporate, and the large-scale ozone depletion is typically over by the end of November (i.e. the results do not exhibit ozone depletion during December). Since cold enough temperatures for the formation of ice-clouds exist during most of the winter-spring seasons shown in the figures, these generalized monthly average results do not exhibit any clear signs of significant denitrifications caused solely by the potentially rapid sedimentation of large NAT-particles (i.e. NAT-rocks) which would have been formed after a long enough exposure for temperatures between the PSC-I forming point and ice forming point (i.e. PSC-II forming point). The behaviour of water vapour basically states that the denitrifications are clearly coupled with the dehydrations, and the conclusion is therefore that it is the sedimentation of ice particles that is causing the exhibited denitrifications on average. However, these results do not rule out the possible sedimentation of large NAT-particles on a more local and shorter time-scale (e.g. daily scale), but as the scope of this study is in the bulk monthly and vortex-scale quantities this is not analyzed further. The actual ozone loss, as seen in Figures 4.9 through 4.11 starts soon after the analyzed area becomes sunlit (on average during August-September). This behaviour is shown by the starting growth of the difference between the passive ozone tracer and regular model ozone. In the early 1980's the relative magnitude of ozone losses is at highest between 50 and 60%. After mid-1980's the relative ozone depletion starts to grow exhibiting frequently values over 80% in the 31-146hPa layer.

Figure 4.12 shows how the two main chemical ozone loss cycles have con-

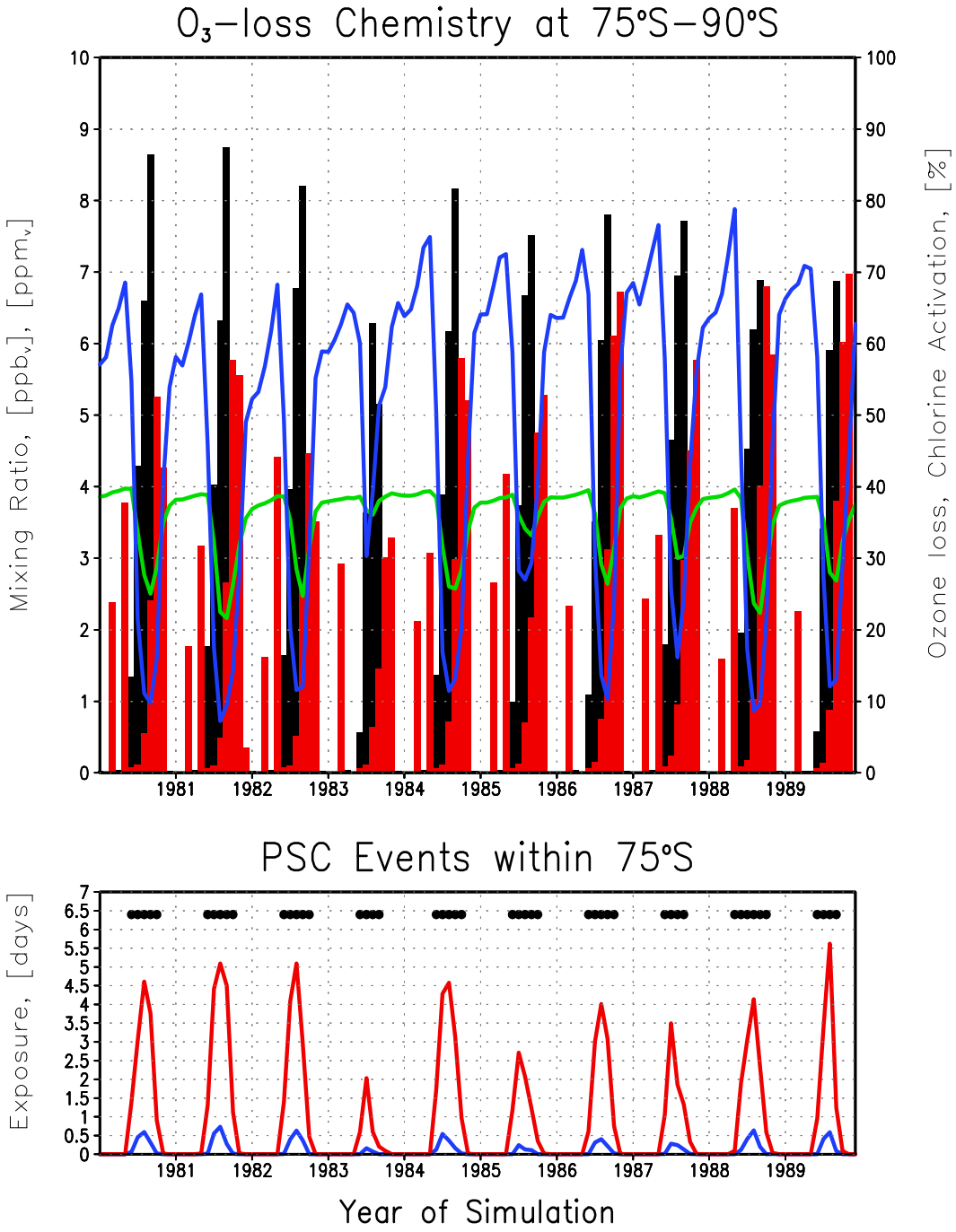

FIGURE 4.9. Simulated average time-series for 1980-1989 of main constituents affecting ozone within 75°S, and between the levels 146hPa and 31hPa. In the upper frame the evolution of chlorine activation is shown by the black bars, the evolution of total nitrogen by the blue line (in ppb_v), the evolution of water vapour (in ppm_v) by the green line, and the relative difference between the passive ozone tracer and regular model ozone by the red bars. In the lower frame the PSC type-I exposure time is given by the red line, the PSC type-II exposure by the blue line, and the areal average events of tempartures below 195K are denoted by black markers.

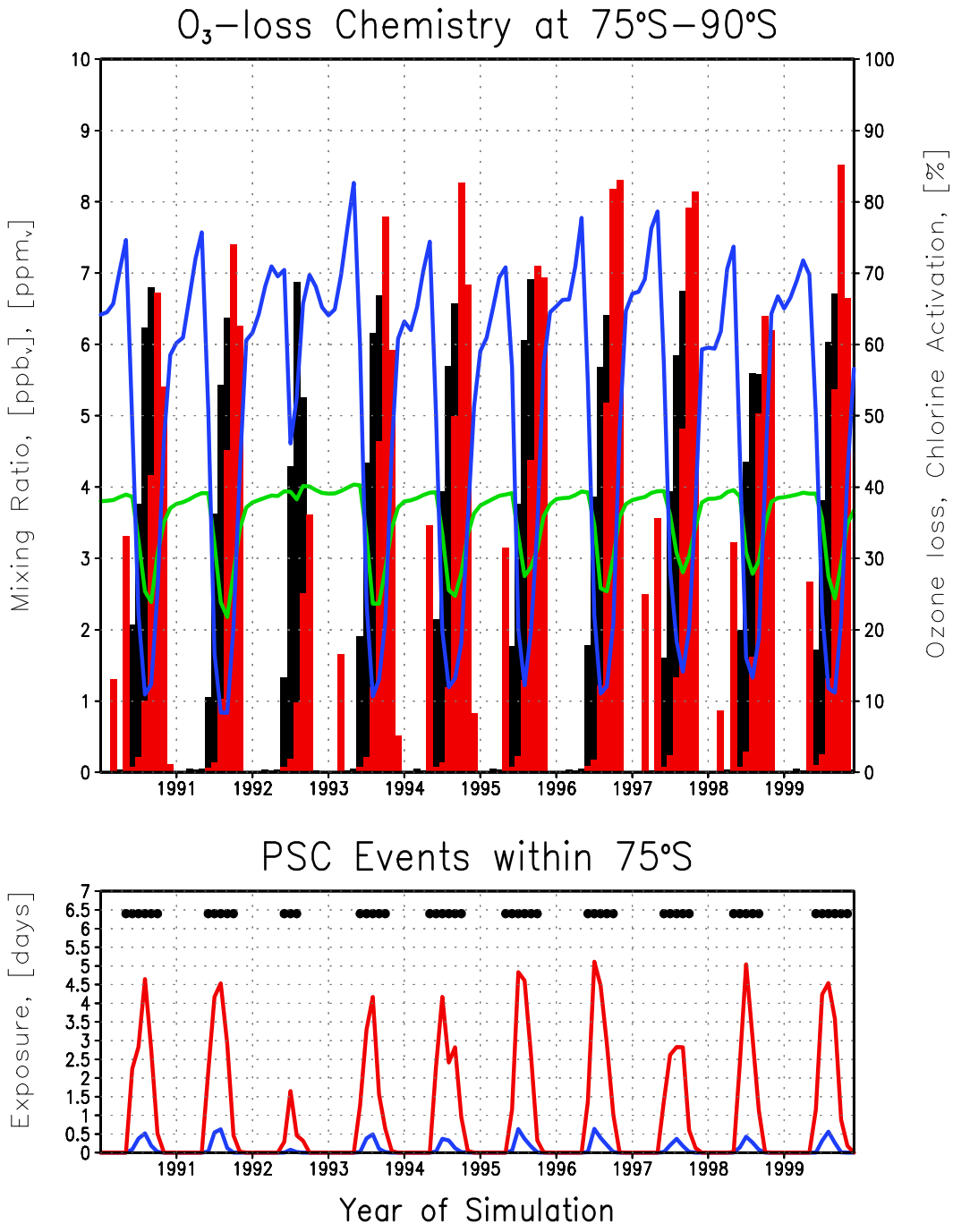

FIGURE 4.10. As in Figure 4.9, but for the years 1990-1999.

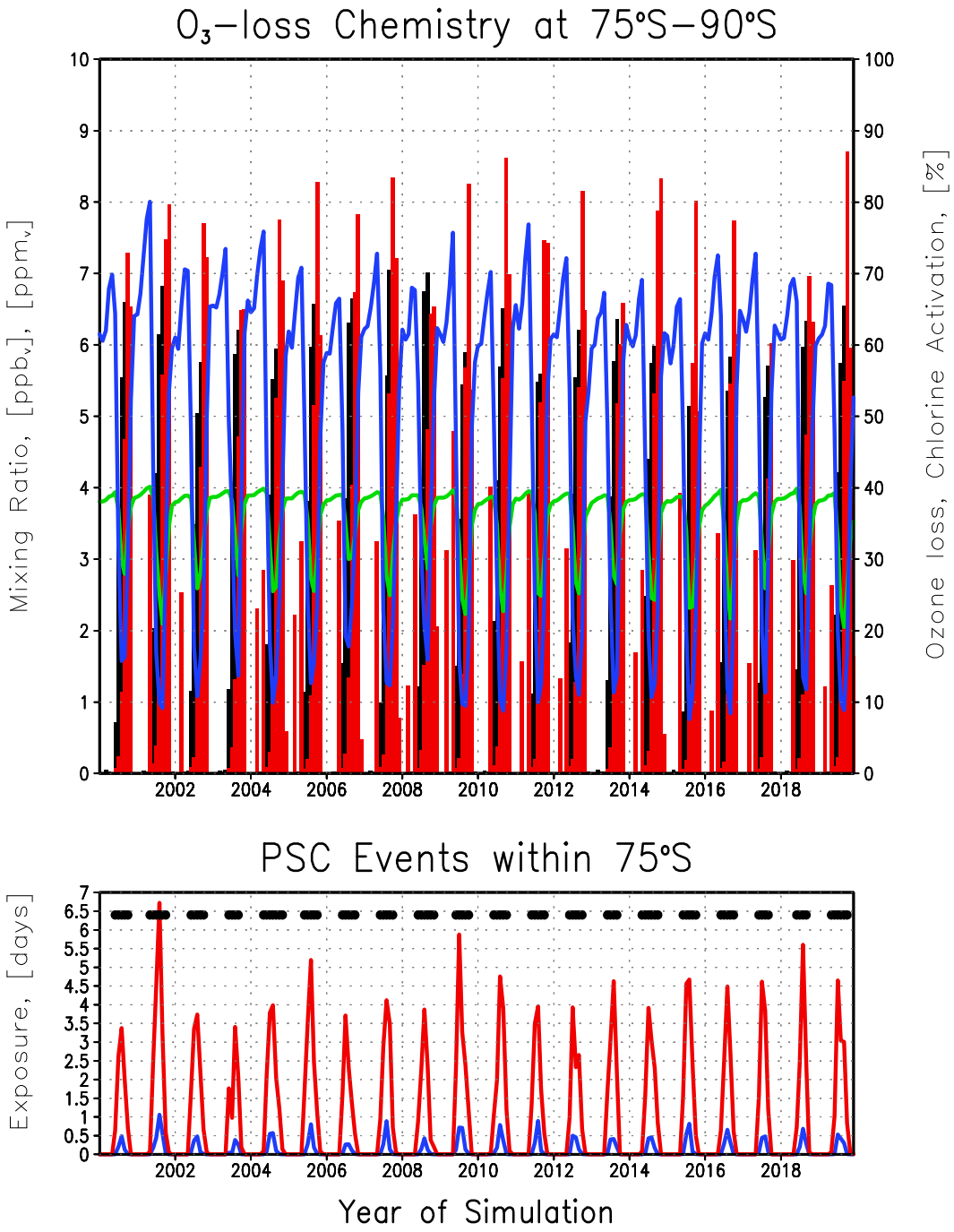

FIGURE 4.11. As in Figure 4.9, but for the years 2000-2019.

tributed to the simulated net ozone loss, as explained in Chapter 3. The relative effect of catalytic ozone loss cycles by active chlorine (i.e. ClO_x) is clearly the most significant as these cycles are responsible for about 60 – 70% of the total ozone loss during the southern hemispheric spring. The rest of the ozone depletion is due to the second most important catalytic cycle during the ozone depletion season, namely the combined effect of BrO and ClO . Actually the coupled ClO – BrO destruction of ozone is almost as important as the ClO_x cycles during August and October. However, it should be kept in mind that the amount of absolute ozone depletion itself is smaller during August as there is only limited amount of solar radiation available within the analysed area. It is also worth noticing that during the ex-ozone depletion seasons, the catalytic cycles of NO_x (summertime), and HO_x (autumntime) are the main contributors of the ozone depletion (not shown). However, the analysis of these cycles and seasons is outside the scope of this study and as Figure 4.12 clearly shows, the chemical depletion of ozone during winter and spring is almost exclusively due to the catalytic ozone destruction by active chlorine and coupled ClO – BrO -chemistry.

The average evolution of chlorine activation itself (in Figures 4.9 through 4.11) seem to be somewhat more profound during the 1980's than during 1990's or during the later decades. However, as it will be repeated in later sections of this chapter, there is no statistically significant trend connected to this phenomenon of chlorine activations. The average total nitrogen (NO_y) between these particular levels (146-31hPa) clearly exhibits expected behaviour. In all cases, when a significant drop in the NO_y -value occurs there is a clear connection with the existence of PSCs type-II. From a monthly average perspective, NO_y is nicely anticorrelated with the behaviour of the PSC type-II exposure tracer. It is also clear that significant chlorine activation occurs during every austral winter-spring season of this 40-year timeseries. The denitrifications, however, do not take place during every single simulated seasons and it is clear that the most significant ozone depletions are connected with the behaviour of total nitrogen. The exceptions for the denitrification are especially the years 1983 and 1992 when the drops in total nitrogen are less significant, and the ozone loss less profound. In these cases, the initiation of the denitrification has the same features as in the other years. The chlorine activation also has similar behaviour. The main difference, in these cases, is the behaviour of temperature, as manifested by the existence of the PSCs. Basically, it can be seen that the ozone destruction starts slowly, as usual, around August. The minor denitrification year 1992 seems to exhibit signs of denitrification due to the large NAT-particles, since the simulated PSC-type-II events, on average, are relatively moderate, and still the value of NO_y drops below $5ppb_v$. Whether this moderate drop of NO_y is due to the sedimentation of large NAT-particles (i.e. grown PSCs type-Ia) or more localized occurrences of PSCs type-II, not shown by this averaged analysis, cannot be readily concluded from this figure. However, it is encouraging to see that this rather simple parameteri-

zation of the gravitational settling of large NAT-particles in the FinROSE-model seems to work. During these non-ozone-depletion cases the formation of ice is relatively moderate due to the warmer conditions. These warmer conditions may be connected to sudden stratospheric warming events which are known to be very rare in the Southern Hemisphere (see e.g. Shepherd et al., 2005). It is, again very encouraging to see that the used driver model (i.e. UMETRAC-model) is capable of reproducing these events. The analyses of warming events have been left outside the scope of this study as they are produced by the driver CCM (i.e. UMETRAC) rather than FinROSE.

Another way for the analysis of the 40-year time-series is to look at the behaviour of total inorganic chlorine levels in the atmosphere. Keeping in mind the fact that since early 1980's the inorganic chlorine loading increased from around 1.6 ppb_v up to around 3.5 ppb_v in the late 1990's, and it is projected to stay above 3 ppb_v until the end of the 40-year simulation period, an obvious conclusion can be made: The behaviour of the difference between the passive ozone tracer and regular model ozone is mainly due to the chemical processes, including the effect of denitrification. Chlorine activation, while being a regular phenomenon, does not alone lead to significant ozone depletion. After the winter season the high southern latitude stratosphere becomes sunlit and the active chlorine is converted rapidly back to the reservoirs (like $ClONO_2$ and HCl), if significant denitrification has not taken place. This means that it is the amount of inorganic chlorine that controls the severity of ozone depletions, and the occurrence and magnitude of the denitrification that controls whether ozone depletion takes place or not during a particular winter and spring. All the shown time-series show nicely how the increase in the inorganic chlorine has made the ozone depletions more severe since the beginning of 1980's. The level of ozone depletion reached during the latter part of 1990's seems to continue also during the future period, meaning that the overall picture stays more or less the same as it has been during the 1990's. The main two factors are in place (i.e. the chlorine activation, and denitrification) throughout the whole 40-year simulation, while during the early years the actual levels of inorganic chlorine were lower, and therefore the ozone depletions less severe. However, it is important to note that even with inorganic chlorine levels below 2 ppb_v , large-scale ozone destruction may happen by large, provided that the temperatures are low enough for the denitrification. The increase in the inorganic chlorine loading is a quite clear manifestation of its importance in ozone chemistry, but it is the low stratospheric temperatures that give way for the ozone depletion processes to happen. Therefore, if the stratospheric temperatures are to decrease as a result of the enhanced greenhouse effect, the probability for significant ozone loss may increase over the northern hemispheric high-latitude stratosphere. This will be analyzed and discussed in the next Sections.

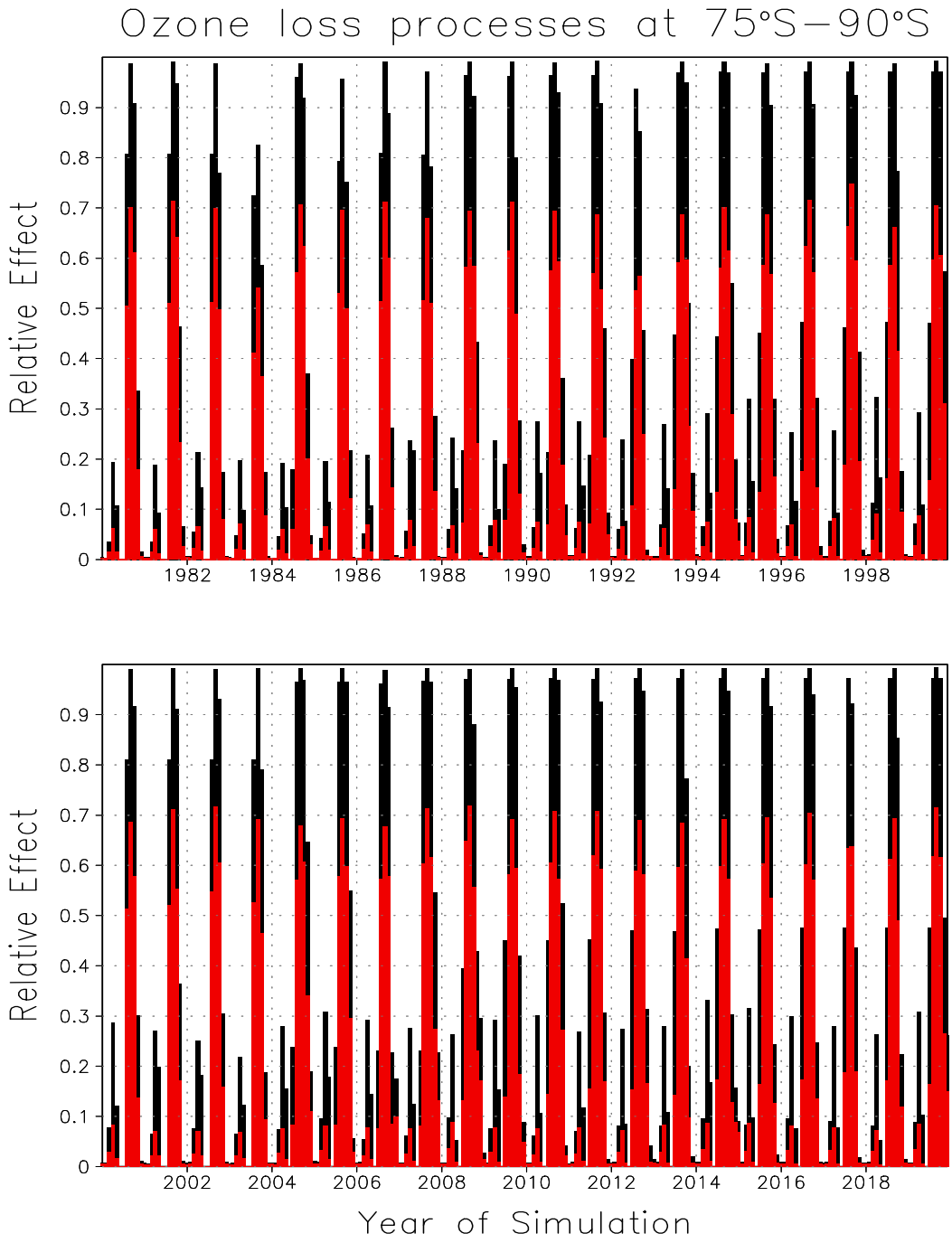

FIGURE 4.12. Proportions of the total ozone loss chemistry due to the two main catalytic ozone loss cycles during the 40-year FinROSE integration. The red portions of the bars show the effect of ClO_x processing, and the black portions show the effect of combined BrO_x - ClO_x chemistry, respectively. The shown values are averaged within the 75°S latitude, and between levels 146hPa-31hPa.

4.6.3 Ozone Evolution over the Arctic Areas

In order to understand the behaviour of the stratospheric ozone over the high northern latitudes, one needs to understand the basic differences between the southern and northern polar processes, as the two hemispheres have rather different conditions. These differences derive from the differences in the planetary wave activity between the hemispheres (as explained in Chapter 2). The differences between the hemispheric geographies (i.e. in the longitudinal distribution of land and sea, as well as continental scale mountain formations) cause wave activity forcing to be much stronger over the Northern Hemisphere than over the south. This means that the propagation of wave activity from the troposphere up to the stratosphere is more common over the Northern Hemisphere, and therefore the Brewer-Dobson circulation is stronger over the Northern Hemisphere than over the southern one (see e.g. WMO, 2003, and Figure 4.3). The axisymmetry of the southern wintertime vortex is very profound, while the Arctic polar vortex has a much more complex structure, and even the formation of the vortex itself is very much dependent on the mean-flow/wave-activity conditions during individual winters. The hemispheric differences in the Brewer-Dobson circulation mean that the level of vortex isolation is less profound in the north than in the south, and therefore the temperatures needed for PSC formation are much less probable in the north.

Keeping these fundamental differences in mind, I show the evolutions of monthly mean total ozone in the area enclosed by the 75th northern latitude during the 40-year simulation period, with comparisons to TOMS total ozone measurements, and driver model total ozone, in Figure 4.13. The situation in the north is rather different from that in the south as the Figure 4.13 shows (see Figure 4.8 for comparison). The overall multi-year monthly mean evolution follows nicely the observed seasonal patterns in both models. However, in the case of FinROSE the modelled total ozone is around 40 DUs lower than the TOMS measurements during summer and in some cases during wintertime maximum FinROSE gives over 100 DUs lower total ozone values than TOMS. In the UMETRAC model the summertime minimum are regularly around 100 DUs higher, and the wintertime maximum are around 50 DUs higher than measurements. Both models also exhibit the observed fact, stating that the total ozone should be higher over the northern circumpolar areas compared to south (see Figure 4.8). In both models the annual amplitudes at 75°–90°N are more or less the same, and around 30 DUs less than the annual amplitudes measured with TOMS. The difference between the two models derives from the chemistry, and emerges due to the transport. Since both models exhibit the expected seasonal behaviour where the total ozone has its maximum during late winter or early spring, and minimum during late summer or early autumn, and since there are clear similarities in the modelled interannual and seasonal patterns, I may conclude that the transport of constituents is similar

in both models. As already stated before, the modelled behaviour of the age of air tracer exhibited (in Figure 4.3) shorter values over the northern pole than over the south, and both values were lower than observed. This behaviour is nicely in line with the general interpretation of the Brewer-Dobson circulation, and so, it may be concluded that the seasonal behaviour of general transport characteristics is reasonable, though the age of air itself is too short.

The differences between FinROSE and UMETRAC are mainly in the chemistry schemes. The UMETRAC-model, being a chemistry-coupled general circulation model includes the essential coupling between transport characteristics and atmospheric composition through radiation. This means that the changes in the composition due to the chemical processing are reflected to the simulated temperatures and winds. Since the UMETRAC-model reproduces its own climatologies for compositional species like ozone (see Figures 4.6 and 4.7) with steady-state equilibriums, and other determinants (like chemical kinetic data) from its own chemistry scheme, and since these compositional features are in balance with UMETRAC's dynamical behaviour, one may say that UMETRAC produces its own balanced aeronomy. When the winds and temperatures from such a model are introduced to a CTM where the transport is formulated in more or less same way, but chemical formulations are different, the realized compositional patterns end up being pattern-wise the same, but in absolute level different. As the Figures 4.6 and 4.7 show, the ozone climatologies derived from FinROSE and UMETRAC have differences between the magnitude and altitude of the tropical ozone maximum, FinROSE being somewhat closer to the measurement-based climatology magnitude-wise, and UMETRAC altitude-wise. This tropical maximum can be considered as an initiation point for the Brewer-Dobson circulation, as the new stratospheric air is injected from the troposphere mainly over the tropics. In the case of FinROSE this initiation starts with values that are basically too low due to the fact that the maximum is located too high, and in the case of UMETRAC this initiation starts with too high values as the tropical ozone maximum is too profound. Since the behaviour of interannual and seasonal ozone characteristics are similar in both models, FinROSE's Brewer-Dobson circulation has less ozone to start with, and transport towards the winter pole, while UMETRAC has too much. As the simulated ozone maximum during late winter to early spring are either too high (UMETRAC), or too low (FinROSE) the reversal period of the Brewer-Dobson circulation (i.e. summer-autumn) starts with either too high values (UMETRAC), or too low values (FinROSE). As already noted, the Brewer-Dobson circulation is too fast (see discussion on Figure 4.3), and both models are continuously fed with too fresh air from the tropical troposphere. The processing of this too young air with different chemical schemes along similar transport results in different aeronomical features of both models, and these differences are further reflected at poles as the transport has different startpoints in these two models.

From the results presented in Figure 4.13, it may be concluded that the FinROSE results are reasonable also over the high northern latitudes, and that while differences with observed ozone levels exist, the FinROSE is capable of producing its own aeronomy which is balanced, but different from the driver model (UMETRAC). I also conclude that the more profound atmospheric chemistry scheme in FinROSE than that in the UMETRAC-model gives somewhat more realistic results. This is especially true in those stratospheric areas where the chemistry drives the compositional features (e.g. production of ozone in tropics or the springtime Antarctic ozone loss). While in the south, the increase in the magnitude of the ozone depletion since 1980's was clear, and the projected behaviour in the near future looked the same as observed during the 1990's, in the northern high-latitude stratosphere, no clear trend is evident in Figure 4.13. Due to the model features described above, the actual behaviour of total ozone shown in Figure 4.13 is not easy to analyse solely from either transport point of view or from chemistry point of view. For example, the FinROSE-model exhibits behaviour during some winters or springs that looks like ozone depletion (see e.g. years from 1988 up to 1990, or year 2008 in Figure 4.13). However, these deficits in wintertime maximum are more or less reflected in the UMETRAC evolutions as well and therefore might be due to the transport. The possible northern winter-/springtime ozone behaviour will be further analyzed in the next Section.

4.6.4 Arctic Ozone Destruction

As already explained, the situation in the wintertime and springtime northern high-latitude stratosphere is far less favourable for PSC formation than in the south, as the temperatures do not exhibit regularly sufficiently low values. While the total inorganic chlorine loading is similar to the south, Antarctic-like ozone destruction in the north would become possible only if chlorine activation and denitrification takes place. As these processes are dependent on the existence of PSCs, and therefore low temperatures, it is easy to conclude that northern high-latitude ozone destruction should be significantly less profound.

Again, as in the case of southern high latitudes, I show the monthly mean evolutions of the main contributors (i.e. total nitrogen, chlorine activation, water vapour, and the relative difference between the passive ozone tracer and with regular model ozone) within the 75th northern latitude circle between the vertical levels of 146hPa and 31hPa in Figure 4.14 for the whole 40-year timeseries. As can be seen, these results are totally different from those in the south. The evolution of total nitrogen stays relatively stable throughout the whole simulation period. While NO_y seems to exhibit some drops during the course of the simulation, the water vapour distribution stays very stable. Interestingly, it seems that even on this average-perspective from around 20% up to 50% chlorine activation is taking

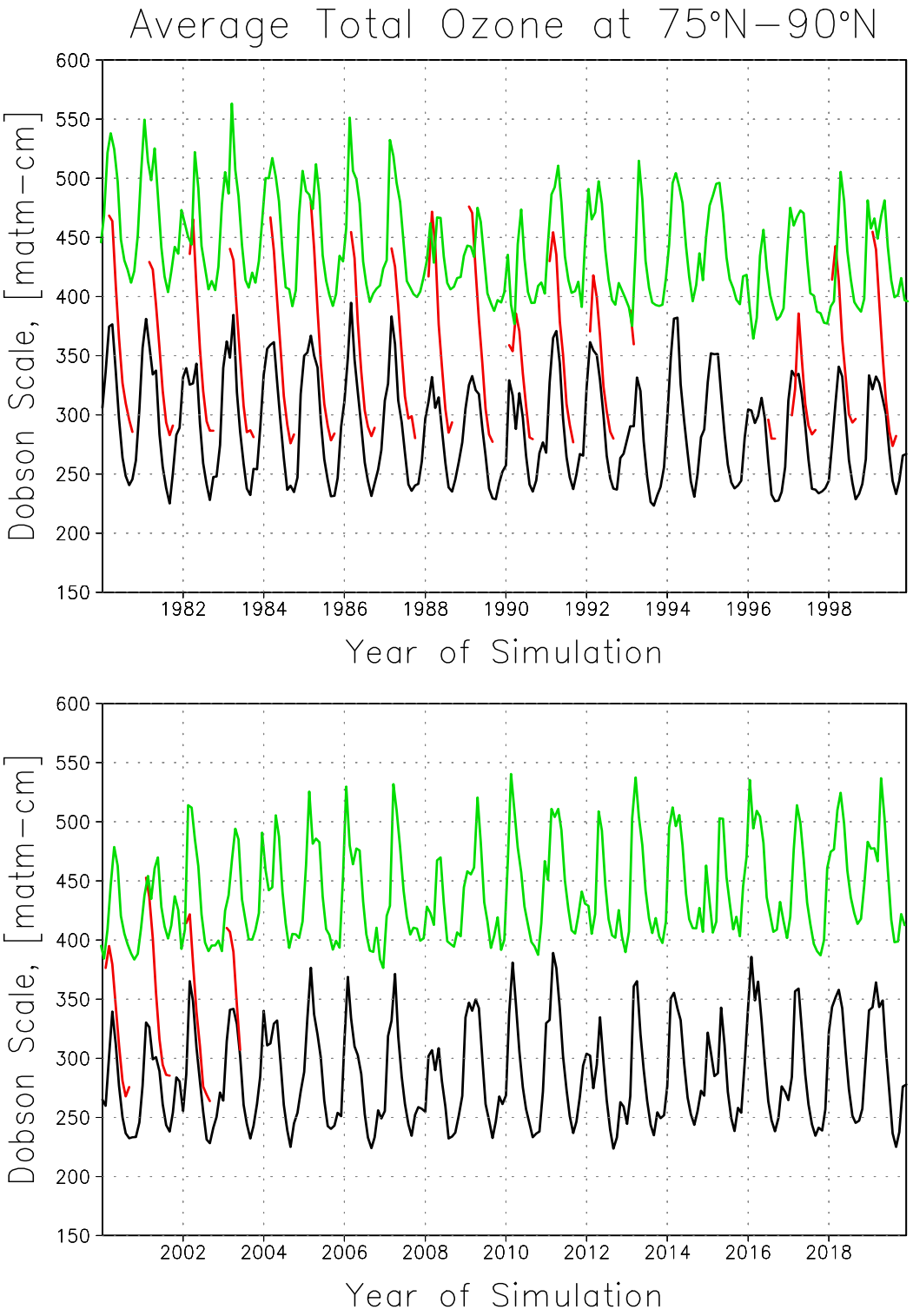

FIGURE 4.13. Comparison of the observed total ozone evolution with the modelled ozone evolution. Time-series are shown as average values within the 75°N-latitude circle. The FinROSE-model ozone values are presented by black lines, the UMETRAC-values as green lines, and the measurements by TOMS-satellite instruments by red lines.

place during almost every winter/spring. The level of the chlorine activations is clearly connected with the average existence of PSCs type-I, while in this averaged analysis no signs of PSCs type-II are found. The evolution of chemical processing (i.e. the relative difference between the passive ozone tracer and the regular model ozone) exhibits no clear signs of systematic trend, except perhaps, the increase during the first half of the 1980's. The cases of higher chlorine activations are clearly connected with the weak, but obvious denitrifications shown, and in turn with the simulated ozone losses.

In general, at 75°N–90°N, the total nitrogen does not exhibit as large drops as it does in the south. This result is basically expected, as the temperatures do not exhibit low enough values for ice-cloud formation (see also discussion on Figure 4.2). Since PSC type-II clouds are a rarity in the north, no extensive ozone depletion results. However, during some years weak signals of denitrifications are present, as the NO_y values drop below $5ppb_v$. A closer look at the behaviour of the PSC-tracers also indicates that while the ice-form PSCs are non-existent, the type-I PSCs are simulated during most of the winters since mid 1980's. This behaviour is consistent with the behaviour of the extreme temperatures shown in Figure 4.2. Another interesting feature in these figures emerges if the behaviour of total nitrogen, water vapour, and the existence of ice-clouds are compared with each other. Basically it seems that while no PSC-type-II processing has taken place, the reproduced NAT-form PSCs give way to some denitrifications. Since no signal of the ice-form PSCs is reflected by the behaviour of water vapour, the only logical conclusion is that during the cases of weak denitrifications the NAT particles have grown to sizes where significant enough sedimentation is possible. This means that denitrification occurs time to time, but the temperatures do not stay low enough, long enough over this altitude range for realization of large scale denitrifications due to ice-form PSCs or large NAT-form PSCs. Nevertheless, during the most evident years (e.g. 2000 or 2013) the drop in total nitrogen over the discussed area is around 40%. These weak signals could be signs of the greenhouse-gas-induced stratospheric cooling, and they will be studied further in the next Section.

Similarly to the analyses in south, Figure 4.15 shows how the different ozone loss processes have contributed to the net ozone loss in the north. As in the southern case, catalytic ozone loss cycles by active chlorine (i.e. ClO_x) are clearly the most significant as they are responsible for about 30 to 60% of the total ozone loss during the northern hemispheric winters/springs. During the 1980's, while the absolute levels of ozone depletions were lower than after mid 1980's, it seems that the processing due to some other process than chlorine, or coupled bromine-chlorine has been significant. This process has been the ozone depletion chemistry due to the NO_x (not shown). The NO_x -chemistry is simulated to have had a more significant role until the early 1990's, and the effects of ClO_x -chemistry and coupled effect of ClO and BrO chemistry become more significant after early 1990's. The comparison of this Figure with the previous timeseries (i.e. Figure

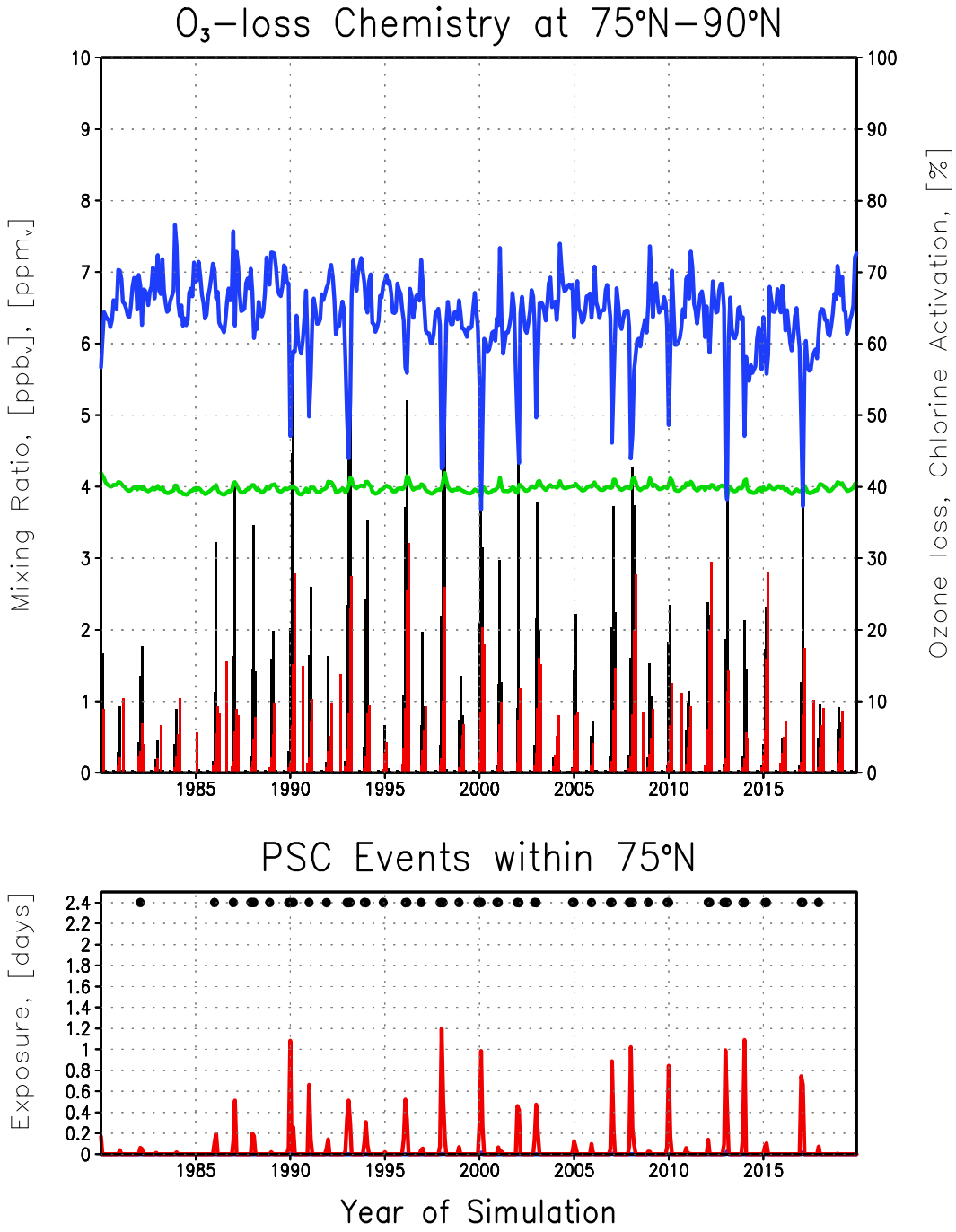

FIGURE 4.14. Simulated average time-series for 1980-2019 of the main constituents affecting ozone within 75N°, and between levels 146hPa and 31hPa. In the upper frame the evolution of chlorine activation is shown by the black line, the evolution of total nitrogen by the blue line (in ppbv), the evolution of water vapour (in ppm_v) by the green line, and the relative difference between the passive ozone tracer and regular model ozone by the red line. In the lower frame the PSC type-I exposure time is given by the red line, the PSC type-II exposure by the blue line, and the events of the tempartures below 195K are denoted by black markers.

4.14) show that each year when the chemical ozone processing indicates arctic-type minor ozone depletion, the ClO_x -processing is the most important process. The changes in the ozone depletion chemistry during the 40-year simulation will be further studied in the next two Sections.

As stated already in the southern case, the chlorine activation, while being a regular phenomenon also in the north, does not alone lead to significant ozone depletion. After the winter season, the stratosphere becomes sunlit, and the active chlorine is converted rapidly back to the reservoirs (like $ClONO_2$ and HCl), provided that significant denitrification has not taken place. In the northern high-latitude stratosphere no signs of Antarctic-type denitrifications exist, and therefore no large scale ozone depletion takes place in the 40-year simulation. While this rather obvious result is in line with the observed behaviour of the Arctic stratosphere, it should be noted, once more, that even in a monthly-mean perspective, the weak signals of these important processes are reproduced. As stated in the case of the Antarctic stratosphere, even inorganic chlorine loading below 2 ppb_v may lead to significant large-scale ozone depletion if the denitrification takes place. Therefore, the possible cooling of the Arctic stratosphere may give way for larger-than-today type ozone depletion events in the north. Although, the comparison between the past and future periods over the arctic areas does not show any clear changes to take place within the simulated period, it should also be remembered that the behaviour of the northern high latitude stratosphere is very different from its southern counterpart, as it is by large a result of the dynamical characteristics. As the northern polar vortex has more complex structures, the processes should be analyzed from a more localized point of view. For example, from the used monthly perspective some signs of the large NAT-particles exist, since in every case when a drop in total nitrogen appears, no signs of ice-clouds or dehydration are exhibited by the model results. In order to study the possible denitrifications caused by the possible formations of large NAT-particles, one should analyze the simulation results from a case-study perspective. Since the scope of this study is in the climate-scale behaviour patterns and changes, I will not analyze these possible occasions of large NAT-particles in detail. However, it should be stated here that if UMETRAC results had had a cold temperature bias over the high northern latitudes, this should have affected the existence of PSCs in the FinROSE results, since the threshold temperatures for the formation of both type-I, and type-II PSCs is quite close to each other (i.e. 6K, or so). Since the FinROSE integration does not exhibit any unrealistic amounts of ice-form PSCs in the north, it may be concluded that the UMETRAC-simulated temperatures give a realistic PSC behaviour over the northern polar areas. Therefore it may also be concluded that the FinROSE-simulated northern hemispheric PSC amounts are reasonable and in line with WMO (2003).

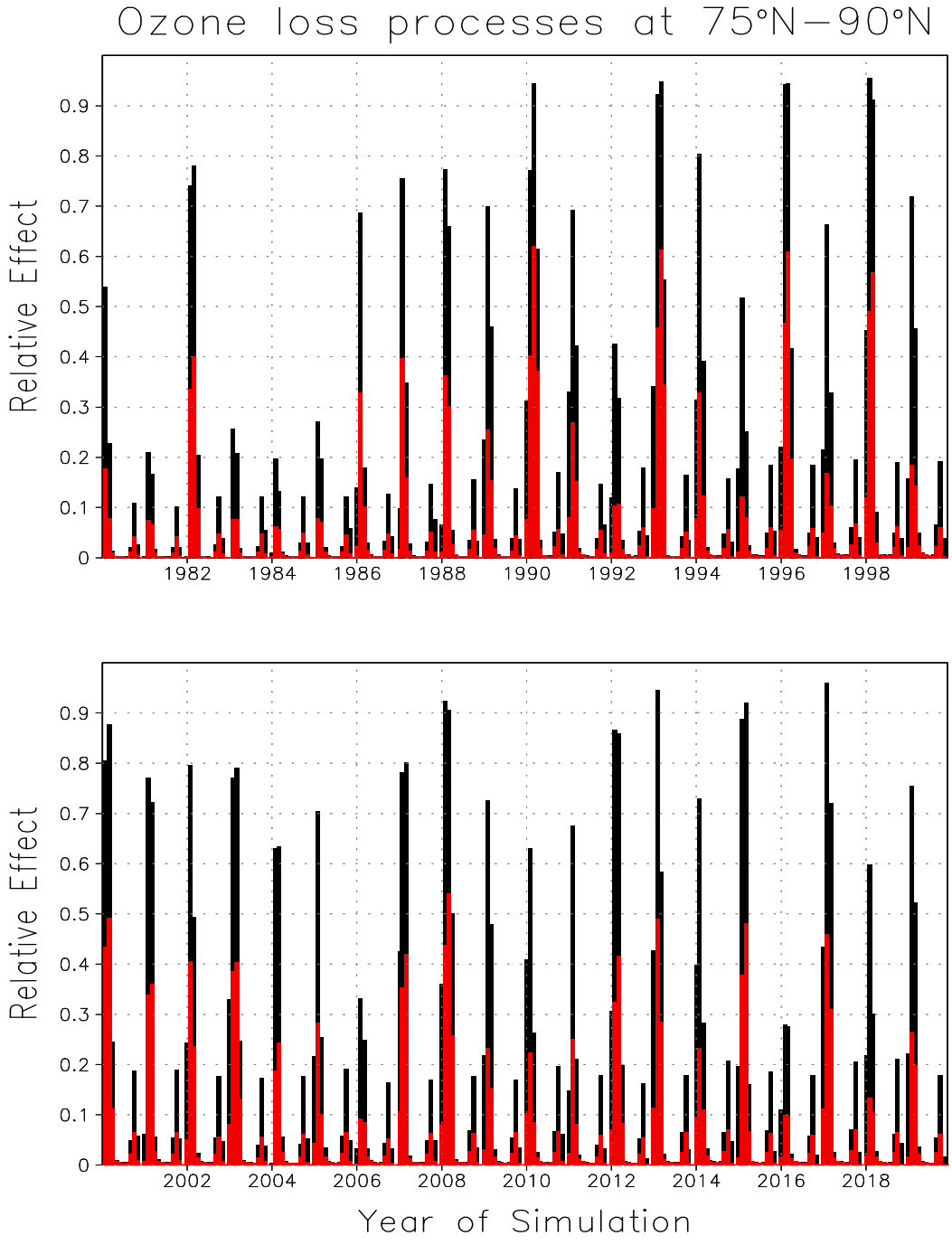

FIGURE 4.15. Proportions of the total ozone loss chemistry due to the two main catalytic ozone loss cycles during the 40-year FinROSE integration. The red portions of the bars show the effect of ClO_x processing, and the black portions show the effect of combined BrO_x - ClO_x chemistry, respectively. The shown values are averaged within the 75°N latitude, and between levels 146hPa-31hPa.

4.7 Analysis of Ozone Changes

In the previous sections of this chapter it has been shown that the FinROSE model is capable of simulating reasonably realistic decadal average behaviour of stratospheric ozone. Moreover, the model results are stable throughout the whole 40-year simulation period with respect to the model's own realization of stratospheric aeronomy, derived from the chemistry-coupled transport characteristics of the driver model (UMETRAC) and compositional characteristics of the FinROSE's own chemistry-scheme. Since the transport characteristics of the driver model include the radiation coupling between atmospheric chemistry and circulation, and therefore the effects of long term changes of green-house gas concentrations (i.e. CO_2, CH_4, chlorine and bromine loadings in this study), it is reasonable to assume that the FinROSE-simulation also carries the same greenhouse-enhancement signal, and it is now possible to apply trend analysis to the achieved results.

As a start point for the analysis of the high latitude ozone changes, I show Figures 4.16 and 4.17. In these figures the differences between the simulated annual average ozone climatologies are shown as a difference between the climatology of 1980-1984 with the respective climatology of 1995-1999 (i.e. near past change), and difference between the ozone climatology of 1995-1999 with the climatology of 2015-2019 (i.e. near future change). Figure 4.16 shows these differences from the mixing ratio perspective, and Figure 4.17 in units of ozone partial pressures. In Figure 4.16, the past period difference shows decreasing of ozone mixing ratios throughout the whole stratosphere. In the Antarctic polar stratosphere this difference has its maximum, being over $300ppb_v$ around 50hPa, while in the north the respective stratospheric decrease is around 100-150ppb_v , depending on the altitude. During the future period, in line with the previous discussions in this chapter, no clear manifestations of either increases or decreases are exhibited. However, model simulates a slight increase of $50ppb_v$ near 50hPa, over the southern polar areas, and a similar increase in the upper stratosphere, while over the northern polar areas an increase of order of $50ppb_v$ is simulated throughout the whole stratosphere above 100hPa. A comparison of the differences in mixing ratios, with the partial pressure differences shown by the Figure 4.17, indicates that the ozone decreases on both poles are clearly manifested, and reproduced by the model. Over the southern polar areas simulated changes are more than -2mPa , near 68hPa from 1980-84 to 1995-99, while over the northern polar areas the corresponding value is more than -1mPa , but at a somewhat lower level than in the south. Since the partial pressure is a measure of the absolute volume of ozone, and therefore directly correlated with the total ozone column abundance, Figure 4.17 also suggests that the FinROSE results are stable since the changes outside the polar stratospheric areas are close to zero, and the changes take place over the expected areas (e.g. high-latitude south). During the future period, again,

the partial pressure perspective only indicates modest changes in the ozone levels. Values are very close to zero in the south during the future period, but a slight growth of around $0.5mPa$ is indicated near 100hPa. The analyses shown in this Section will be further deepened in the next Section where the statistical significance of these changes will be discussed using the framework of trend analysis.

4.8 Ozone Trend Estimates

In order to gain responses to the original objectives of this study (see Chapter 1), I will now present my trend estimates for both the near-past and near-future polar stratospheric ozone changes. In this section I will first validate the annual average ozone trends calculated from the FinROSE results against the corresponding trend estimates calculated using the TOMS ozone measurements, and compare these trends with those exhibited by the UMETRAC results. Secondly, I will show seasonally and zonally averaged trend estimates for both total ozone, and vertical distributions of ozone mixing ratios during the past period, and the future periods.

Figure 4.18 shows the latitude distribution of average annual trend estimates of the FinROSE and UMETRAC total ozone for the past period (1980 to 1999), and the comparison with corresponding TOMS (version 8) total ozone trend estimates. Due to the technical limitations of the TOMS-instrument (explained in the beginning of this Chapter) these annual TOMS-trends are calculated only between 60°N and 60°S. The Figure also shows the trend estimates of both models (i.e. FinROSE and UMETRAC) for the near future period (2000-2019). The trend estimates are calculated applying a standard linear regression (i.e. a least mean square fit) to the monthly mean values. The trend errors, based on the Student's T-test, are given at the 95% significance level. Basically the error bars show if the regression coefficient of the least mean square fit is significantly different from zero at the 95% confidence level. Both models give similar trend estimates as gained from the TOMS measurements, and the overall agreement with measurements is good. During the past period the FinROSE results over the latitudes where TOMS data have been applied with statistical significance (i.e. within 60°S and 60°N), both the actual values and uncertainty intervals of the FinROSE trends exhibit similar behaviour as in case of TOMS. In the vicinity of 60°S the FinROSE's annual average decreasing trend is just slightly less than the TOMS-derived trend. In the case of UMETRAC, the magnitude of the southern trends is somewhat smaller than the corresponding FinROSE trends, and the trend errors exhibit somewhat narrower error ranges. In the vicinity of the northern 60th latitude, the TOMS trends exhibit a turnover that is not reproduced by either model. However, the trend values, as well as the trend errors are again in good agreement with the measured estimates. Over the high polar latitudes

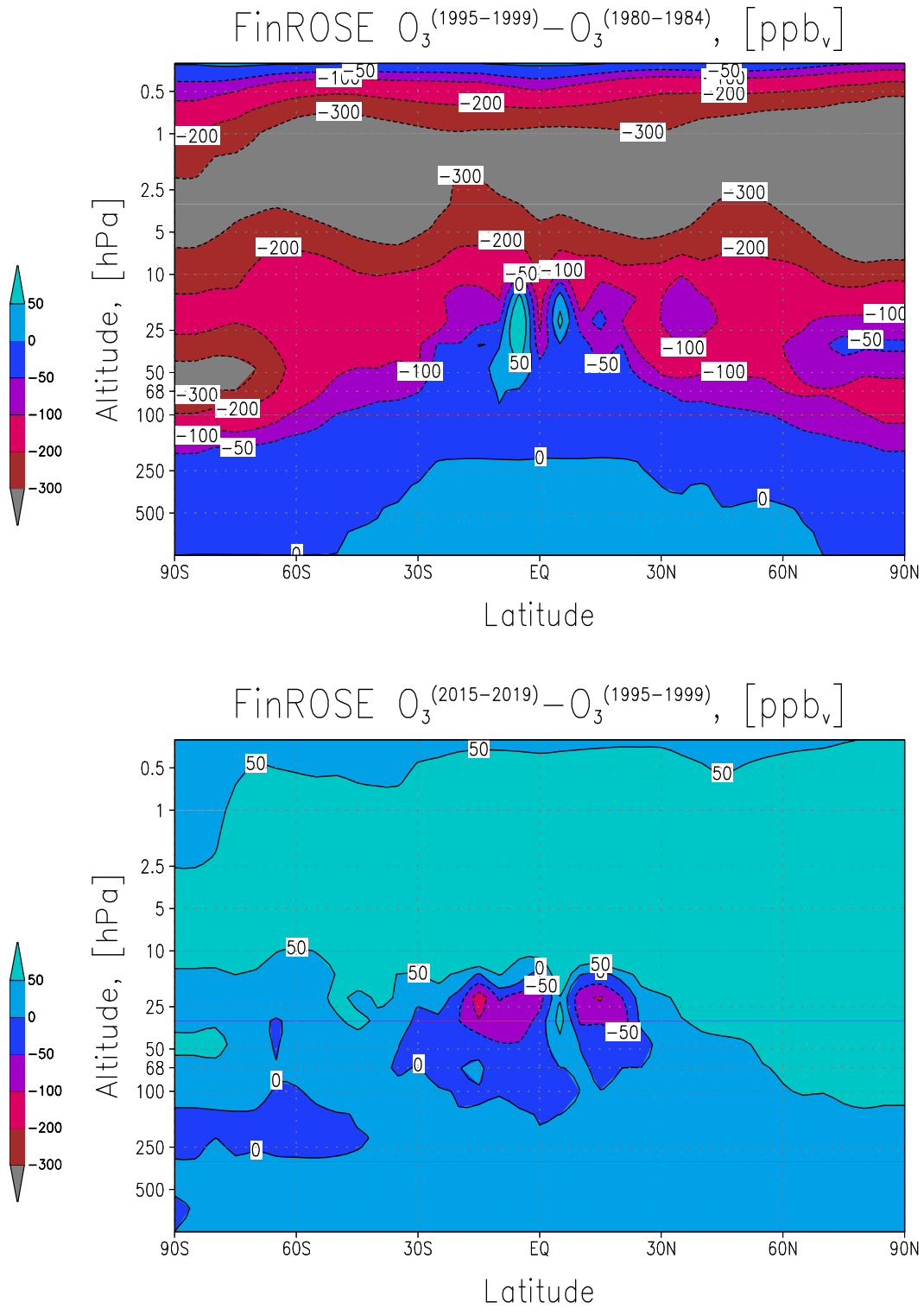

FIGURE 4.16. Ozone changes in average annual zonal distributions. Top frame gives the change between 1980-1985 and 1995-1999. Lower frame shows the difference between 1995-1999 and 2015-2019. Values are shown as mixing ratios.

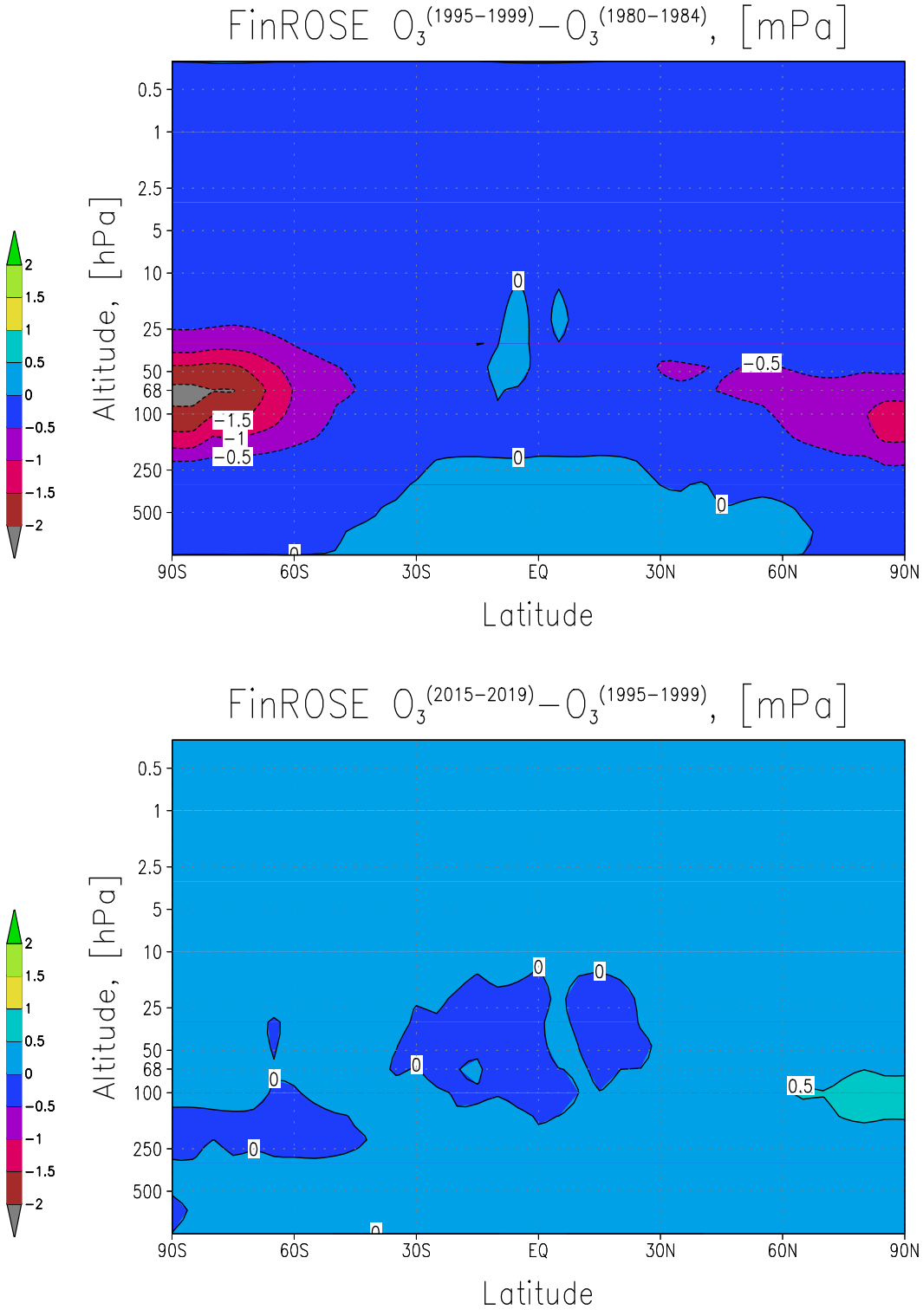

FIGURE 4.17. Ozone changes in average annual zonal distributions. Top frame gives the change between 1980-1985 and 1995-1999. Lower frame shows the difference between 1995-1999 and 2015-2019. Values are shown as ozone partial pressures.

both models give large, statistically significant negative trend estimates. Over the Antarctica the trend is almost -8% /decade in the case of FinROSE, and in the case of UMETRAC, the trend is around -6% /decade. Over the northern polar areas, the FinROSE gives a trend of around -3.5% /decade, and UMETRAC gives around -5.5% /decade. These polar values are very much in line with the trend estimates shown by e.g. WMO (2003, Chapter 4, fig 4-31), Hadjinicolaou et al. (2002) or Fioletov et al. (2002).

During the future period the average annual trend estimates (in Figure 4.18) of both models are similar over the high southern latitudes. Both models exhibit statistically non-significant small 2 to 3% positive trends per decade. Over the northern polar areas the results of the two models are almost alike; the UMETRAC trend estimates give a positive trend around 3% /decade which is clearly significant at 95% confidence level while FinROSE gives basically the same trend with a somewhat larger error range while still significant at 95% level. From the annual average perspective both models are therefore suggesting that over the high southern latitudes, a small increase in total ozone may take place by 2019, but since the statistical significance is low, the ozone depletion may stay more or less the same as it has been during the 1990's. Over the northern polar areas, however, on the annual average point of view, the statistically significant negative trend over 1980-1999 is simulated to be replaced by a statistically significant positive trend which in turn could be a sign of a start of the ozone recovery. These results are in line with those presented by Figures 4.16 and 4.17.

Similarly to Figure 4.18, Figure 4.19 shows the latitude distributions of seasonal total ozone trend estimates for the past period. As in the case of average annual trend estimates, the seasonal estimates of both models are also in good or reasonable agreement with the TOMS trends. The northern high latitude winter months (i.e. December, January, and February) exhibit in both models very similar behaviour. For example, over the northern high latitudes the trends fall between -5% /decade and -8% /decade, being significant at the 95% confidence level. These results suggest the importance of dynamics in the northern polar region, as already stated in earlier sections. During the spring months (March through May), both models agree over the high northern latitudes reasonably well with the measured trends. While TOMS gives a significant negative trend of around -7% /decade, the FinROSE reproduces a trend of around -5% /decade which is still significant at the 95% confidence level and the UMETRAC reproduces a clearly significant trend around -9% /decade. In WMO (2003) it was stated that most models underestimate the amplitude of the seasonality due to the underestimation of the springtime ozone losses. From a comparison of these winter- and springtime trend estimates with somewhat lower trend estimates discussed by WMO (2003) (i.e. between -2% /decade and -5% /decade), I may conclude that the trends captured by either FinROSE or UMETRAC, are not generally underestimating the seasonality of the ozone behaviour. However, it remains somewhat unclear

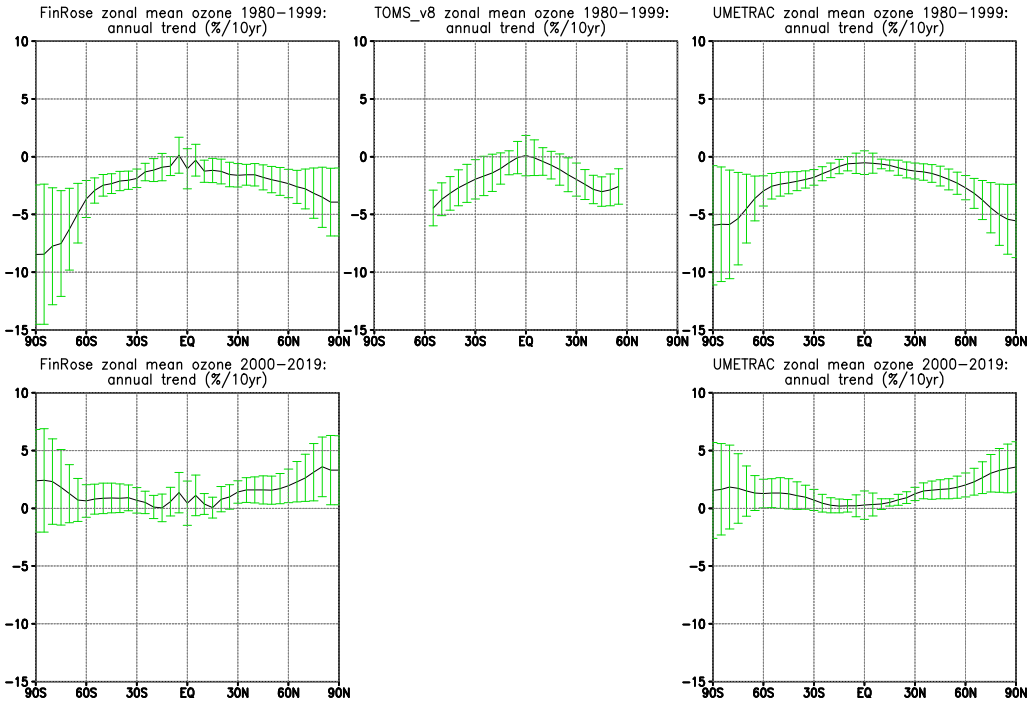

FIGURE 4.18. Annually averaged total ozone trends [% /decade]. The errorbars indicate the confidence intervals at 95% level. The confidence levels are calculated using the Student's T-test.

whether this good agreement is due to the successful reproduction of circulation characteristics, and profound treatment of chemistry, or whether the result is just coincidental.

The southern high latitude trends, shown in Figure 4.19 follow the observation based trends similarly to the north. During the austral winter (June-August), both models are reproducing the observed trends nicely. During the austral spring (September-November), the most visible feature in this figure is the large, statistically significant (at 95% confidence level) negative trend of total ozone. Around 80°S, the TOMS and FinROSE trend estimates agree with around -18% /decade trend, while UMETRAC simulates around -12% /decade statistically insignificant trend. In the case of FinROSE also the trend errors are in good agreement with the TOMS trend errors, suggesting that the interannual variability simulated by FinROSE is of same order as that of TOMS. While over the northern polar areas the dynamics were suggested as a reason behind the similarities in the model trend estimates, over the south these differences are in line with the discussions given in previous sections, suggesting that the ozone depletion chemistry is of primary importance. As already discussed, the chemistry scheme implemented to FinROSE has somewhat more profound treatment of both gas-phase chemistry as well as a more profound treatment of polar stratospheric clouds and their gravitational

settling than that implemented in UMETRAC.

Another interesting feature shown by Figure 4.19, are the trend estimates for other than winter-spring high-latitude cases. For example, the statistical significance of the austral summertime trend, given by FinROSE, over Antarctica seems to give better comparison with measurements than the trend estimates by UMETRAC. However, the analysis of summertime ozone behaviour, midlatitudes, and tropics is outside the scope of this study, and the analysis of these model features is left to another work.

In Figure 4.20 the seasonal trend estimates for latitudinal total ozone behaviour in the near future (2000-2019) are shown for both FinROSE and UMETRAC. In general terms both models agree that the wintertime and springtime total ozone will increase over the poles. For the winter-spring seasons of the north this increase is around 3-5% /decade, and in the south during austral winter-spring, the increase is around 2-3% /decade in the case of FinROSE, and 2-5% /decade in the case of UMETRAC. While the trend estimates are in agreement, the confidence levels, however, are somewhat different. During the winter months (December through February), the positive northern polar trends in the UMETRAC simulation are clearly significant at the 95% confidence level while the corresponding FinROSE trends are statistically significant only around the 60°N. Since both models are basically similar with respect to the atmospheric transport, this indicates that the differences are due to the greater variability produced by the chemistry scheme in FinROSE. A similar difference is also clear in the case of southern high-latitude winter and spring. The results of Austin and Butchart (2003), as well as those in Austin et al. (2003b) suggested that the turnover of ozone trends would start around 2005. This turnover should further enhance after 2020. My results are very much in line with these results. However, differences between these results exist. While the trend estimates from UMETRAC show a slight but significantly positive trend during the future, FinROSE results rather indicate that the negative ozone trends are levelling off during the near future, and that this will be exhibited as increased interannual variability. From the results of both models it is, however, quite straightforward to draw a conclusion (supported by e.g. Weatherhead et al., 2000 or Austin and Butchart, 2003) that no unambiguous signs of the ozone recovery are likely before the year 2020. As these kinds of analyses are highly speculative and disturbed by e.g. interannual variability (see e.g. Weatherhead et al. 1998, 2000), the rest of this type discussion will be left to the next chapter. However, summarizing these trend estimates for total ozone, I may say that: i) The simulated patterns in the near past agree with the observed patterns well, ii) The usage of the CTM-approach seems to give somewhat more realistic trend estimates than the driver model (UMETRAC), iii) The near future positive trends over the high winter-spring latitudes are less significant in the case of FinROSE than in the case of UMETRAC probably because interannual variability is larger in FinROSE. Furthermore, the future ozone trends

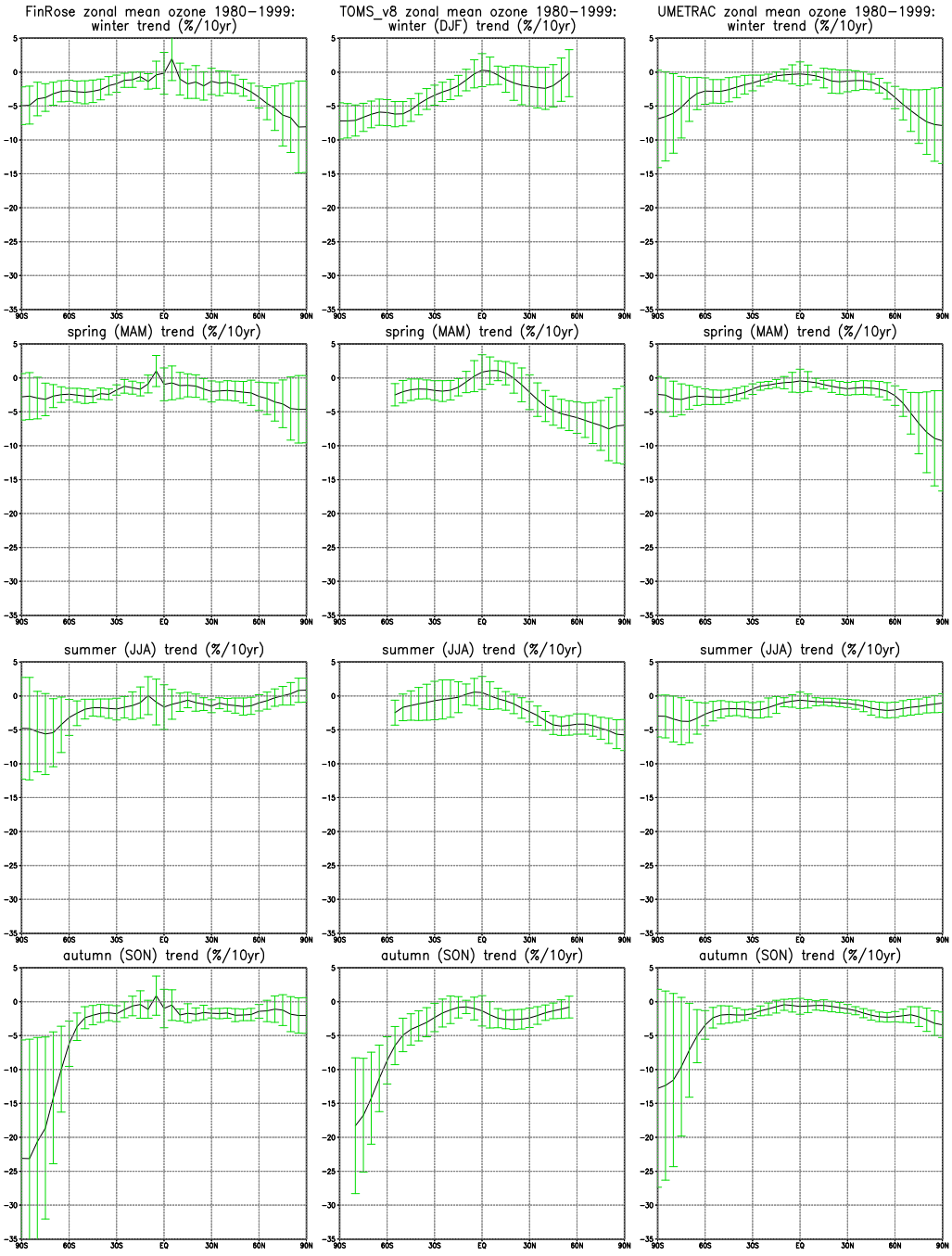

FIGURE 4.19. Seasonally averaged total ozone trends [% /decade]. The errorbars indicate the confidence intervals at 95% level. The confidence levels are calculated using the Student's T-test.

estimated by UMETRAC and FinROSE results do not give clear manifestations about the statistically significant ozone recovery suggesting the need for longer model integrations for the predictions of ozone recovery.

Figure 4.21 shows vertical cross-sections of the FinROSE-simulated seasonal trends for the past period focusing over the high latitudes. During the past period negative trends above 250hPa and below 10hPa are typical during all seasons. During the northern hemispheric winter, the statistically most significant (confidence 95%, or more) trends are between -5% /decade to -10% /decade above 100hPa, and north of the 65°N latitude. The maximum trend during the northern hemispheric winter is, however, located between 250hPa and 150hPa, being around -15% /decade (without statistical significance). This large negative trend is associated with trends in tropopause height, and it will be further discussed below. During the northern hemispheric spring the lower stratospheric decreasing trend of ozone disappears above 40hPa while the negative trend below 40hPa stays negative. Similarly to the wintertime trend estimates, a statistically significant trend between -5% /decade to -10% /decade is found between 150hPa and 50hPa, while the maximum negative trend of around -15% /decade is located between 250hPa and 150hPa. In the spring, this upper tropospheric, lower stratospheric trend is significant at 90% level within 75°N.

Over the southern hemispheric high latitudes (in Figure 4.21) the wintertime trend estimates are somewhat different. While downward trends are typical over the whole domain shown, the statistical significance of the downward ozone trends south of 75°S, and below 10hPa, is weaker. At the 95% significance level a trend between -5% /decade to -10% /decade is found only between 25hPa and 10hPa, and the statistically most significant trends are exhibited south of the 75°S around 30hPa. During the austral spring, however, the situation is quite clear; The Antarctic ozone depletion is manifested with trend estimates below -40% /decade south of the 75°S latitude between 150hPa and 50 hPa. These trend estimates are also significant at 99% level. These trend estimates of the Antarctic ozone depletion are basically well understood, and known to be related to the increasing halogen amounts (see e.g. WMO, 2003). These seasonal trend estimates are also in line with the observation-based trend estimates shown by Randel and Wu (1999).

Simulated trends for the future period are shown in Figure 4.22. A very general conclusion of the northern polar stratospheric ozone trends is that they are slightly positive, but statistically not significant within the area of interest. The same is true in the case of southern hemispheric wintertime trends (i.e. summer months from June to August). During the austral spring a small downward trend of ozone is found close to 30hPa south of 70°S, though without statistical significance. Austin and Butchart (2003) concluded that these kinds of trend estimates are indicating that the ozone trends are affecting the temperatures. The work by Shine et al. (2003) is stating that the future temperature trends are probably dominated by the increases in the greenhouse gases. In addition, WMO (2003) is

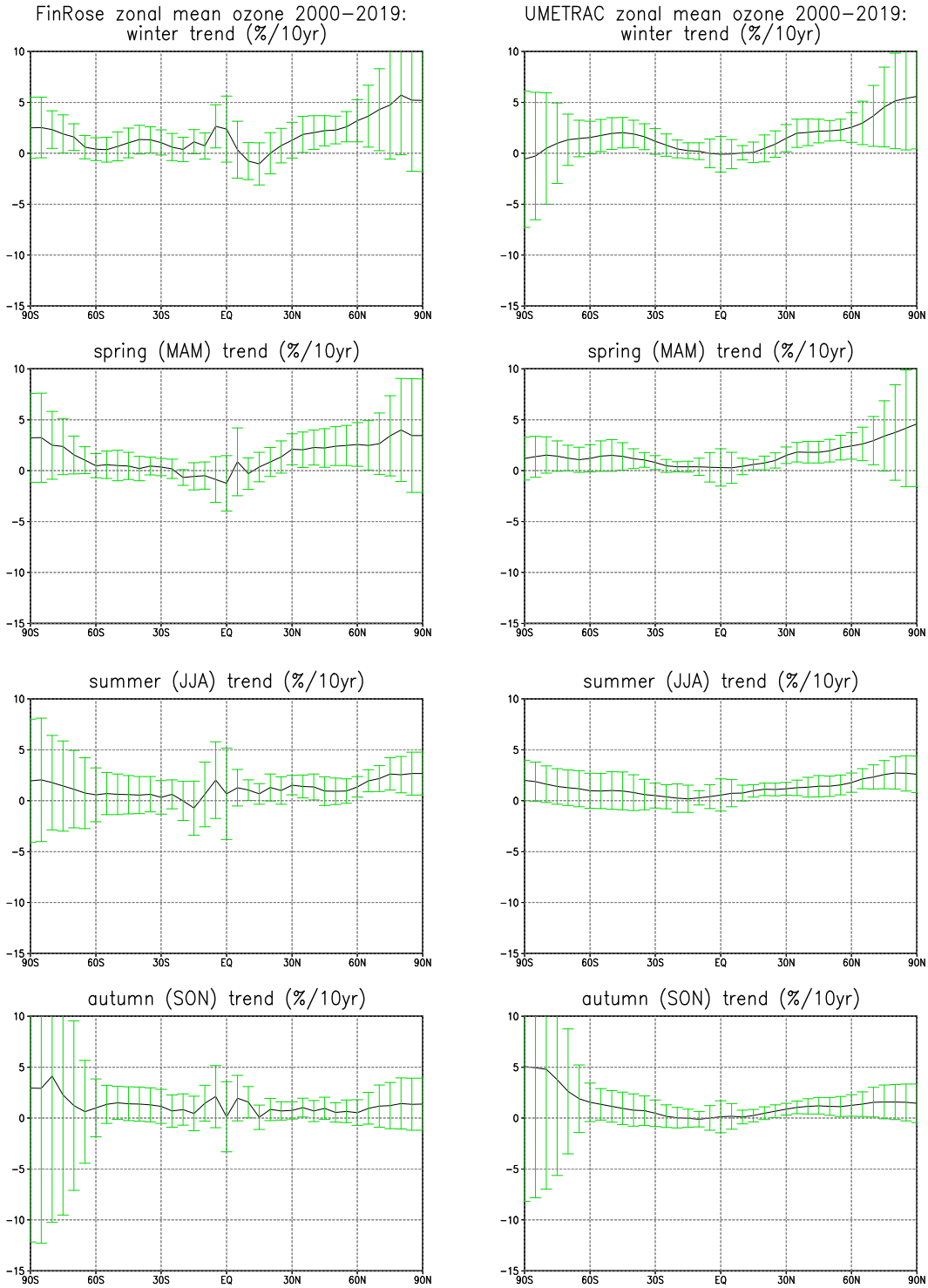

FIGURE 4.20. Seasonally averaged total ozone trends [% /decade] for the future period (2000-2019). The errorbars indicate the confidence intervals at 95% level. The confidence levels are calculated using the Student's T-test.

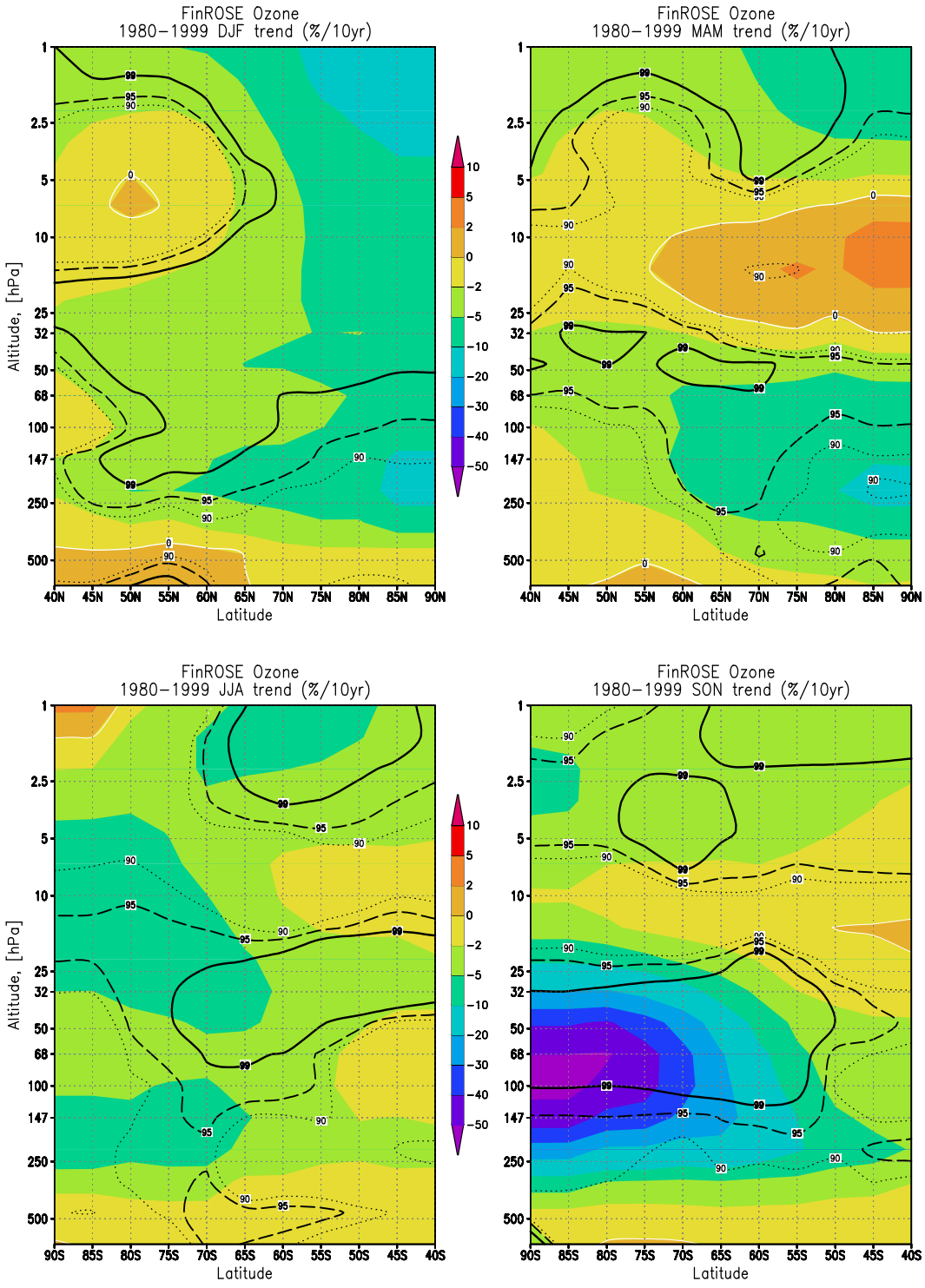

FIGURE 4.21. Vertical distributions of the seasonal ozone concentration trends [% /decade] for the past period (1980-1999). The significance levels are indicated with dotted black lines for 90% significance, with dashed for 95% significance, and with solid black line for 99% significance. White solid line shows the zero trend level.

stating that due to the decreases in the atmospheric chlorine loading, an increasing trend in stratospheric ozone will be seen over the next 50 years. As already seen in the case of annual and seasonal total ozone trend estimates for the future, no clear signal of the start of recovery of ozone is seen in the FinROSE results during the first two decades of the 21st century, and the behaviour of ozone depletion is more like levelling of. Due to the climate change the stratospheric cooling has a potential for enhancing the polar ozone depletion. However, based on the analyses of the ozone trends alone, it is not straightforward to say, if this mechanism is in any way exhibited in the shown results.

The negative ozone trend close to the tropopause in high northern latitudes during winter and spring, shown in Figure 4.21 is in line with a number of recent studies (see e.g. WMO, 2003). The observed dependence of the column total ozone on the tropopause height is quite clear, though the level of understanding is still somewhat limited. In general, the observations have shown that northern hemispheric tropopause over mid- and high-latitudes have risen during the past few decades which imply decreases in total ozone. The connection between the temperature changes, tropopause heights, and ozone changes is discussed in detail in WMO (2003). The results of Austin et al. (2003a) have shown that in the driver model used in this study (i.e. UMETRAC), a statistically significant decrease in tropopause pressures is exhibited over a wide range of latitudes, and furthermore, that over the mid-latitudes this downward trend is about 1hPa/decade, which in turn is in line with the observed changes (Santer et al., 2003). In WMO (2003) it was concluded that these trends are basically not due to the changes in stratospheric ozone, and thus radiatively driven, but due to the changes in tropospheric circulation. As a conclusion on this subject, I may now state that the 40-year simulation with FinROSE also exhibits this observed connection between the tropopause heights and ozone. However, as WMO (2003) states these changes are tropospheric circulation driven, and therefore I leave any further discussions on this particular matter, together with the discussions on the expected future developments, as a subject for a future work.

4.9 Analysis of Denitrification Changes

As stated by e.g. WMO (2003), the relationships between the ozone depletion, changes in atmospheric halogen loadings and low temperatures are quite clear, and well understood. Therefore, the possible cooling of the stratosphere is of great importance. In order to study the ozone recovery due to the emission regulations, and climate change effects on ozone depletion, one needs to have at least a coarse way for the separation between the effect of changing halogen loadings and stratospheric cooling. This separation can be made if the effects of halogen regulations are considered as precursors for the ozone recovery, and possible

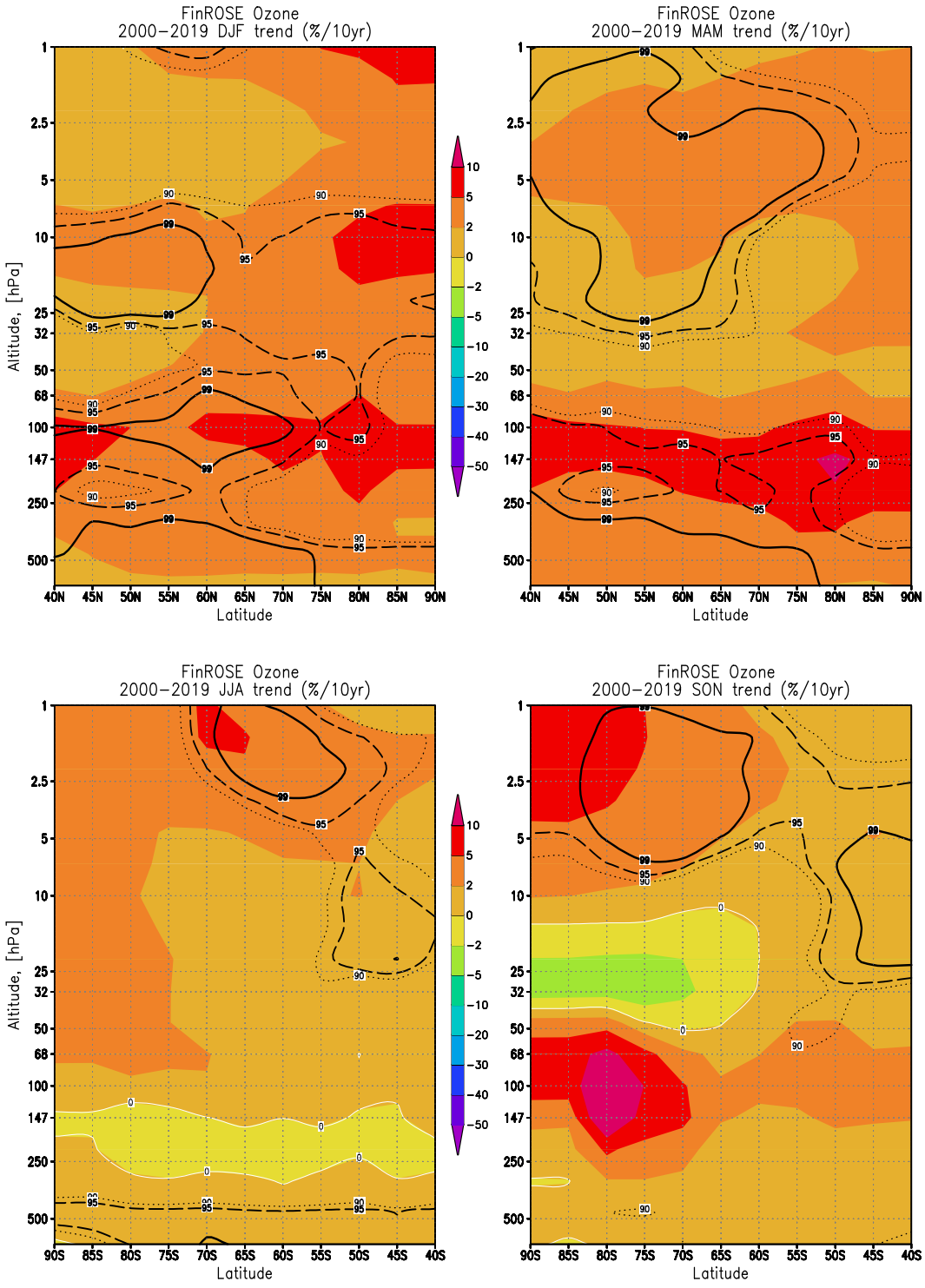

FIGURE 4.22. Vertical distributions of the seasonal ozone concentration trends [% /decade] for the future period (2000-2019). The significance levels are indicated with dotted black lines for 90% significance, with dashed for 95% significance, and with solid black line for 99% significance. White solid line shows the zero trend level.

trends in denitrifications as precursors for ozone-climate interactions. From the model's point of view these two major players are both connected with the formation of PSCs. The results shown in the previous sections are clearly in line with the well-understood mechanisms behind the ozone depletion (see e.g. WMO, 2003), stating that large-scale ozone depletion is possible only if there is enough active chlorine, and low-enough temperatures. Low temperatures give way for the formation of ice-form PSCs, or NAT-form PSCs persisting long enough for the grow-up to sizes where sedimentation becomes an effective removal mechanism for atmospheric nitrogen. While chlorine activation is clearly an essential process for chemical ozone depletion itself, it is the process of denitrification that is required for a large-scale ozone loss since the mechanical removal of nitrogen in turn gives way for the actual ozone loss processes due to chlorine or bromine. As already shown in the previous sections, the process of denitrification, while regular, and frequent in south, does not take place in the north on a large-scale climatological basis with Antarctic-like profoundness. However, in the northern polar case, occasions where denitrification has taken place exist to some degree (see e.g. WMO, 2003). These events take place on a more local scale, and are not due to the sedimentation of the ice-form PSCs, but due to the sedimentation of grown NAT-form PSCs. These events in turn are reflected in the behaviour of northern hemispheric polar ozone.

As was explained in Chapter 2, the springtime polar stratosphere may cool as a result of several processes, including the increases in WMGHGs, ozone loss, possible stratospheric water vapor increases, and natural variability. In order to estimate the possible trends in the behaviour of PSC induced denitrifications which are consequences of stratospheric cooling, I show Figure 4.23. This figure shows the vertical distributions of simulated seasonal NO_y trends. It should be remembered here that the UMETRAC simulation included a prescribed projection for increasing of the NO_y in the atmosphere, and here I'm basically looking for possible decreases. Therefore, the purpose of the Figure 4.23 is to show if the FinROSE results are exhibiting any, seasonally localized, changes in the behaviour of NO_y , contrary to the general increasing projections, over the wintertime and springtime polar areas due to the changes in stratospheric temperatures.

As Figure 4.23 shows clear negative trends are seen over the both poles during the respective winter periods. The statistical significance of these trend estimates, however, is weak, since in most of the cases the trend estimates are significant at confidence levels lower than 90%. During the winter months (December-February) there is a clear negative trend of more than -5% /decade between the levels of 150hPa and 25hPa in the north, while the winter season in the south (i.e. June-August) exhibits downward values that exceed -10% /decade between the levels 50hPa and 30hPa. The overall patterns of these wintertime trends are also very different. Over the Antarctica the trend is clearly isolated by statistically significant positive values suggesting that there is a clear connection between the ozone

depletion itself and the simulated NO_y trend. Over the northern wintertime high latitudes the negative values are seen on much broader areas extending to the mid-latitudes at around 40hPa. The analysis of Figure 4.23 indicates that some connection between the temperatures and NO_y is possible since the NO_y trend estimates (while not statistically significant) are in line with those given by the regular temperature trend analysis discussed by Austin & Butchart (2003), Austin et al. (2003b), Shine et al. (2003), as well as WMO (2003).

The springtime NO_y trends over northern polar areas (in Figure 4.23) are smaller than the trends in winter. However, negative trends (e.g. less than -3% /decade) extend further in the south close to the level of 50hPa (i.e. around 20km) than in winter and these trends are actually significant at 95% significance level. This result is in line with the discussion given with respect to the Figure 4.2, suggesting that the actual PSC events have become more frequent in the vicinity of the northern wintertime vortex edge, either due to the larger and longer persisting vortex or due to colder vortex. The springtime (SON) results for the south are qualitatively similar to those for the north but without statistical significance. In the southern case, however, the absolute values are actually smaller than in the north, and the level of decreasing NO_y is somewhat lower than in the northern case. The results shown in Figure 4.23 (as well as in Figure 4.2) are also in line with WMO (2003), where it was noted that the Antarctic ozone depletions have become more persistent during the 1980's, and that during the 1990's the vortex has lasted until late November to early December.

The simulated near-future trends of the high-latitude wintertime and springtime NO_y are shown in Figure 4.24. Again, these results correlate with the simulated behaviour of near future temperatures. During the northern hemispheric winter months the model predicts a statistically significant negative trend of more than -3% /decade in the middle stratosphere around 15hPa, north of 70°N. In the lower stratosphere, in the levels of ozone maxima, however, the trend is positive, and statistically insignificant. During the northern hemispheric spring, the negative, statistically insignificant trends off less than -2% /decade dominate between the levels of 50hPa and 20hPa, and lower down the trends are generally positive. This result suggests that in the near future, the enhanced denitrifications are probable above the ozone maximum and close to the polar vortex edge areas. In the southern winter, denitrifications, similarly to the north, are simulated to increase further at the higher levels around 15hPa. However, these trend estimates are not statistically significant. Lower down the southern wintertime trends (around 40hPa) of NO_y are positive but statistically non-significant, and further down, around 140hPa, insignificantly negative. During the austral spring, similarly to the north, the negative trends, around 20hPa, increase in magnitude exceeding -5% /decade between the latitude belts of 65°S and 75°S where these trend estimates are significant at 95% confidence level. These simulated NO_y trends are suggesting that over the polar areas future increases in the denitrifications are

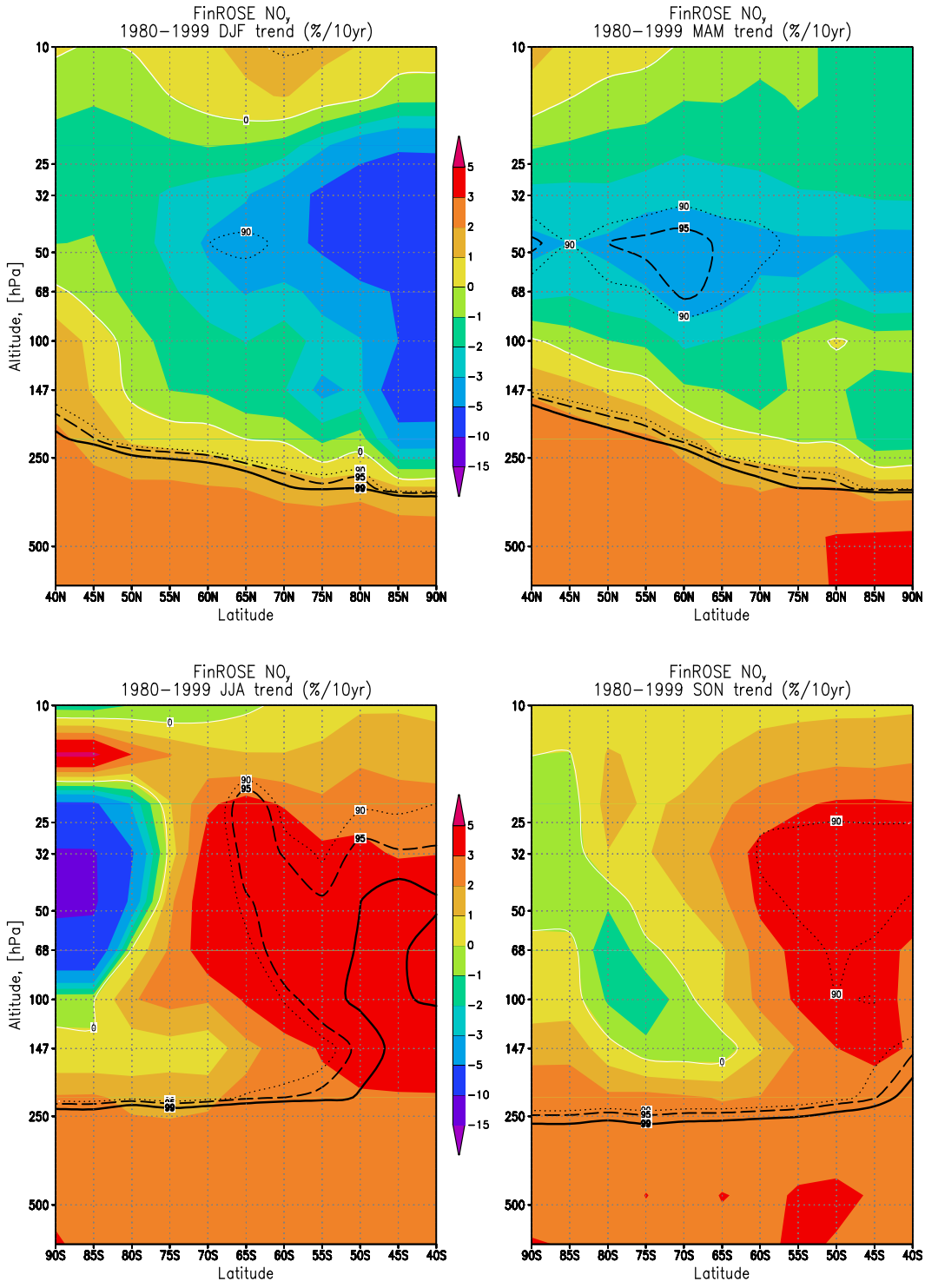

FIGURE 4.23. Vertical distributions of the seasonal total nitrogen (NO_y) concentration trends [% /decade] for the past period (1980-1999). The significance levels are indicated with dotted black lines for 90% significance, with dashed for 95% significance, and with solid black line for 99% significance. White solid line shows the zero trend level.

most probable in the upper parts of the ozone maximum. This result is comparable with the suggestion by Austin and Butchart (2003) that the best place to look for the future atmospheric climate change induced ozone change is the upper stratosphere. The NO_y trend estimates also suggest that the cooling of the northern polar stratosphere does not lead into a clear, statistically significant, decreasing wintertime trend of NO_y during the 40-year simulation.

The effect of the denitrifications on the total ozone column depends on the vertical extent of the denitrification. The depths of the simulated denitrifications are illustrated in Figure 4.25 as a ratio between the monthly average NO_y and the 40-year average NO_y binned by thirds. Over the Antarctica the situation is rather straightforward as the denitrifications are deep (i.e. between, say, 170hPa, and 15hPa) throughout the whole simulation. Over the Arctic the overall situation is also quite as expected; the reductions are both smaller in magnitude, and shallower in vertical extent. Taking the ratios below 0.66 (i.e. the ratio between monthly average NO_y and 40-year average NO_y is less than two thirds) as an indicator for moderate denitrification, such values over the north are typically limited to altitude range of 70hPa to 17hPa corresponding to a depth of around 6km. These results in turn correspond nicely with the values shown by Hintsa et al.(1998), Kondo et al.(2000), as well as by Fahey et al.(2001). The effect of the depths of the denitrifications on column ozone losses was basically seen already in the evolutions of the ozone itself. An interesting feature in Figure 4.25 is the frequency of the moderate denitrifications in the north, since the values below 0.66 seem to become somewhat more common after late 1990's between 50hPa and 20hPa. This behaviour is in line with the previous NO_y trend estimates, again suggesting that the largest future changes are to be found above the actual ozone maximum. In the high-latitude south, however, Figure 4.25 does not give any clear signs of enhanced wintertime and springtime reductions of NO_y .

In this work, a highly simplified scheme for large NAT particle sedimentation was implemented based on the work by Fahey et al. (2001). This simple parameterization makes the formation of effectively sedimenting particles possible above the temperatures required for the ice-form PSC formation. Since only the large enough solid PSC particles cause denitrification (see e.g. WMO, 2003), and since the temperatures below the frost point are extremely rare in the 40-year simulation over the northern polar areas, the model results shown so far are suggesting that the NO_y removal due to the large NAT particles is basically the reason behind the simulated moderate denitrifications. The short persistence of the temperatures allowing for the growth of the NAT particles, however, prevents the reproduction of strong denitrifications in the simulation. I may also state that these model results are, in general, quite reasonable, and agree with the conclusions made by WMO (2003) on this subject.

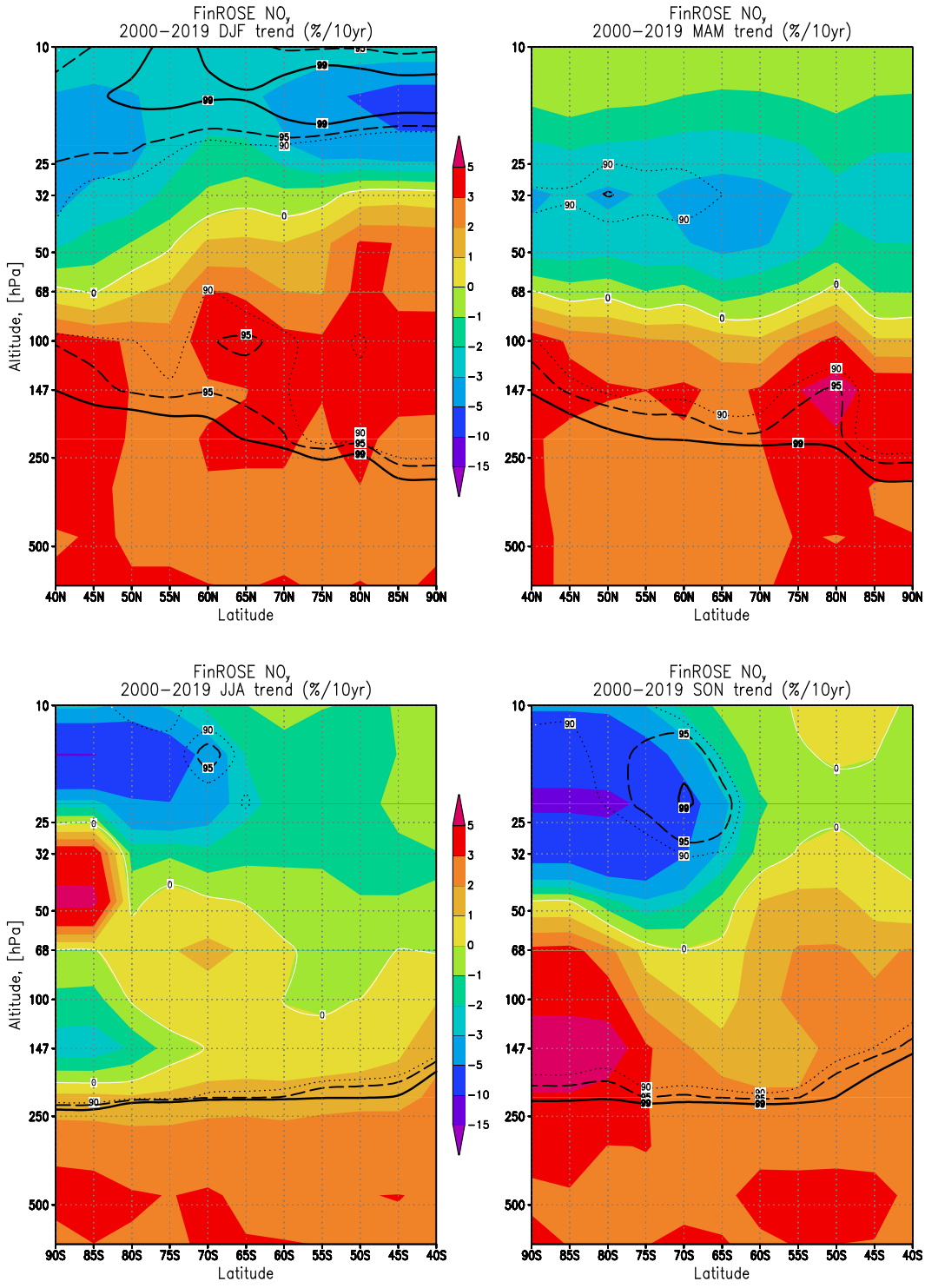

FIGURE 4.24. Vertical distributions of the seasonal total nitrogen (NO_y) concentration trends [%/decade] for the future period (2000-2019). The significance levels are indicated with dotted black lines for 90% significance, with dashed for 95% significance, and with solid black line for 99% significance. White solid line shows the zero trend level.

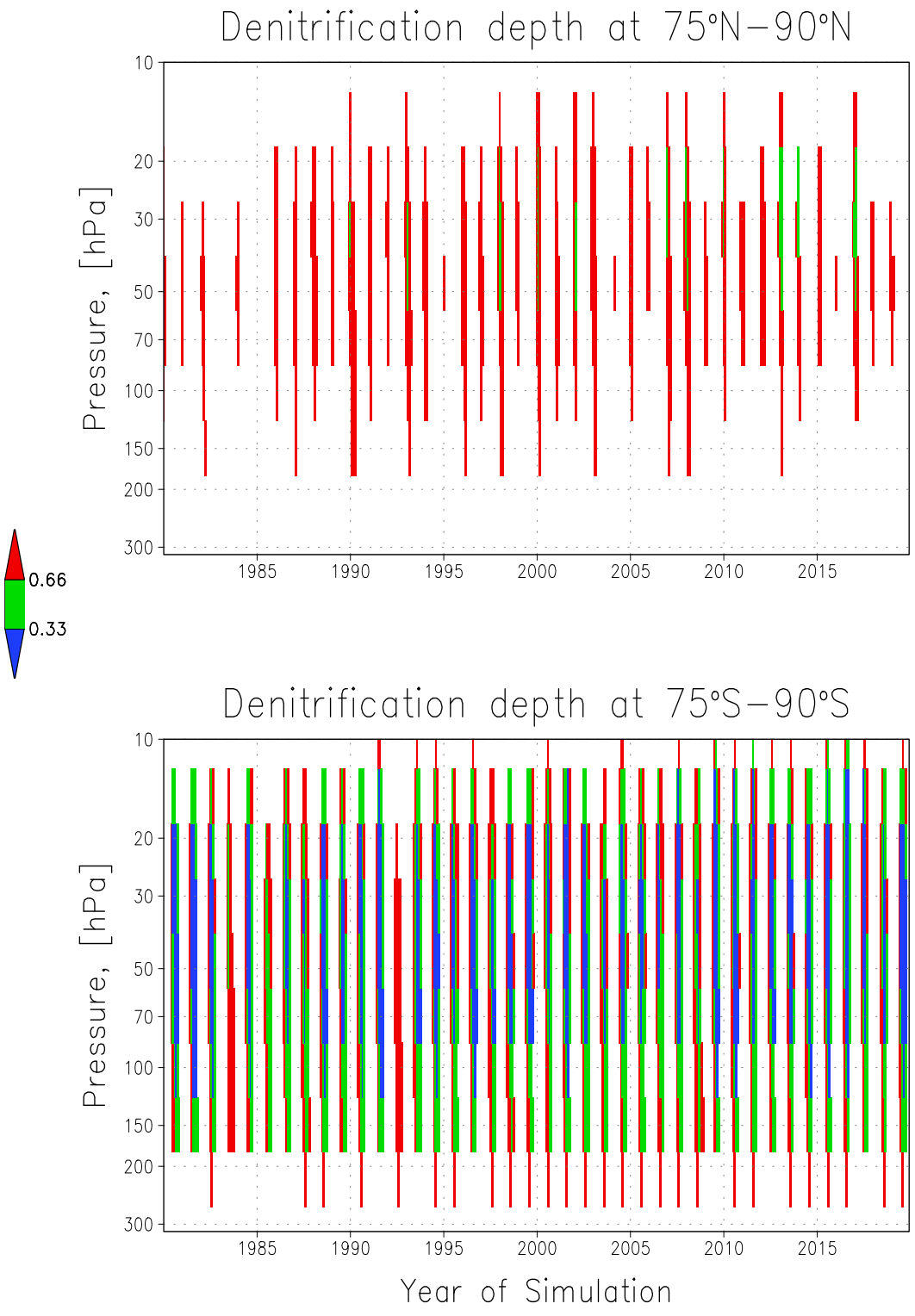

FIGURE 4.25. Vertical distributions of reduced monthly mean NO_y at 75°N–90°N (upper frame), and at 75°S–90°S lower frame. The values shown are the ratios between the actual monthly averages and averages for the whole 40-year simulation (i.e. 1980-2019).

4.10 Changes in the Chemical Processing of Ozone

It is now clear that neither the vertical trend estimates for ozone and total nitrogen, nor the simulated denitrification depths reveal any unambiguous signs of either the start of the ozone recovery, or signs of enhanced ozone depletions in the polar stratospheric areas due to the climate-change related cooling (except for the possible changes in the tropopause height). The lack of statistical significance in simulated NO_y trends, however, cannot be directly connected to the UMETRAC-simulated dynamical changes, and consequent changes in the temperatures. Over the polar areas, the FinROSE results basically indicate that the denitrifications will continue as they have since mid 1990's. Mainly due to the natural variability there will be winter-cases over the northern polar areas where the denitrification mechanism will take place due to the sedimentation of large NAT particles (i.e. grown PSCs type-Ia), and in the southern polar stratosphere the ice-form PSCs will cause the deep denitrifications during the near future in a similar manner as they have during the near past. The actual amounts of chlorine and bromine species in the atmosphere will then in turn steer the magnitudes of the ozone depletions in the near future.

Figure 4.26 summarizes the projected effect of increasing atmospheric chlorine and bromine loading on stratospheric ozone, and compares this effect with the behaviour of NO_y and normalized ozone evolution over the South Pole at the level of 46hPa. The values have been normalized simply between the time-series maximum and zero for each parameter shown. The analysis of this figure shows how the two major players have affected the behaviour of ozone. The increasing chlorine loading is clearly driving the development of the deepening minimum ozone from early 1980's until the mid 1990's while the strong denitrifications, expressed here as effective denitrification (i.e. in terms of 1-$[NO_y\ ]/[NO_y\ ^{max}]$), take place over the South Pole on annual basis during the 40-year simulation (with somewhat less profound years being 1983 and 1992, and to some degree also the year 2017). Since the beginning of the time-series the amount of activated chlorine (ClO_x) increases together with the total chlorine loading. The same is even more visible in the case of total bromine loading and the amount of active bromine (BrO_x). Throughout the whole simulation, catalytic chlorine chemistry is extensive enough to cause the simulated ozone depletions. The relative effect of catalytic chlorine chemistry is showing rather year-to-year-type variations than similar correlation with the chlorine loading projection as the actual chlorine activation does. Since the actual magnitude of the separate catalytic chemical cycles is dependent on the amount of both ozone itself, and on the amount of activated radicals, this behaviour is as expected in the southern polar stratosphere. However, the behaviour of chlorine activation could be signalling that the processes leading to the observed Antarctic ozone depletion do not necessarily need all the available activated chlorine, and even lower amounts of chlorine can produce large

ozone destruction if the denitrification is deep enough over large areas.

The evolution of total inorganic atmospheric bromine, in Figure 4.26, has similar features as the chlorine does; the increase from the beginning of 1980's to early 2000's is quite clear. As already discussed, the bromine peak lags some five years behind the chlorine. Another interesting feature, shown in the figure is the overlapping of the bromine loading and the actual amount of active bromine. This is in line with the earlier statement in Chapter 2 that most of the bromine is already in active form. This result also shows that even on a monthly mean scale all the available bromine is in active form. The coupling between the chlorine chemistry and bromine chemistry is also visible in Figure 4.26. During those years when the magnitude of chlorine chemistry stays low (e.g. year 1992), the magnitude of coupled ClO – BrO -chemistry is also low.

Figure 4.27 gives a similar analysis as Figure 4.26, but for the North Pole. In order to have a comparison with the south, the normalizing of this figure has been done using the same minimum and maximum values as in the case of South Pole. As one may expect, the figure gives rather different results than in the south. Again, the amount of activated chlorine follows nicely the development of the chlorine loading from the beginning of 1980's until the late 1990's. Interestingly, it seems that, while the chlorine activations are more or less typical on annual basis, the magnitude of chlorine chemistry often stays low compared to the south. For example, in the early 1980's much higher values for the chlorine catalyzed ozone depletion chemistry at this particular level occur in the south than in the north. As already stated, the magnitude of the different catalytic cycles, or the chemical loss in general, depends both on the amount of depleted substance itself, and on the amount of catalyzing radicals. In the northern case, I have already shown that the model derives too low values for winter-spring ozone maximum. The FinROSE's incapability for reproducing the actual magnitudes of the northern hemispheric high latitude ozone distributions then yields to too low amounts of ozone, and furthermore to reduced levels of depletion chemistry itself. Since the mixing ratios of stratospheric ozone are typically in the ppm-scale, and the levels of activated chlorine at ppb-scale the resulting effect of having too low ozone levels to start with is expected to be bigger than the effect of ozone depletion chemistry itself. This, off-course, has its effect also on the needed chemical processing for ozone depletion magnitude itself. The unperturbed winter-spring maximum, due to the Brewer-Dobson circulation should be bigger in the northern polar areas than in the south, and as stated already, this is not the case in the FinROSE simulation. The explanation lies both in the chemistry and transport; The age of air results indicated (see Figure 4.3) that the stratospheric air is too young, and that this young air forms the equilibrium quantities different than they would be if the air would be older.

The two discussed models (FinROSE and UMETRAC) have their own chemistry schemes which in turn force the compositional equilibrium levels for e.g. ozone

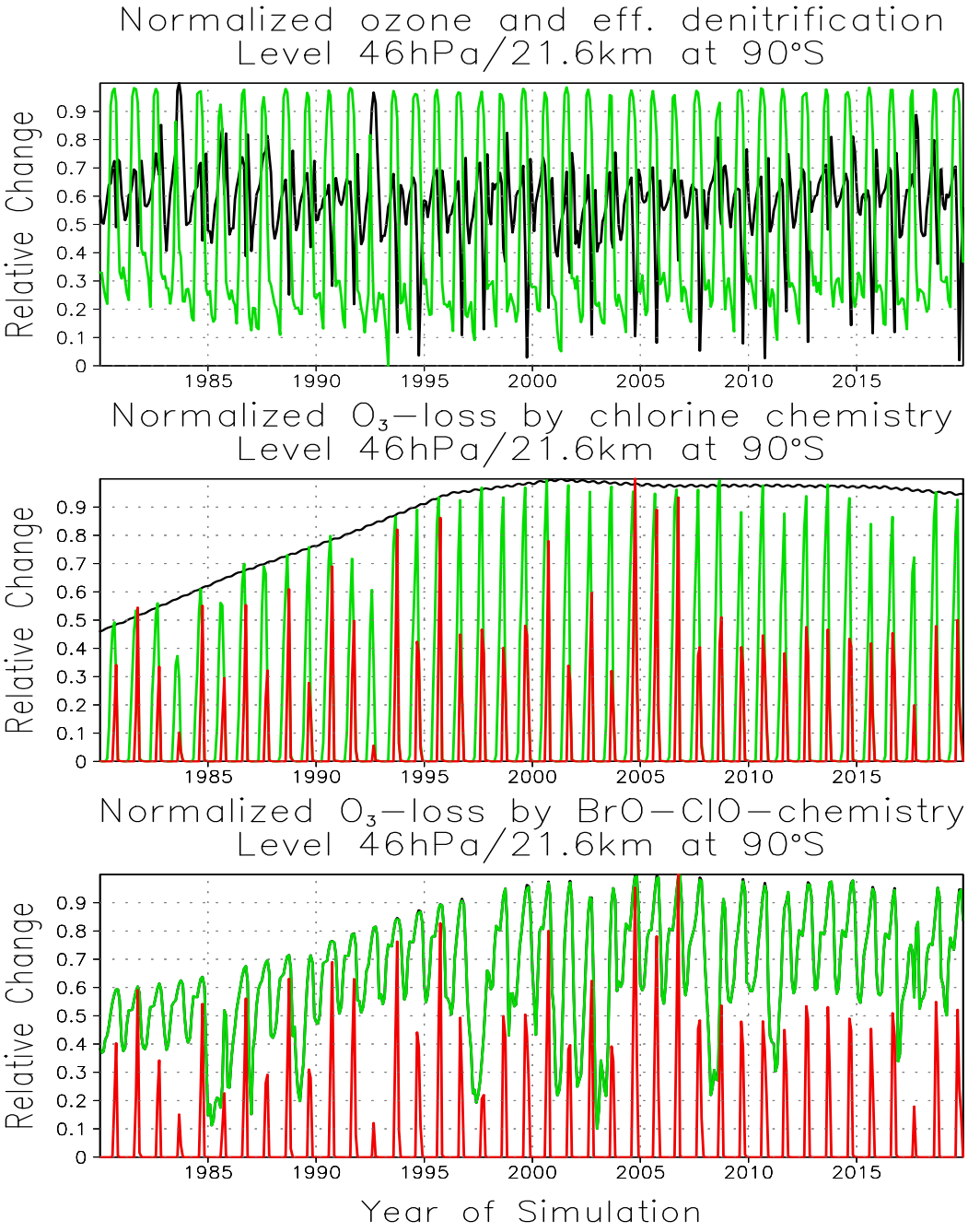

FIGURE 4.26. Normalized monthly mean evolutions of the main processes of ozone depletion over the South Pole at 46hPa. Upper frame shows the normalized evolution of ozone by black line, and the normalized evolution of effective denitrification (1-$[NO_y]/[NO_y{}^{max}]$) by green line. In middle frame the normalized evolutions of total inorganic chlorine (Cl_x), active chlorine (ClO_x), and ozone loss due to the chlorine chemistry are shown by black, green, and red lines, respectively. The bottom frame shows the evolutions of total bromine (Br_x), active bromine (BrO_x), and ozone loss due to the coupled BrO -ClO chemistry by black, green, and red lines, respectively. Note that the evolution of Br_x (black line) is almost completely covered by the evolution of BrO_x (green line).

production and loss over the tropics. Since the FinROSE results are stable throughout the 40-year simulation, it is quite safe to say, once more, that the results over the northern hemisphere high latitudes are imperfect, but reasonable. Furthermore, the described problem is mainly seen on the northern hemispheric ozone alone. The northern hemisphere is more dynamically driven than the south. In southern polar areas the ozone depletion mechanisms due to the axisymmetrical nature of the vortex, and profound denitrifications make the evolution of springtime ozone abundantly chemically driven. This is further emphasized due to the evolutions of chlorine or bromine loadings as they are coupled with the expected projections, or historical measurement-based evolutions, and due to the fact that the evolution of temperature is based on it's evolution in the forcing model. This coupling of the chlorine and bromine loadings with the expected projections also means that while the ozone chemistry clearly suffers from the inadequate reproduction of the Brewer-Dobson circulation, the total loading amounts of halogens are always at reasonable level. This would have not been the case if the modelled amounts of chlorine species would have been produced directly from their source gases, like CFCs, because the slow conversion of the source gases to either chlorine reservoirs or to active forms would have been dependent on the aging process, which in turn would have not been long enough. However, it should be stated that the inadequate reproduction of the Brewer-Dobson circulation is the most severe problem of the FinROSE model itself, and that this problem actually forbids the sensible implementations for the treatment of the source gases. However, I may conclude that the effects caused by the low amounts of ozone, and resulting low level of catalytic ozone depletion are of different magnitude compared to the effects caused by the problems in transport characteristics. Therefore, relatively speaking, I assume that the ozone chemistry is reasonably reproduced also in the north since no unexpected behaviour is exhibited by the model results, and the results are comparatively representative (e.g. the shown trend estimates for the near past).

The results exhibited in Figure 4.27 are based on the evolutions at one single model gridpoint. Therefore the magnitudes and frequencies of denitrifications are more profound in these cases than the results previously discussed (i.e. see Figures 4.9 - 4.11, 4.14, and 4.25). The magnitudes of the North Pole ozone depletions in this Figure 4.27, are basically shown as the missing tops of the annual cycles which in turn have clear correlation with the magnitudes of denitrification events. During some winters and springs in and after the early 1990s the level of denitrification reaches 70%. During those years (e.g. 1990, 1993, 2000, 2008, 2013, etc.) when this around 70%-denitrification is taking place the chlorine and bromine catalyzed ozone chemistry has also visible values. In the case of lower or non-existent levels of denitrification, the model exhibits practically no chlorine or bromine catalyzed chemistry on a monthly average scale. This clear coupling between the denitrifications and chlorine chemistry is a clear manifestation of

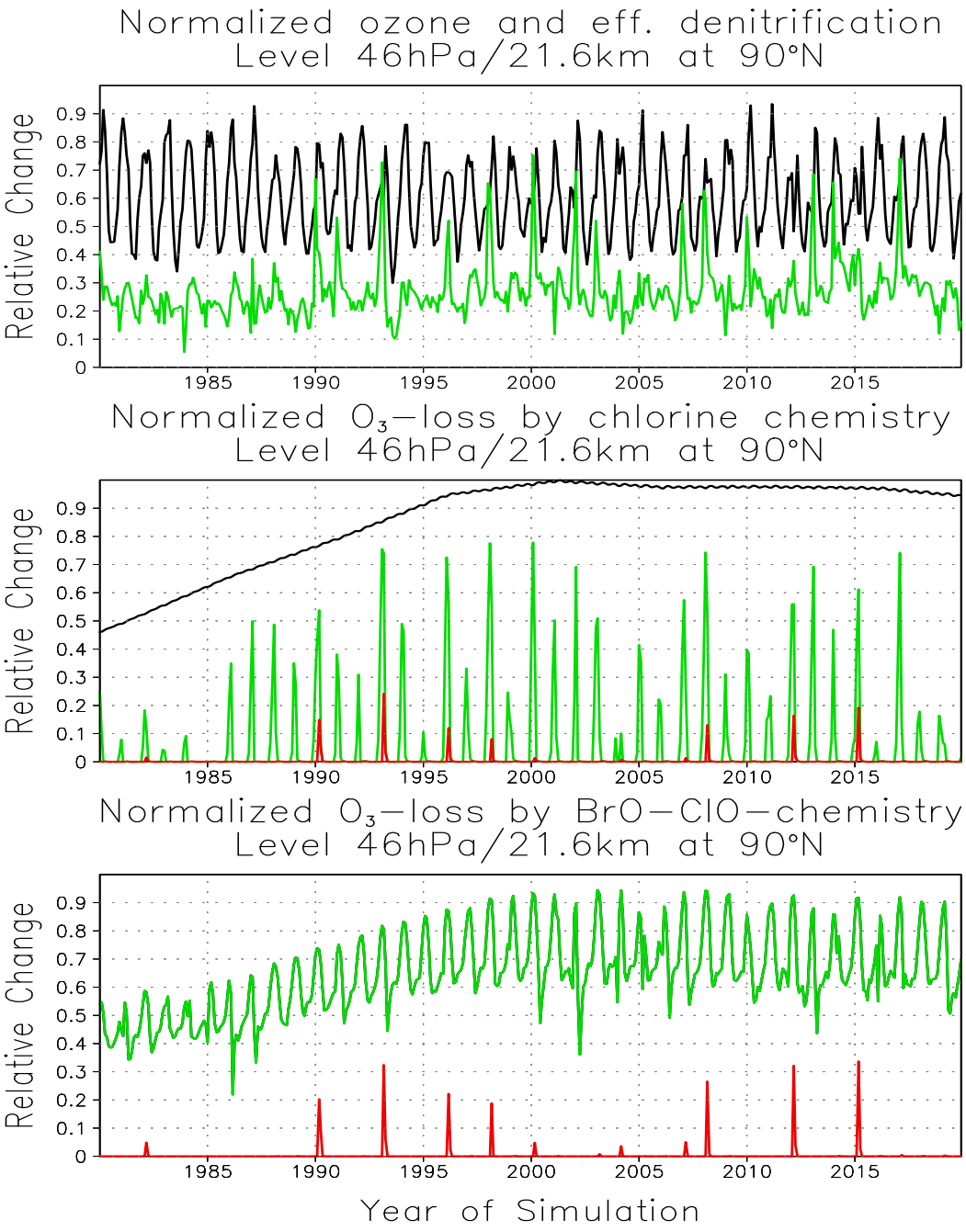

FIGURE 4.27. As in fig 4.26, but over the North Pole at 46hPa.

the importance of denitrification magnitude on the ozone depletion. The actual amount of activated chlorine does not have as visible correlation with the ozone amounts as was the case in the south. It can be actually stated that the activation of chlorine alone does not guarantee the ozone depletion. Remembering that the ozone depletion chemistry itself is dependent on the availability of the solar radiation, this interpretation is clear. The required low temperatures for chlorine activation are taking place effectively enough for causing the resulting, basically annual, chlorine activations, but when the solar radiation becomes available, after the winter period, the activated chlorine converts back to the reservoirs, if no denitrification has taken place. In the case of denitrification events, the mechanical loss due to the sedimentation of either ice-clouds or enlarged NAT-particles makes the chemical destruction of ozone possible as the conversion of activated chlorine back to the reservoirs is not possible. The frequency of these northern denitrification events (in Figure 4.27) seems to increase after early 1990's, after which the frequency stays more or less the same. This result is in line with the trend estimates shown by Figures 4.23, and 4.24, and with the discussions on Figure 4.2, and Figure 4.25.

With respect to the bromine chemistry, an interesting feature in the FinROSE results (i.e. Figure 4.27) is the relative magnitude of coupled bromine-chlorine chemistry compared to the south. It basically seems that the normalized effect of BrO -ClO -coupled ozone depletion is more profound in the north than in the south. This was basically seen already in Figures 4.9-4.11, and 4.14. However, my analysis is not showing any significant trend in these changes during the 40-year simulation (not shown). Otherwise, the evolution of bromine, active bromine, as well as bromine-chlorine catalyzed ozone depletion chemistry is in line with the conclusions made by Chipperfield and Pyle (1998) and WMO (2003).

The monthly mean magnitudes of the ozone depletion and the effects of the chlorine and coupled bromine-chlorine chemistry on total ozone above the poles are shown in Figure 4.28. As described in Chapter 2 one of the main consequences of the stratospheric ozone depletion is an increase in the surface UV radiation which in turn is mostly dependent on the amount of total ozone (in clear sky conditions). The magnitude of the ozone depletion can be derived from the difference between the inert ozone tracer and regular model ozone. Figure 4.28 shows the actual magnitudes of the depleted ozone due to the two main catalytic mechanisms which were already shown to be almost exclusively responsible for the ozone depletions in the southern polar stratosphere, as well as in the northern polar stratosphere during the most profound ozone depletion cases (see Figures 4.12, and 4.15 for comparison). Over the South Pole the overall monthly mean magnitude of the ozone loss is clear. Typically the values exceed 150DUs after early 1990's, and even during the early half of the 1980's the absolute depletion is typically more than 120DUs. This behaviour is, again, a clear manifestation about the importance of the amount of halogen loading in the atmosphere. Over

the North Pole the simulated maximum values are around 60DUs, and in general, quite low or negligible. The modelled 40-year evolution of the ozone depletions is repeating the results revealed by the previously shown trend estimates over both poles. The signals of the ozone-climate coupling or the turnover for the ozone recovery are not clearly manifested by this figure, as the levels of the total ozone depletions seem to stay high until the end of the simulation over the South Pole. Over the North Pole the situation is more or less the same, though the absolute levels are lower. This expected behaviour is in line with the discussions and conclusions portrayed with the ozone trend estimates.

The total loading of the atmospheric chlorine during the early 1980's was much less than during the turn of the century. However, the actual levels of early 1980's were still high enough for the total ozone depletions shown. While this conclusion is based on the use of one single gridpoint, and thus does not exhibit areal increases of the ozone depletion, it suggests that if deep denitrifications are taking place, even the values below the regulation goals of the Montreal Protocol (i.e. below $2.1 ppb_v$) may cause significant ozone depletions similar to those simulated for the first half of the 1980's. In Figure 4.28 the dependence of the coupled BrO -ClO chemistry on the availability of ClO_x is quite clear. In every case the magnitude of the BrO -ClO chemistry is close to the magnitude of ClO_x chemistry, independent on the absolute magnitude of the ozone depletion itself. Due to the fact that the atmospheric loading of total bromine is expected to increase somewhat longer in the atmosphere, as seen in Figure 4.1, than the chlorine loading, the relative effect of coupled BrO -ClO chemistry may become more important in the future. However, no clear signs of the increase in this relative importance of coupled BrO -ClO chemistry are seen in this figure.

Over the North Pole, the absolute magnitudes of ozone depletion are much lower than in the south. As already explained, this is due to the fact that the temperatures do not drop low enough for vertically abundant, deep denitrification. Since the absolute values of the monthly ozone depletions are, while somewhat low, still in line with the values found in common literature (e.g. WMO, 2003). Therefore, it can be concluded that the inadequate representation of the Brewer-Dobson circulation has apparently no major impact on the simulation of the ozone depletions (e.g. far too low or too high ozone depletions). However, there is no straightforward way to make any conclusions on how the ozone depletion would have evolved if the absolute amounts of stratospheric ozone would have been higher, as they should have been. Considering the previously stated fact that the magnitude of the ozone depletion is dependent on the amount of ozone itself, which in turn is some orders of magnitude higher than the typical values of activated chlorine, it seems logical to conclude that the resulting ozone depletion would have been higher if the Brewer-Dobson circulation over the northern hemisphere would have been better presented. Since the FinROSE's chemistry scheme is reproducing realistic behaviour of the ozone depletion itself, I may say again that

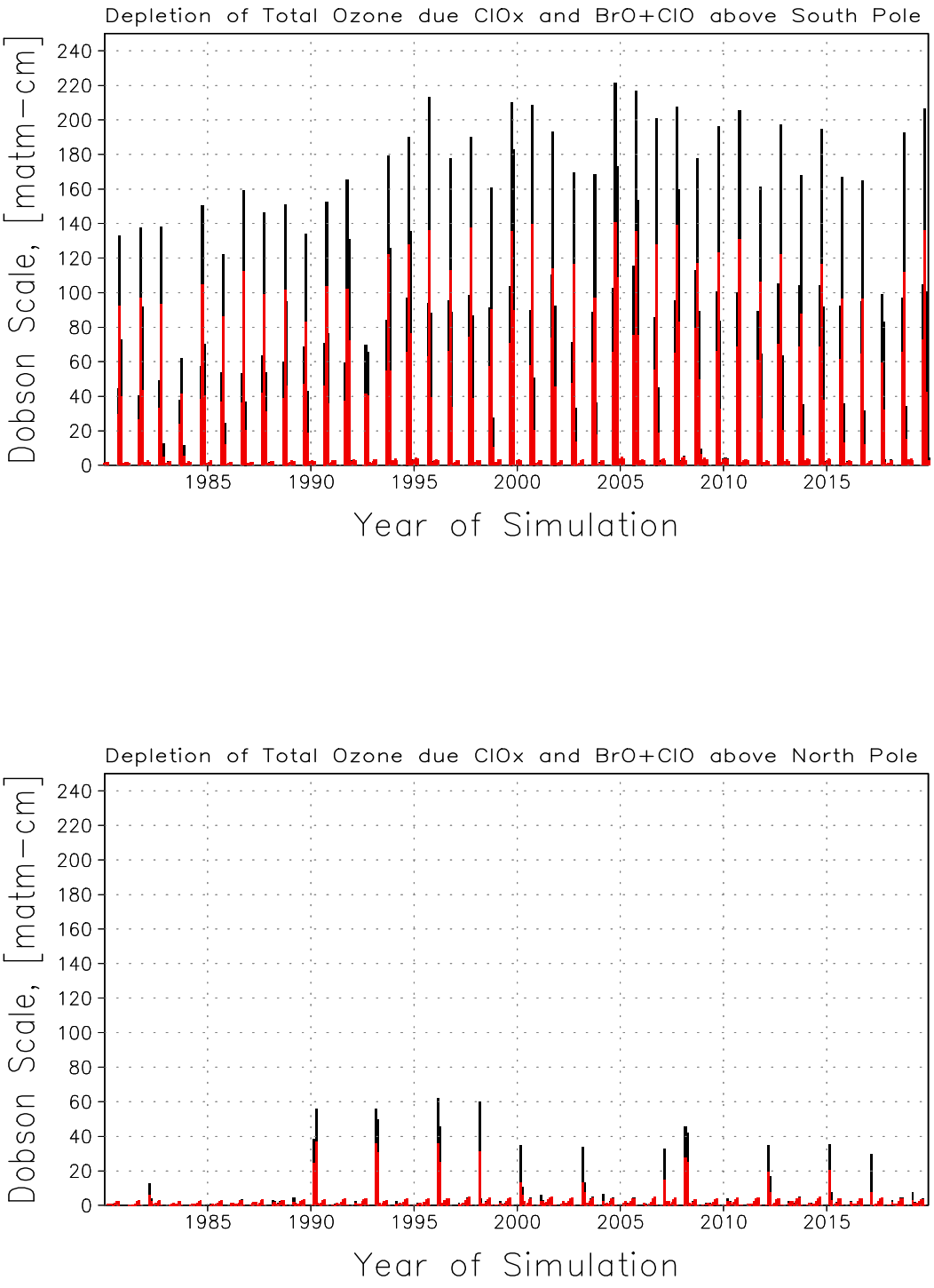

FIGURE 4.28. The effect of chlorine and coupled bromine-chlorine chemistry on total ozone above poles derived from the difference between the inert ozone tracer, and regular model ozone. Upper frame shows the simulated ozone depletion above the South Pole, and the lower frame shows the respective ozone depletion above the North Pole. Red bars indicate the contribution by the ClO_x chemistry, and the black bars give the contribution due to the combined ClO_x -BrO_x chemistry.

the results are, in general, reasonable, and encouraging.

4.11 Ozone-Climate Interactions

Ozone-climate coupling mechanisms are rather complicated. While climate change affects the temperature of the stratosphere, it also affects the transport of ozone due to the direct Brewer-Dobson circulation changes and indirectly by radiative feedback mechanisms due to the compositional changes. This positive radiative feedback derives from the fact that reduced ozone, due to the low temperatures causing denitrifications, and consequent ozone depletions, would cause further cooling in the stratosphere due to the less absorption of stratospheric ozone. Since this radiative feedback has a potential for strengthening the ozone depletion, WMO (2003) concludes that the non-linearly coupled dynamical and chemical effects causing changes on ozone are not easily separable. WMO (2003) also concludes that this separation has to be made case-by-case. Since the objectives of this study are not focusing on these separations directly, and only climatological scale features have been analyzed, these case-by-case studies have been left for future studies.

As shown by the previous sections, the processes connected to the wintertime and springtime ozone depletions in the high-latitude stratosphere are well reproduced by the FinROSE model. The model results exhibit clear connections between the existence of low temperatures and consequent formation of PSCs and ozone depletion. The process of chlorine activation is dependent on both the available surfaces for heterogeneous processing (provided by PSCs), and the availability of inorganic chlorine. The process of denitrification allows for the activated chlorine to react with ozone, as the nitrogen which readily composes chlorine reservoirs has been mechanically sedimented to lower atmospheric levels, mainly due to the large size of the ice-form PSCs (over the southern polar areas), but also possibly due to the sedimentation of the grown NAT-form PSCs. These together mean that the main factors affecting the strength of the ozone depletion are the amount of total inorganic chlorine and the areal magnitude, and vertical extent of temperatures favourable for the formation and permanency of PSCs. As the formation temperature for the ice-form PSCs is a few Kelvins lower than that for PSCs type-I (i.e. NAT-form or STS-form PSCs), all the available chlorine would be already activated before the ice-clouds or large NAT particles form. This means that if chlorine exists in the stratosphere, at least some ozone destruction will take place over those places where large PSC particles form. If the vertical extent of the areas where large PSCs may form is deep enough, the ozone depletion grows more severe.

In order to analyse the possible effects of climate change, as revealed by the changes in the stratospheric temperatures, on high latitude stratospheric ozone, I

show correlation plots of O_3 , NO_y , and chlorine activation against the temperatures at the 46hPa level averaged within 75°S–90°S and 75°N–90°N in Figures 4.29 and 4.30. The plots include all the individual monthly averages, binned by the season during the near future and the near past. At the analysed model level (in Figures 4.29 and 4.30) the ozone mixing ratio scale from $1ppm_v$ to $4ppm_v$ compares roughly with layer total ozone from 15DU to 55DU, respectively. The ozone deficiency shown, is based on the calculation of the difference between the inert tracer ozone and regular model ozone multiplied by the relative contribution of ClO_x and $ClO_x + BrO_x$ ozone depletion cycles to the total chemical ozone loss (as they have been stored during the model integration). Therefore, the shown ozone deficiency reflects the changes in ozone mixing ratios due to the ozone depletion chemistry caused by the two main catalytic depletion cycles (see Chapter 2 for discussion). The chlorine activation is expressed as the ratio ClO_x /Cl_x . In order to distinguish the possible late austral spring results from the values simulated for September and October, the November results have been marked separately in the southern case (i.e. in Figure 4.29).

In the southern case Figure 4.29 exhibits no unexpected "outliers", and the individual months are nicely clustered (as illustrated by e.g. the green markers in the middle panel of Figure 4.29, indicating the NO_y behaviour during March-May). The monthly behaviour of austral wintertime chlorine activation is quite clear, as the values are clustered along temperatures and actual values themselves. This clustering reveals the gradual increasing of chlorine activation, starting from June values around 30%, and ending at August up to 90%, and more. The chlorine activation is then gradually cancelled by more continuous manner, during the austral spring (orange markers in Figure 4.29), reflecting a less clear monthly clustering than during the winter season. With respect to the differences between the past and future periods, no clear separation can be made, implying that the process of chlorine activations will remain similar in the near future as in the near past.

In the case of NO_y , the correlation with temperature during the austral winter (red markers in Figure 4.29) shows clearly how the most effective denitrification takes place at temperatures around 190K and below. This result is clearly suggesting that the sedimentation of grown NAT particles is partly responsible for the simulated denitrification, and that after the ice-forming threshold is broken the denitrification becomes complete. As in case for chlorine activations, the past and future periods seem to reflect similar behaviour. It is also suggested by Figure 4.29 that some possibilities for prolonged denitrifications during the late Antarctic spring in the near future exist at around 20km since the values for the near future Novembers (open black circles) are somewhat more frequent in the temperature region between 195K and 205K than the values for the past Novembers (closed black circles).

The Antarctic wintertime ozone deficiencies (red markers in the topmost

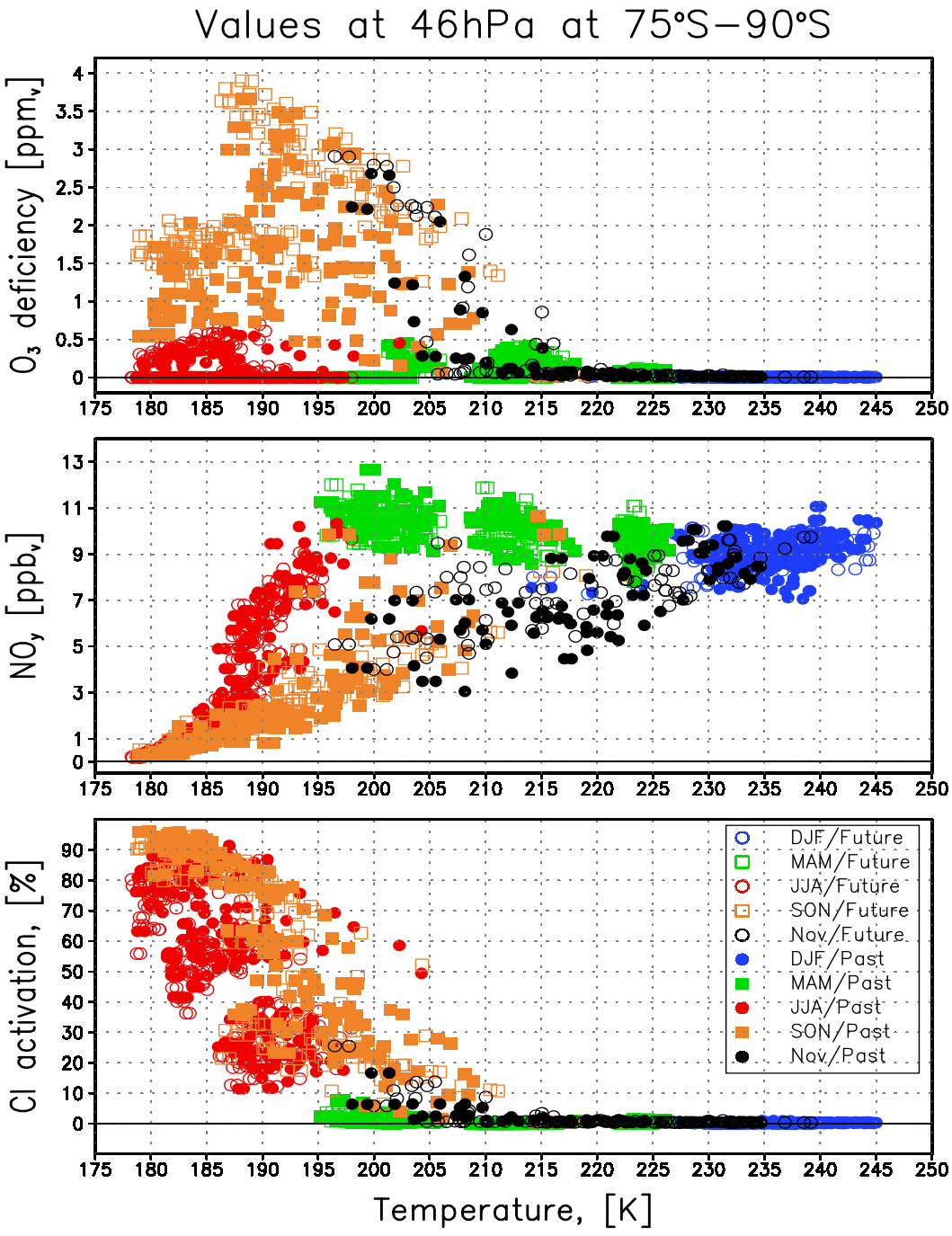

FIGURE 4.29. Scatterplot for temperature versus O_3 deficiency, NO_y mixing ratio, and chlorine activation (ClO_x /Cl_x). The monthly average values are shown by season for polar area enclosed within the 75°S-latitude at 46hPa (around 21km). Marker coding: DJF-Past–blue closed circles, DJF-Future–blue open circles, MAM-Past–green closed squares, MAM-Future–green open squares, JJA-Past–red closed circles, JJA-Future–red open circles, SON-Past–orange closed squares, SON-Future–orange open squares, NOV-Past–black closed circles, NOV-Future–black open circles. The past refers to the period 1980-1999, and future refers to the period 2000-2019. See text for further explanations.

frame of Figure 4.29) show the combined influence of chlorine activations and denitrifications on ozone depletion. During the Antarctic winter areas south of 75°S are basically not sunlit, and the ozone deficiencies stay low. After the initiation of the photochemistry during the Antarctic spring, the ozone deficiencies (shown by the orange markers in Figure 4.29) start to increase, and top at almost $4ppm_v$, below 190K, corresponding to depleted layer total ozone amount around 50DUs (i.e. almost complete loss). The gradual recovery from the ozone depletion season during the late spring is relatively smooth and continuous. The simulated values for near future ozone deficiencies (open orange squares) exhibit somewhat different behaviour compared to the past (closed orange squares). During the future period, the monthly clustering of ozone deficiencies is somewhat more separable between the month of September (ie the lower cluster at around $1.7ppm_v$ marked with open orange squares) and later spring months (i.e. October and November; open orange squares and open black circles, respectively) than during the past. This result suggests that the Antarctic springtime ozone depletions may become more profound during the late austral spring in the near future, especially during November, while the actual magnitude of the depletion stays the same (roughly between 50% and 75% during November at around 20km, and almost complete loss during October). Since the austral summer and autumn cases (i.e. blue and green markers in Figure 4.29) do not reveal any significant ozone deficiencies or chlorine activation levels, though some signs of lowered NO_y levels during December-February are evident, these seasons are not further analyzed.

In the northern case (i.e. Figure 4.30) the situation is more moderate, as expected. The behaviour of wintertime chlorine activation reveals, similarly to the south, gradually increasing values during winter (i.e. blue markers in Figure 4.30) that "top" at around 80%. The steepness of this gradual chlorine activation is comparable with the southern case, though the extreme maximum is missing, as the values below 190K are rare, and values below 186K, completely missing. As in the southern case, Figure 4.30 exhibits no clear differences in chlorine activations between the past and future periods.

The denitrifications in Figure 4.30 (blue and green markers) show clearly the effect of the grown NAT sedimentation, as the lowest values are basically between 190K and 195K. It also seems that during the near future these low values between $3ppb_v$ and $7ppb_v$, indicating denitrifications efficiencies up to around 75%, become somewhat more frequent, while the minimum values are similar to those in the near past. This result, in line with previous results is in turn suggesting that ozone depletions, like the one observed during the northern hemispheric winter-spring 2004-2005 (discussed in Chapter 1) may become more frequent in the future near the altitude of around 50hPa (i.e. around 20km). It should also be noted that the steepness of the NO_y -temperature-slope in Figure 4.30 is of same order as in the south (i.e. Figure 4.29). This suggests that the process of denitrification is first initiated by the sedimentation of the grown NAT particles, and if the temperatures

drop below the frostpoint the denitrification is continued, and completed by the sedimentation of ice-form PSCs (as it is in case of Antarctica, shown in Figure 4.29).

The behaviour of the ozone deficiency in Figure 4.30 reflects again the combined influences of denitrifications and chlorine activations, and the availability of solar radiation on ozone: The ozone deficiencies stay low during the dark wintertime periods, and elevated values appear during the spring. The springtime deficiencies (green markers in Figure 4.30) have their maximum at around $1ppm_v$, corresponding to 15DUs in layer total ozone terms. While the steepnesses of the NO_y versus temperature, and chlorine activation versus temperature plots were roughly similar both in south and north, the shape of the ozone deficiency versus temperature scatter is somewhat different in the northern case compared to the south. Over the Antarctic region higher than $1ppb_v$ ozone deficiencies were frequently found during the springtime below 210K, while in the Arctic these ozone deficiency values are found in colder temperatures (i.e. 190K-200K). This is signalling the differences in the persistence of PSCs between the Arctic and Antarctic.

In the Arctic stratosphere, the PSC events are short in time, and typically rather shallow (see Figure 4.25). While the denitrification at around 20km may be as strong as 75%, the remaining NO_y seems to be high enough for chlorine deactivation after the PSCs have vanished. This in turn is somewhat self-evident, as the remaining NO_y mixing ratio is of the same order as the amount of chlorine loading (i.e. around $3.5ppb_v$). Therefore if the denitrifications are to get stronger, and values of remaining NO_y drop clearly below the total chlorine levels, then the ozone depletion should become more efficient. In Figure 4.29 (red markers) the steep wintertime drop in NO_y content takes place at around ice frostpoint. Whether this is associated with the NAT sedimentation or ice sedimentation is not quite clear, and will be left as a subject for future studies. However in Figure 4.30 a similar feature, i.e. steep NO_y drop, from around $6ppb_v$ down to $3ppb_v$ seems to take place at 190-195K, suggesting that denitrification leaving less than, say, $3ppb_v$ of NO_y might be possible in the north if the duration of NAT sedimentation is long enough. Using the ozone deficiency values in Figure 4.29 during the near future Septembers (i.e. the cluster of open orange squares in Figure 4.29 at around $1.7ppm_v$) as precursors of the early stages of the ozone depletion during each individual season, as they represent the values of ozone depletion right after the polar night, it seems that below 195K the corresponding values of NO_y during the local spring (i.e. the open orange squares representing Septembers and Octobers in Figure 4.29) are typically around $3ppb_v$ or less. While these values clearly occur already below 195K in both the Antarctic case (Figure 4.29), and the Arctic case (Figure 4.30), the remaining NO_y content in the Arctic case is typically over $3ppb_v$. Based on these figures I may now suggest that in order to have substantial ozone loss in the springtime Arctic, denitrification should be strong

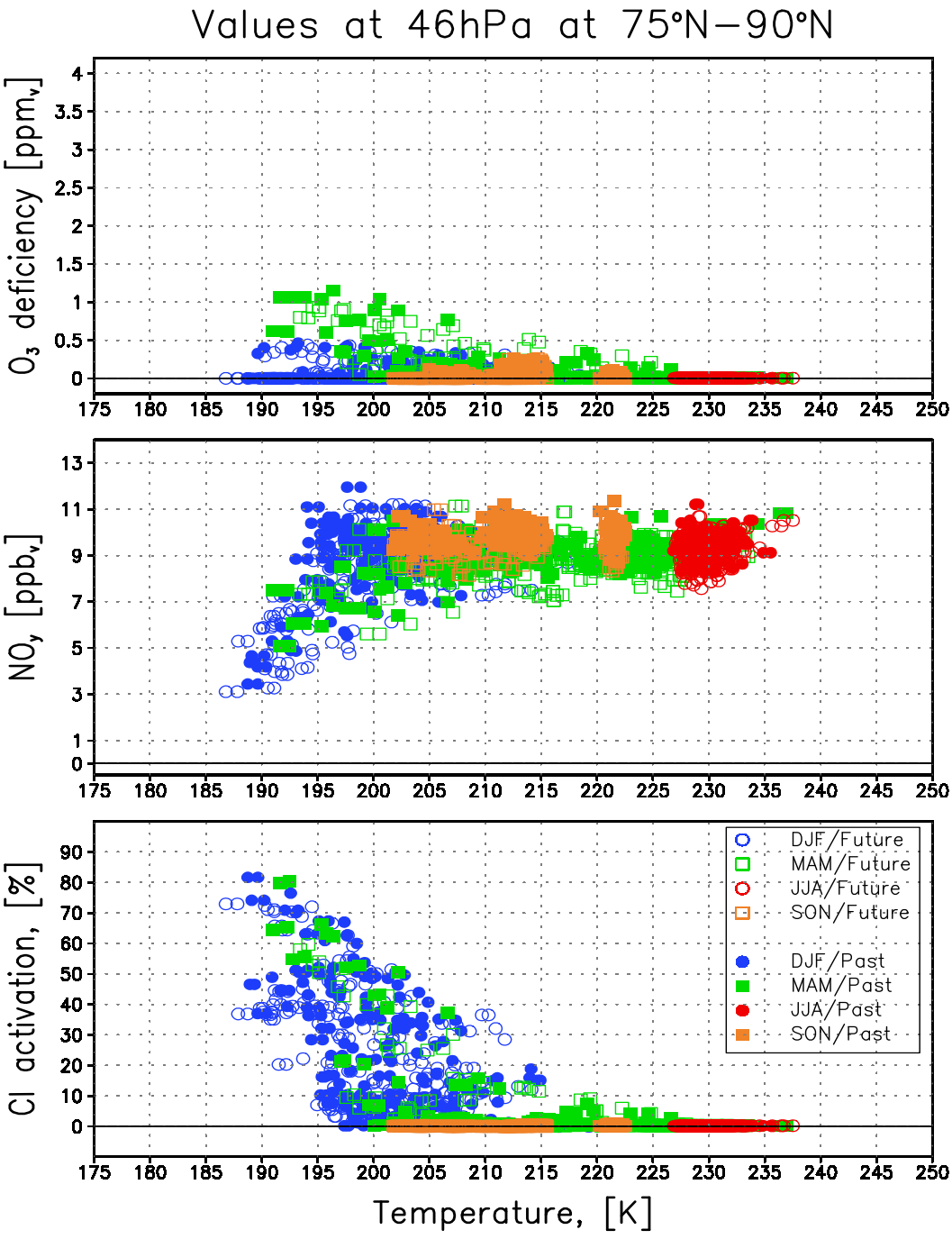

FIGURE 4.30. Scatterplot for temperature versus O_3 deficiency, NO_y mixing ratio, and chlorine activation (ClO_x /Cl_x). The monthly average values are shown by season for polar area enclosed within the 75°N-latitude at 46hPa (around 21km). Marker coding: DJF-Past–blue closed circles, DJF-Future–blue open circles, MAM-Past–green closed squares, MAM-Future–green open squares, JJA-Past–red closed circles, JJA-Future–red open circles, SON-Past–orange closed squares, SON-Future–orange open squares. The past refers to the period 1980-1999, and future refers to the period 2000-2019. See text for further explanations.

enough to leave the remaining NO_y be around $3ppb_v$ or less during the early spring. I will leave further studies on this suggestion as a subject of a future study. Another conclusion from these analyses is also related to the remaining NO_y : As the emission regulations are expected to decrease e.g. the atmospheric chlorine loading, the needed magnitude of denitrification will increase accordingly. A more detailed analysis of the relations between the needed levels of denitrifications and chlorine loadings will also be left as a subject of a future research.

Using the results shown in Figures 4.29, and 4.30, an estimation of the temperature relations of ozone loss, chlorine activation and denitrification is also possible for the shown circumpolar areas and level (i.e. 46hPa). In case of both the Antarctic and Arctic winters, below 205K, the chlorine activation increases on the average by 4% for a 1K decrease in temperature. The corresponding relation for wintertime Arctic and Antarctic denitrification at around 20km is on average around $0.5ppb_v$ /K (for temperatures below 205K). In the case of ozone deficiency, the corresponding average value for Antarctic spring is almost $100ppb_v$ /K, while the somewhat gentler average slope in the Arctic spring is almost $60ppb_v$ /K. In terms of Dobson Units, the values for this layer are roughly 1.5DU/K for the Antarctic spring, and slightly less than 1.0DU/K for the Arctic springtime.

Recently, quantitative relations between the stratospheric temperatures and the Arctic springtime ozone losses were found and discussed by Rex et al. (2004) and Tilmes et al. (2004). The results of Rex et al. (2004) show that an empirical relation between the Arctic wintertime and springtime ozone depletions and climate change exist. Based on the observations, it was shown that in the stratosphere, for each Kelvin cooled, a 15DU total column ozone reduction is realized. In broad terms, an ocular analysis of the results presented by Figure 4.28 shows that during the first 15 years of the model simulation the average total ozone depletion have increased approximately 50-70DU. With respect to the results shown by Rex et al. (2004) these ozone depletion increases correspond roughly to a cooling of 2-3K/decade which in turn is qualitatively in line with the cooling trend estimates of Austin and Butchart (2003), or WMO (2003). This means that the simulation results of FinROSE, using the UMETRAC temperatures, are comparable with the results of Rex et al. (2004), and the ozone losses are reasonably well simulated without any significant underestimations discussed e.g. by Harris et al. (2002), and WMO (2003). In addition, using the ozone deficiency relations between 1.0DU/K and 1.5DU/K, as shown and discussed above, and assuming that the model layer average total ozone amount is roughly 10-15% of the total column ozone amount, this ozone depletion chemistry driven temperature relation translates to approximate values between 10DU/K and 15DU/K in terms of the surface total ozone column, meaning that for each Kelvin decreased the total ozone column abundance decreases around 7DU (derived from the Arctic springtime estimates) up to 15 DU (derived from the Antarctic springtime estimates). This in turn suggest that while the estimated ozone loss magnitudes are

not underestimated in the southern springtime vortex, an underestimation probably occurs over the Arctic springtime high latitudes. The underestimation of the Arctic ozone losses is, at least partly, due to the transport problems, since the ozone depletion is dependent also on the available ozone amounts themselves, and since it is now known that due to the problems in the simulated Brewer-Dobson circulation, in this work, the Arctic ozone levels are generally too low. On the other hand, the values presented here, while based on the use of monthly averages, do not explicitly take the asymmetrical nature of the Arctic polar vortex into account, since the usage of monthly averages enclosed by the 75°N circumpolar latitude belt may not serve as a good estimate for the Arctic polar vortex even on a monthly mean perspective.

Over the Antarctic areas an isolated and extremely cold vortex is expected to exist also in the future due to the regular circulation characteristics of the southern hemisphere middle atmosphere. Therefore ozone depletion will also be seen in the future, as long as enough chlorine is available, and both magnitude-wise and altitude-wise deep denitrifications will take place. During the duration of the shown 40-year simulation, the atmospheric loadings of the inorganic chlorine stay high, and therefore no clear decrease of the ozone depletions is seen before the end of 2019. These results are in line with the estimates given by e.g. WMO (2003). A more recent study by Knudsen et al. (2004) predicts that the ozone depletion may even become stronger by 2010-2015, and after around 2020, a slight recovery would take place. While the results of this study do not explicitly show any significant increases in the near future ozone depletion, this possibility is not completely ruled out as e.g. the areal extent of the ozone depletion may be increasing (see e.g. Figure 4.2), and the duration of the ozone depletion season may get prolonged until later spring (see Figure 4.29). The changes in the areal extent of the depleted ozone over the Antarctica have been recently addressed by Newman et al. (2004). In the northern high latitude stratosphere, however, no large-scale deep denitrifications take place in the FinROSE simulation, and therefore no clear climate-change induced increases before 2019 in the northern polar ozone depletions are exhibited by my results either. This is due to the fact that the temperatures, while cooling, do not cross the threshold for ice-cloud formation, or persist long enough for vertically deep events of the grown NAT particles in a climate-perspective. However, the chlorine activations will continue to happen on annual basis, and over those areas where local denitrifications take place also the ozone depletion becomes more profound. Furthermore, in the future, the enhanced denitrifications and resulting ozone depletions are expected to be more likely in the upper parts of the ozone layer (e.g. Austin and Butchart, 2003; WMO, 2003).

According to WMO (2003) the models typically suggest that over the Antarctica the observed stratospheric cooling can be explained by either combined WMGHG and stratospheric ozone changes or stratospheric ozone changes alone during

any season. Over the Arctic, however, models typically underestimate the springtime cooling, suggesting that CCM models may not reproduce correctly the ozone depletion feedback of the cooling, or there are shortcomings in the profoundness of the compositional treatments of the CCMs (like water vapour), or the natural variability itself is underestimated by the CCM-models. A general conclusion by WMO (2003) was, however, made for both south and north; i) Over the northern polar areas the observed springtime cooling during 1980-2000 is not only due to the stratospheric ozone depletion but also due to large dynamical variations, while ii) over the southern polar areas the stratospheric cooling is mainly due to the ozone depletion, and that iii) the annual average stratospheric cooling is mainly due to the effect of increased WMGHGs and stratospheric water vapour. WMO (2003) also concluded that increases in WMGHGs and changes in ozone are closely coupled, and that chemical and dynamical processes should not be analysed separately. For example the study by Hadjinicolaou et al. (2002) argued that the dynamically driven model trend of stratospheric ozone accounts for at least half of the observed northern hemispheric trend averaged over December-February.

Beyond the time periods of this study (i.e. after 2020), WMO (2003) expects that increases in methane and nitrous oxide concentrations will have a more profound effect. Therefore, if longer simulations are to be performed, the processes coupled with the methane and nitrous oxide (N_2O) should be taken into account. As regards the effects of eventual major volcanic eruptions, it is expected that the eruptions would not affect the general ozone evolution, but rather enhance chemical ozone depletion in timeframes of three to four years, though there is a great deal of uncertainty when the behaviour of stratospheric aerosol loadings in the future are addressed. Tian and Chipperfield (2005) have recently created a new fully interactive CCM with state of the art descriptions for stratospheric processes, including the radiation couplings not only with ozone (as in this study), but also with N_2O, methane, and water vapour. In this study other species than ozone (e.g. WMGHGs) were specified according to observational estimates or commonly accepted future scenarios, with an additional parameterization for methane oxidation. This new model by Tian and Chipperfield (2005) which is based on the use of the same dynamical core model as the UMETRAC model used in this study (i.e. Cullen, 1993) simulated about 15% higher ozone values in the Arctic winter/spring and up to 90% higher ozone values in a significantly smaller ozone hole over the Antarctic by 2050. They also found that the significant increase in O_3 more than offsetted the effect of climate-change driven stratospheric cooling during the late austral spring.

4.12 Discussion

Chemical-Transport-Models (CTMs) driven by the externally provided wind and temperature fields (and as in this study by the surface pressure fields) are very useful for the simulation of various atmospheric processes. The main purpose of this study was to use the winds and temperatures resulting from a 40-year chemistry-coupled GCM (i.e. CCM) simulation, to drive the FinROSE chemistry transport model for the study of the past and future behaviour of the ozone layer. Global CTM models have been widely used for such multi-year simulations of the stratosphere (e.g. Chipperfield, 1999; Rummukainen et al., 1999; Egorova et al., 2001; Hadjinicolaou et al., 2002, and Chipperfield, 2003). Typically these simulations are based on the observational meteorologies (e.g. analyses of the numerical weather prediction models, like the ECMWF model). However, studies where a CTM model has been driven with a chemistry-coupled climate model are rather rare. However, Brasseur et al. (1997a) used this approach on a shorter timescale (i.e. on seasonal scale).

The results discussed in this work are, to large degree, within the envelopes of the model results discussed in WMO (2003). Since the results shown and analyzed are based on a simulation designed mainly during 2002 and executed during early 2003, the results should be considered mainly from that perspective (e.g. the Ozone Assessment 2002, by WMO (2003) was not available during the design-phase and completion-phase of the simulation). However, after 2003, significant stratospheric model development has taken place, and e.g. the recent results by Chipperfield et al. (2005), Mann et al. (2005), Rex et al. (2004), and Tian and Chipperfield (2005) were unknown prior to the actual model simulation presented in this study. The results shown and discussed should be considered, first of all, as a proof for the applicability of the CTM-CCM approach itself in climate scale studies, as well as a general documentation of the 40-year simulation. It is clear that a number of other possibilities for the usage of these results, and for the CTM-CCM approach in general, exist. The applicability of the CTM-approach coupled with CCM winds and temperatures is therefore concluded to be an effective framework especially in the field of atmospheric chemistry studies, while the applicability in transport-type studies is somewhat restricted. However, the CTM type analyses could also be used for analyzing the CCM results in general, and therefore, the CTM approach has a potential for adding value to the CCM type results also in the case of atmospheric transport process studies.

The quality of the CTM-type model studies is very much dependent on the quality of the transport characteristics and temperatures of the meteorological analyses used, as well as on the profoundness of the chemistry scheme of the CTM itself. With respect to this study, the uncertainties associated with the CCM have been discussed by Austin et al. (2003b). The shortcomings in the realized Brewer-Dobson circulation, and the large natural variability of the north-

ern polar vortex, increased the uncertainty of the trend analyses. However, the reproduced trend estimates for the northern polar areas are very much in line with the results discussed in WMO (2003). The results from the FinROSE's 40-year simulations are stable with respect to the general evolutions reproduced by the model's externally driven transport, and FinROSE's own chemistry scheme. It is clear that every model produces its own aeronomy, and its own balances between the radiation driven processes, dynamically driven processes, and chemistry driven processes. Therefore, the driver model and FinROSE-simulated evolutions are different, and dependent on e.g. the reproduction of features like ozone depletion. In this study the drive for transport and temperatures for chemistry were taken from a CCM simulation. This means that, in case of dynamically, or thermo-dynamically driven atmospheric processes, the FinROSE-reproduced patterns follow those gained by the driver simulation, which in turn are dependent on the radiation couplings, or used WMGHG projections within the CCM itself. In the case of chemistry-driven processes, like the springtime Antarctic ozone hole, it is therefore fair to say that the FinROSE model is capable of making a more independent simulation over the southern continent than over the Arctic. It should also be noted that FinROSE simulated no other clearly erroneous results than the less profound annual ozone amplitude. The FinROSE's inability to reproduce reasonable age of air distributions, and its insufficient Brewer-Dobson circulation, are actually well-known problems of the CTMs (Hall et al, 1999).

In general, all the shown results in the previous sections indicate that the ozone evolution is more predictable in the winter-spring Antarctic stratosphere than in the northern polar stratosphere where the natural interannual variability is greater. Since the result analyses in this study are based on the average quantities (i.e. zonal averages, monthly means etc.), the discussed results do not reveal all the fine-scale features that the simulation contains. This means that, for example, there might be single, short-time (e.g. from a few model timesteps to a few days) cases of PSC-type-II events over the northern polar areas. However, it is fair to state that the inclusion of the effects caused by large NAT particles (i.e. sedimentation and denitrification) clearly improves the results exhibited in this study, as the moderate Arctic denitrifications are being reproduced in absence of ice particles. These results suggest, in line with other studies (e.g. WMO, 2003) that the denitrification caused by gravitational settling of ice particles is not causing Antarctic type denitrifications over the Arctic. Furthermore, I may also conclude that the model results captured the typical interannual variability of ozone in the northern polar stratosphere as well, though the absolute levels were too low. While there was evidence of denitrifications due to the large NAT-form PSC sedimentation, the close threshold for the ice-formation was not by-passed, and no unrealistic ice-form PSCs were reproduced.

According to WMO (2003), the largest uncertainties in stratospheric model studies of ozone depletion are due to the unrealistic representation of denitrifica-

tion processes. In order to have more realistic behaviour, especially in the Arctic, the 40-year simulation presented in this study has been furnished with a simplified scheme for the denitrifications resulting from the growing of the NAT particles to sizes where sedimentation may become truly effective. Since this work is based on a single simulation, and focuses on the analysis of climate-scale average quantities, it is not straightforward to draw any self-evident conclusions on the effect of the more profound treatment of denitrification. A number of studies on polar denitrification cases exist (e.g. Fahey et al., 1990; Rex et al., 1997; Waibel et al., 1999; Kondo et al., 2000; Santee et al., 2000, just to mention a few). In agreement with the present study, the model results of e.g. Chipperfield and Pyle (1998) and Waibel et al. (1999) have shown that the Arctic ozone loss is dependent on the level of denitrification.

In the northern polar stratosphere, the chlorine activation is an annual phenomenon. However, since the temperatures do not "drop" low enough, no large scale ozone depletion is expected before the end of 2019. The Arctic polar vortex, having more complex, and weaker structure, is not expected to be cooled so much that vortex-wide existence of PSCs type-II would become possible. However, the Arctic polar vortex will probably experience ozone depletions having the same nature as they have had so far (e.g. the latest winter, 2004-2005, prior to this study). It is also possible that these more local perturbations may cause elevated levels of UV over the populated northern hemisphere high-latitude areas if the ozone depletion affects the ozone distributions during the following summer as well. This matter has been recently addressed by Fioletov and Shepherd (2005). If the cooling of the stratosphere continues, as expected, even larger-scale wintertime and springtime depletion is possible as the situation is already close to having ice clouds formed. The expected loading of total inorganic chlorine will stay high even after my integration. The key question therefore is: Will the temperatures drop below ice-formation temperatures on larger scales before the projected chlorine loadings have reduced to levels where ozone depletion would be considered history. An important precursor for this is the behaviour of the early 1980's ozone depletion events. As was noted before, even chlorine levels below 2.1 ppb_v may cause large-scale ozone depletion. Whether the regulations stated by the Montreal protocol (UNEP, 2000) are enough in a cooled stratosphere remains unanswered in this work since longer simulation timeframe is needed. However, it should be remembered that during the preindustrial times the chlorine loading of the atmosphere was low. While the ice-form PSCs have existed during the preindustrial times as well, due to natural causes, the timescale of the winter-spring season may be too short for the production of significant ozone loss if the chlorine loading is low. The actual magnitude of the ozone depletion depends on the existence of low temperatures, as they cause denitrification. Since the level of chlorine is expected to stay high during the timeframe of this study (i.e. 1980-2019), it is easy to conclude that the Antarctic ozone depletions are expected continue as they are until

the end of 2019.

In this study the radiative coupling and dynamical features like planetary wave drag and Brewer-Dobson circulation are a result of those reproduced by the driver model UMETRAC, while the chemistry, and transport of the long-lived species, and the photochemistry of the short-lived species have been simulated by the FinROSE's own chemistry-transport scheme. While a clear possibility for incompatibilities between the driver model and the CTM exist, the problem would have been the same if analyses from an observation-based numerical weather prediction model would have been used. Therefore, it is reasonable to assume that should the driver model carry any signals on possible changes in the aeronomical features due to the increases in WMGHGs this signal would be transferred to the results of the FinROSE model as well.

Eventual changes in the atmospheric wave-drive itself (e.g. changes in the tropospheric circulation due to the climate change) were explicitly left outside the scope of this work. WMO (2003) states that the contribution of this phenomenon in the observed ozone trends over the northern hemisphere during the near past period (in WMO, 2003; past refers to 1979-2000) is probably less than 30%. However, the effects and changes of tropospheric dynamics on the long term changes were recently addressed by Wohltmann et al. (2005), and their results show that from 30% up to 50% of the long-term total ozone trends are explained by the long-term pressure changes over Europe. As was shown in Figure 4.21, also FinROSE signalled this result as there was a clear downward trend of ozone in the vicinity of the tropopause. The recent results of Mann et al. (2005) show that the contribution of mountain waves to the formation of large NAT particles on a vortex scale may be responsible for as much as 80% of the total denitrification over the northern polar areas. Since the results of the driver model have not been analyzed from this point of view, it is impossible to compare the FinROSE results against the results by Mann et al. (2005). However, in the future, this effect should also be taken into consideration when the actual experiments are designed.

WMO (2003) concludes that if the past ozone variability due to dynamical changes has been caused by natural variability; these changes are not applicable for representing the future. However, if the dynamical changes, observed so far, are due to the climate change, then e.g. the cooling of the stratosphere should be regarded as a possible cause for further decreases in future total ozone columns (WMO, 2003), and therefore as a possible mechanism for delaying the eventual recovery of the ozone layer due to the halogen regulations. Since the signal of climate change is very difficult to isolate, the changes in the stratospheric ozone behaviour due to the increases in WMGHGs are also very difficult to distinguish. In this quest, the use and the maturity of the CCMs become very important. In WMO (2003) it was stated that the GCMs do not even agree on the sign of the dynamical changes, like changes in planetary wave drag. In general, should the

planetary wave drag become weaker, one might expect that the high-latitude ozone would decrease due to the transport. However, the models, so far, have not agreed on this subject (see WMO, 2003 for further details). The weaker planetary wave drag would also increase the age of air in the middle atmosphere, and therefore the photochemical equilibrium of the stratosphere, and life times of the photolytically active stratospheric compounds. The reverse would happen, if the planetary wave drive would become stronger (see Butchart and Scaife, 2001). The timescales associated with the lifetimes of the photolytically active trace species (like those in total inorganic chlorine family) affected by the planetary wave drag changes imposed on the Brewer-Dobson circulation are large compared to the response of the ozone transport. Therefore, the changes in the Brewer-Dobson circulation are affecting the chemical ozone loss together with the changes in stratospheric chlorine loading.

5 Future Aspects and Final Remarks

In the future, several developments of the FinROSE model are needed. These developments include at least considerations of better horizontal resolution and other grid alternatives, implementations required by the inclusion of the source gas treatments, and detailed analyses about the ozone processes over the tropics. As mentioned in the previous chapters, the inadequate reproduction of the Brewer-Dobson circulation forms the most challenging problem for the future developments of FinROSE itself. Only after that, the implementations for the treatment of the source gases can be made in an orderly fashion. Furthermore, as the understanding of the chemical kinetics, quantum yields, heterogeneous processing, and microphysics of the PSCs are under constant scientific research, frequent updates are needed. It should also be kept in mind that the understanding of the composition of the stratosphere, and the changes that are taking place, is of great importance, if we want to make plausible predictions about the future climate and surface UV radiation levels. As WMO (2003) summarized, the stratosphere has been cooling during the last two decades due to the changes in stratospheric ozone, changes in WMGHGs, as well as due to the changes in water vapour. WMO (2003) also concludes that stratospheric cooling due to the ozone depletion has been the dominating mechanism in the lower stratosphere, while the upper stratospheric cooling has been explained by both ozone changes and changes in the WMGHGs. The cooling due to the increases in stratospheric water vapour is thought to be as important as the increase in ozone over the midlatitudes, and more emphasis on this phenomenon should be given when further developing the model itself.

In this work I have merely touched the surface of those numerous possibilities that one may have while using CTMs. Several other applications on the use of the CTM approach may be easily listed. These applications include the use of the CTM approach for the derivation of the upper vertical boundary conditions for the GCMs as well as for the CCMs. This idea has been applied in case of the FinROSE model in an EU/FP5 funded project, RETRO. CTMs may also be used as a feasible platform for testing new parameterizations and implementations (e.g. PSC schemes, and aerosol modules), or they can be used as box model solvers in trajectory type applications. The usage of CTMs as a part of an operational satellite data production system has already been tested (Hassinen et al., 2004). Chemical data assimilation of satellite measurements into operational atmospheric air quality models and applications is also in a range of CTM usage. One possibility could be a CCM/GCM parallel CTM code to be used as an intelligent analyzer of the CCM/GCM results (e.g. in the case of community type climate models). These issues, along with those already discussed in previous sections, and along with numerous unmentioned issues remain as challenges for the future.

6 Conclusions

In conclusion of this work I will now make a reference to my original objectives stated in Chapter 1, and make conclusions as they are relevant with respect to those objectives.

Objectives 1 through 3: CTM applicability, result analyses, and ozone trends

I have now presented the standard configuration, and documented the results of a 40-year stratospheric simulation executed with a global chemistry transport model, FinROSE. The climatological perspective of the 40-year simulation covered the period from 1980 until the end of 2019 and focused on the behaviour of atmospheric ozone in the high latitude stratosphere. The used model (FinROSE) included profound gas-phase chemistry, heterogeneous processing on polar stratospheric clouds, liquid binary aerosols, and simplified scheme for the NAT growth (see Chapter 3). The chemical transport model was driven with winds and temperatures from a transient climate simulation done with a chemistry-coupled climate model UMETRAC. The version of the FinROSE model used for this study was run with a horizontal resolution of 11.25° by 5° (Lon-Lat) with 24 vertical levels from the surface, up to ∼0.15hPa (∼ 62km). For the boundary conditions of the long-lived tracers the model used the specifications and future projections from the driver model (Austin and Butchhart, 2003). These values were presented in Figure 4.1. The results were analyzed and discussed from a climatological high-latitude perspective in Chapter 4.

For this study, the chemical transport model FinROSE, was improved and developed in several ways from its original version (Rose and Brasseur, 1989). These improvements included the replacements for the advection scheme (Lin and Rood, 1996), the replacement for the photodissociation calculation scheme (Kylling, 1992; Kylling et al, 1997; Mayer et al., 1998), the updates for the chemical kinetics (e.g. Sander et al., 2000; Bloss et al., 2001), the improvements for the heterogeneous processing, and some updates/improvements for the chemical mechanism of the model. For this study the model was also implemented for the usage of the UMETRAC CCM-type model data (e.g. vertical grid, and boundary conditions). The original plans for the simulation were made during 2002, and therefore the developments in e.g. chemical kinetics after mid-2002 were not taken into account.

In general, during the past period, the model results of this study show a good or moderate agreement with the measured total ozone (TOMS). The timing, depth and deepening of the Antarctic ozone hole was captured well in the simulation. According to my results the simulated age of air distributions were too young, meaning that the Brewer-Dobson circulation, reproduced by the transport scheme

of the model and driven by the driver model winds, was too strong. While the inadequate reproduction of the Brewer-Dobson circulation turned out to be the most significant limitation associated with the FinROSE model itself, the overall results were both stable and in line with the other model results and observations (see e.g. WMO, 2003). Therefore I conclude that the presented results stand as a demonstration of the applicability of the coupled CTM-CCM approach.

The statistical analyses of this work show that the observed decadal total ozone trends calculated from TOMS-measurements (version 8) from 1980 to 1999, and from the FinROSE results for the same period were in close agreement (ie. within a few percents). The model trend estimates gave also the same level of significance as those achieved from TOMS ozone analyses. In general, during the past period, the model results show a good comparison with the measurement-based trend calculations (TOMS). This is mainly due to the fact that the timing, depth and deepening of the Antarctic ozone hole were captured well in the simulation, and no unexpected results were exhibited over the northern polar areas. My statistical analyses show that the observed decadal total ozone trends calculated from TOMS-measurements from 1980 to 1999 and from the FinROSE results for the same period were in close agreement. The trend estimates derived from the FinROSE simulation gave also the same level of significance as those achieved from TOMS ozone analyses. During the future period, the trend estimates revealed no clear signs of the ozone recovery: The estimated decadal total ozone trends will more likely level off over the high southern latitudes and no significant increases or decreases are expected over the northern high latitude regions.

Objective 4: Model-Simulated Processes

Over the Antarctica the effect of heterogeneous processing was well exhibited in the results of this study, as the chlorine activation and denitrification were complete especially during the latter part of the past period (ie. 1990's). Over the Arctic regions the effect of chlorine activation was present in the model during the coldest winter-spring months. However, since the temperatures were typically well above the ice-forming point in the stratosphere, no massive denitrification took place, and the ozone destruction stayed much less effective than in the high southern latitudes. The fact that the FinROSE results were exhibiting the effects of large NAT particles on the simulated, rather shallow denitrifications in the northern polar stratosphere is very encouraging. The NO_y reductions of up to 75% were simulated, and furthermore these NO_y reductions took place at temperatures clearly above the ice-forming point without any signals of dehydration. The importance of this result is even more emphasized from the cold-pole problem perspective (see e.g. Austin and Butchart, 2003; Austin et al., 2003b). There were also no obvious signs of the increases in the vertical extent of these denitrifications over the wintertime northern polar areas. The simulated denitrifications over

the northern polar wintertime areas were clearly far weaker than those over the Antarctica, and caused mainly by large NAT particles. While this was not clearly seen from the monthly averages, the actual denitrifications over the Antarctica were also taking place, or initiated, due to large NAT particles, before the stratospheric vortex temperatures cooled below the ice formation threshold (see Figure 4.11). This result is in line with the conclusions of Tabazadeh et al. (2000) and discussions given in Carslaw et al. (2002).

One of the main challenges of the CTM-type models has been their inability to reproduce the Arctic winter-spring ozone losses (e.g. Harris et al., 2002 and WMO, 2003), and that they underestimate the ozone losses in general (e.g. Krämer et al., 2003). In this study, however, the problems with the Brewer-Dobson circulation were greatly deteriorating the analyses of the actual magnitudes of the past ozone changes, and their comparison with the observed changes over the northern polar areas. Therefore, the analyses were focused mainly on the relative importance of ozone depleting processes. Recently, Chipperfield et al. (2005) have shown, however, that if the latest findings on the mechanisms behind the ozone depletion are implemented into a state of the art CTM, realistic ozone losses are reproduced also over the Arctic. From this perspective, my results over the northern high latitudes should be considered to be only reasonable or qualitative, and should be discussed from a relative point of view. However, since the shown trend estimates were in close agreement with the observed values, as well as the general stability of the FinROSE results was good, I conclude that the general results of this study are representative in case of polar ozone behaviour. Furthermore, it was shown that the approximate monthly average estimates of ozone loss efficiencies were in close agreement with those presented by Rex et al. (2004).

Objective 5: Near Future Ozone

WMO (2003) defines and uses the ozone recovery term in the following way: i) The timeframe until 2000 is referred as the ozone depletion era, ii) The time frame from 2000 to 2020 is referred as the start of the ozone recovery, i.e. the time-frame when the date of the minimum spring column ozone appears, and iii) The full recovery which is the time when the decadally averaged spring column ozone returns to the levels equivalent to 1980. In general, the same behaviour was also manifested by the results of the 40-year FinROSE simulation within the addressed period (i.e. 1980-2019). However, there were no clear signs of the start of the recovery before 2020. The results are more likely showing that the ozone depletion phenomenon is levelling off, and that the actual recovery would become possible only after a further decrease in chlorine levels. A number of recent model studies on stratospheric ozone imply that the recovery, or at least the phase-out of the springtime Antarctic stratospheric ozone depletion will start around 2020 (e.g. Shindell et al., 1998; Nagashima et al., 2002; Rosenfield et al., 2002; Schnadt

et al., 2002; Austin & Butchart, 2003, and Austin et al., 2003b).

In this study, the near past and near future polar ozone variations were simulated for four decades. Therefore, the reproduced changes in ozone are derivatives of natural variability, climate change, and halogen induced catalytic ozone depletion. The coupling between the ozone depletion and climate change makes predictions of the ozone depletion very challenging since there is no straightforward way to isolate the ozone changes due to increased halogen chemistry from the changes that the depleted ozone has on stratospheric temperatures (e.g. WMO, 2003). In this work, the coupling between these two major players was "delivered" into the FinROSE results from an external CCM simulation that takes these ozone-climate couplings into account. While it is not easy to make the separation between the climate change effects and the effect of changes in halogen loadings, the results of this study show at least that: i) No significant recovery of Antarctic ozone was simulated by the model, ii) That over the Arctic areas no massive denitrifications were simulated, and iii) That temperatures favourable for ice-form PSC cloud formation were not simulated, on a monthly average scale, in the Arctic during the near future. Therefore, I may conclude that while the results shown in this study do not provide clear signals of ozone-climate coupling, they provide some generalized ideas about different mechanisms that are sensitive to the stratospheric cooling due to the climate change and ozone depletion.

Over the Antarctica, the period until the end of 2019 was rather similar to the latter half of the past period (1980-1999). This rather expected result is due to the fact that enough inorganic chlorine will be available for massive destruction of ozone also in the near future, and due to the fact that the stratospheric temperatures drop below freezing point on annual basis, causing vertically deep and almost complete denitrifications also on annual basis. Over the Arctic high latitudes the expected cooling of the stratosphere due to increased greenhouse gas concentrations did not exhibit any massive-scale, vertically profound denitrifications, though reductions up to 75% were detected around 20km altitude. However, even after such NO_y reduction, the remaining NO_y mixing ratio was high enough for cancelling the massive ozone depletions at the denitrified level, after the springtime disappearance of PSCs. It was therefore suggested that for significant Arctic denitrification the remaining NO_y should be around or less than $3ppb_v$. It was also suggested that in order to have significant ozone depletion during the future when the inorganic chlorine levels in the atmosphere are expected to decrease, the needed reductions of NO_y , due to the PSC sedimentation, are increased accordingly. These results are therefore suggesting that the increases in the GHG-concentrations will not lead to any enhanced northern stratospheric ozone destruction before 2020.

The results of this study are clearly showing problems on the Arctic side, as the Brewer-Dobson circulation was inaccurately simulated. However, the simulated trend estimates are suggesting, in line with WMO (2003) that Antarctic like

ozone depletion over the high northern latitudes during the near-future period is highly unlikely. From the fact that observed-like low Arctic ozone events were simulated both during the past and future periods, it is expected that similar events will take place also during the future depending mainly on the amount of available halogens in the atmosphere, and the magnitudes of the NO_y reductions due to the PSC sedimentation. It was also noted, in line with Austin and Butchart (2003) and WMO (2003), that the results of this study were demonstrating the effects of stratospheric cooling at the upper levels of the stratosphere. However, this effect is less significant from the column total ozone perspective.

In this study high-latitude stratospheric ozone changes were addressed. From this perspective the changes in those tropospheric processes, like planetary-scale and synoptic-scale disturbances and height of the tropopause that affect the upper tropospheric-lower stratospheric ozone have not been directly addressed. While the results shown were exhibiting some signals of the changes in tropopause heights (i.e. downward ozone trends close to the level of tropopause), the possible changes in the stratospheric planetary wave drag driving the Brewer-Dobson circulation were somewhat hard to analyse due to the insufficient reproduction of the Brewer-Dobson circulation, and were explicitly left out from the analysis and discussions.

In summary, I seal this work as follows: 1) The CTM models are reproducing sound results when driven with CCM winds and temperatures, 2) The near future springtime ozone depletions will stay similar to those observed during the past decade, and finally 3) The atmospheric halogen loadings drive the changes in the near future ozone depletions, while the magnitudes of the denitrifications drive the magnitudes of individual ozone depletion seasons.

References

Andrews, D. G., J. R. Holton, and C. B. Leovy (1987), Middle Atmospheric Dynamics, 489 pp., Academic Press.

Atkinson R, Baulch DL, Cox RA, Hampson RF, Kerr JA, Rossi MJ, Troe J, (2000), Evaluated kinetic and photochemical data for atmospheric chemistry: Supplement VIII, Halogen species - IUPAC subcommittee on gas kinetic data evaluation for atmospheric chemistry, Journal of Physical and Chemical Reference Data, Vol.29, No. 2, pp.167-266.

Austin, J. (2002), A Three-Dimensional Coupled Chemistry-Climate Model Simulation of Past Stratospheric Trends. Journal of the Atmospheric Sciences: Vol. 59, No. 2, 218-232.

Austin, J. and N. Butchart (2003), Coupled chemistry-climate model simulations for the period 1980 to 2020: Ozone depletion and the start of ozone recovery, Q.J. Roy. Meteorol. Soc., 129, 3225-3249.

Austin, J., N. Butchart, C. Claud,, C. Cagnazzo, A. Hauchecorne, J. Hampson, J. Kaurola, J. Damski, L. Thölix, U. Langematz, P. Mieth, K. Nissen, L. Grenfell, W. Lahoz, S. Hare, and P. Canziani, (2003a), EuroSPICE: The European Project on Stratospheric Processes and their Influence on Climate and the Environment - Description and brief Highlights. In: SPARC newsletter no 21, July 2003, pp. 15-19.

Austin, J., Butchart, N. and Knight, J. (2001), Three-dimensional chemical model simulations of the ozone layer. 2015-2055. Q. J. R. Meteorol. Soc., 127, 959-974.

Austin, J., Butchart, N. and Shine, K. P. (1992), Possibility of an Arctic ozone hole in a doubled-CO2 climate. Nature, 360, 221-225.

Austin, J., Shindell, D., Bruhl, C., Dameris, M., Manzini, E., Nagashima, T., Newman, P., Pawson, S., Pitari, G., Rozanov, E., Schnadt, C. and Shepherd, T. G. (2003b), Uncertainties and assessments of chemistry-climate models of the stratosphere. Atmos. Chem. Phys., 3, 1-27.

Backman L., Damski, J., Thölix, L. and Kaurola, J. (2004), A Chemistry-Transport Model Simulation of Middle Atmospheric Ozone from 1980 to 2019 Using Coupled Chemistry GCM Winds and Temperatures, Proceedings of the XX Quadrennial Ozone Symposium 1-8 June 2004, Kos, Greece., Vol.II, pp. 729-730.

Bloss, W. J., S. L. Nickolaisen, R. J. Salawitch, R. R. Friedl and S. P. Sander, (2001), Kinetics of the self-reaction and 210 nm absorption cross section of the ClO dimer, J. Phys. Chem. A, 105, 11226-11239.

Brasseur, G. P. (Ed.) (1997), The Stratosphere and Its Role in the Climate System, NATO/ASI Series, Series 1: Global Environmental Change, Vo. 54, 366 pp., Springer Verlag, Berlin.

Brasseur, G. P., C. Granier, and S. Walters (1990), Future changes in stratospheric ozone and the role of heterogeneous chemistry, Nature, 348, 626-628.

Brasseur, G. P., D. A. Hauglustaine, S. Walters, P. J. Rasch, J.-F. Müller, C. Granier, and X.-X. Tie (1998), MOZART, a global chemical-transport model for ozone and related chemical tracers, 1. Model description, J. Geophys. Res., 103, 28,265-298,289.

Brasseur, G., F. Lefèvre and A. Smith (1997b), Chemical-transport models of the atmosphere. Chapter 16 in Perspectives in Environmental Chemistry, pp. 369-399, ed., D. L. Macadly, Oxford Univ. Press, NY.

Brasseur, G. P., and S. Madronich (1992), Chemistry-transport models. *Climate system modeling,* K. E. Trenberth, Ed., Cambridge University Press, 491–517.

Brasseur, G. P., J. Orlando, and G. Tyndall (Eds) (1999), Atmospheric Chemistry and Global Change, Oxford University Press, New York.

Brasseur, G.P., A. K. Smith, R. Khosravi, T. Huang, and Stacy Walters (2000), Natural and Human-Induced perturbations in the Middle Atmosphere: A Short Tutorial, Geophys. Monograph, 123, 7-20, 2000.

Brasseur, G., and S. Solomon (1984), *Aeronomy of the Middle Atmosphere (2nd ed. in 1986).* D. Reidel Publishing Company, The Netherlands, 452 pp.

Brasseur, G. P., X. Tie, P. J. Rasch, and F. Lefèvre (1997a), A three-dimensional model simulation of the Antarctic ozone hole: Impact of anthropogenic chlorine on the lower stratosphere and upper troposphere, J. Geophys. Res., 102, 8909-8930.

Broek, van den , M. M. P., J. E. Williams, A. Bregman (2004), Implementing growth and sedimentation of NAT particles in a global Eulerian model. Atmospheric Chemistry and Physics Discussions, 4, 3089-3126, 2004 SRef-ID: 1680-7375/acpd/2004-4-3089.

Butchart, N., and A. A. Scaife (2001), Removal of chlorofluorocarbons by increased mass exchange between the stratosphere and troposphere in a changing climate. Nature, 410, 799-802.

Carslaw, K. S., J. A. Kettleborough, M. J. Northway, S. Davies, R. Gao, D. W. Fahey, D. G. Baumgardner, M. P. Chipperfield, and A. Kleinböhl (2002), A vortex-scale simulation of the growth and sedimentation of large nitric acid hydrate particles, J. Geophys. Res., 107(D20), 8300, doi: 10.1029/ 2001JD000467.

Carslaw, K. S., B. Luo, and T. Peter (1995), An analytic expression for the composition of aqueous HNO3-H2SO4 stratospheric aerosols including gas phase removal of HNO3, Geophys. Res. Lett., 22(14), 1877-1880.

Chapman, S. (1930), On Ozone and Atomic Oxygen in the Upper Atmosphere, Philosophical Magazine and Journal of Science 10 (September), 369-383.

Chipperfield, M. P. (1999), Multiannual simulations with a threedimensional chemical transport model, J. Geophys. Res., 104, 1781-1805.

Chipperfield, M. P. (2003), A three-dimensional model study of long-term mid-high latitude lower stratosphere ozone changes, Atmos. Chem. Phys., 3, 1-13, 2003.

Chipperfield, M. P., D. Cariolle, P. Simon, R. Ramaroson, D. J. Lary (1993), A three-dimensional modeling study of trace species in the Arctic lower stratosphere during winter 1989-1990. J. Geophys. Res., 98, 7199-7218.

Chipperfield, M. P., W. Feng, and M. Rex (2005), Arctic ozone loss and climate sensitivity: Updated three-dimensional model study, Geophys. Res. Lett., 32, L11813, doi: 10.1029/ 2005GL022674.

Chipperfield, M. P. and Jones, R. L. (1999), Relative influences of atmospheric chemistry and transport on Arctic O3 trends, Nature, 400, 551-554.

Chipperfield, M. P., and J. A. Pyle (1998), Model sensitivity studies of Arctic ozone depletion, J. Geophys. Res., 103, 28,389- 28,403.

Crutzen, P.J., (1970), The influence of nitrogen oxides on the atmospheric ozone content. Quart. J. Roy. Meteor. Soc., 96, 320-325.

Crutzen, P. and Arnold, F. (1986): Nitric acid cloud formation in the cold Arctic stratosphere, a major cause for the springtime "ozone hole", Nature, 324, 651-655.

Cullen, M. J. P., (1993), The unified forecast/climate model. Meteor. Mag., 122, 81-94.

Damski, J., Backman, L., Thölix, L. and Kaurola, J. (2003), A Chemistry-Transport Model Simulation of Middle Atmospheric Ozone from 1980 to 2019 Using Coupled Chemistry GCM Winds and Temperatures, International Conference on Earth System Modelling, 15-19 September 2003, Max Planck Institute for Meteorology, Hamburg, Germany.

Davies, S., et al. (2002), Modeling the effect of denitrification on Arctic ozone depletion during winter 1999/2000, J. Geophys. Res., 108(D5), 8322, doi: 10.1029 / 2001JD000445.

Davies, S., G. W. Mann, K. S. Carslaw, M. P. Chipperfield, J. A. Kettleborough, M. L. Santee, H. Oelhaf, G. Wetzel, Y. Sasano, T. Sugita (2005), 3-D microphysical model studies of Arctic denitrification: comparison with observations. Atmos. Chem. Phys. Discuss., 5, 347-393.

DeMore, W. B., S. P. Sander, D. M. Golden, R. F. Hampson, M. J. Kurylo, C. J. Howard, A. R. Ravishankara, C. E. Kolb, M. J. Molina (1997), Chemical kinetics and photochemical data for use in stratospheric modeling, Evaluation No. 12, JPL Publication 97-4.

Dessler, A. E., J. Wu, M. L. Santee, and M. R. Schoeberl (1999), Satellite observations of temporary and irreversible denitrification, J. Geophys. Res., 104, 13,993-14,002.

Drdla, K., A. Tabazadeh, R. P. Turco, M. Z. Jacobson, J. E. Dye, C. Twohy, and D. Baumgardner (1994), Analysis of the physical state of one arctic polar stratospheric cloud based on observations, Geophys. Res. Lett.,21, 2475-2478.

Egorova, T. A., E. V. Rozanov, M. E. Schlesinger, N. G. Andronova, S. L. Malyshev, I. L. Karol, V. A. Zubov (2001), Assessment of the effect of the Montreal Protocol on atmospheric ozone, Geophys. Res. Lett., 28(12), 2389-2392, 10.1029/2000GL012523.

Evans, S. J., Toumi, R., Harries, J. E., Chipperfield, M. P., and Russell III, J. M. (1998), Trends in the stratospheric humidity and the sensitivity of ozone to these trends, J. Geophys. Res., 103, 8715-8725.

Fahey, D. W., S. Solomon, S. R. Kawa, M. Loewenstein, J. R. Podolske, S. E. Strahan, and K. R. Chan (1990), A diagnostic for denitrification in the winter polar stratosphere, Nature, 345, 698- 702.

Fahey, D. W., et al. (2001), The detection of large nitric-acid particles in the winter Arctic stratosphere, Science, 291, 1026-1031.

Farman, J.C., B.G. Gardiner and J.D. Shanklin (1985), Large losses of total ozone in Antarctica reveal seasonal ClOx/NOx interaction, Nature, 315, 207-210.

Fioletov, V. E., G. E. Bodeker, A. J. Miller, R. D. McPeters, and R. Stolarski (2002), Global and zonal total ozone variations estimated from ground-based and satellite measurements: 1964-2000, J. Geophys. Res., 107(D22), 4647, doi: 10.1029/ 2001JD001350.

Fioletov, V. E., and T. G. Shepherd (2005), Summertime total ozone variations over middle and polar latitudes, Geophys. Res. Lett., 32, L04807, doi: 10.1029 2004GL022080.

Fortuin, J. P. F., H. Kelder (1998), An ozone climatology based on ozonesonde and satellite measurements, J. Geophys. Res., 103(D24), 31709-31734, 10.1029/ 1998JD200008.

Fueglistaler, S., B. P. Luo, C. Voigt, K. S. Carslaw, and Th. Peter, (2002). NAT-rock formation by mother clouds: a microphysical model study. Atmos. Chem. Phys. Discuss., 2, 29-42.

Gauss, M., G. Myhre, G. Pitari, M. Prather, I. S.A. Isaksen, T. K. Berntsen, G. P. Brasseur, F. J. Dentener, R. G. Derwent, D. A. Hauglustaine, L. W. Horowitz, D. J. Jacob, M. Johnson, K. Law, L. J. Mickley, J.-F. Muller, P.-H. Plantevin, J. A. Pyle, D. S. Stevenson, J. K. Sundet, M. Van Weele, and O. Wild (2003), Radiative forcing in the 21st century due to ozone changes in the troposphere and lower stratosphere, J. Geophys. Res., 108(D9), 4292, doi: 10.1029/ 2002JD002624.

Graf, H.F., I. Kirchner, and J. Perlwitz, Changing lower stratospheric circulation (1998), The role of ozone and greenhouse gases, J. Geophys. Res., 103, 11251-11261.

Granier, C., and G. Brasseur (1991), Ozone and other trace gases in the Arctic and Antarctic regions: A three-dimensional model simulation, J. Geophys. Res., 96, 2995-3011.

Granier, C., and G. P. Brasseur (1992), Impact of heterogeneous chemistry on model predictions of ozone changes, J. Geophys. Res., 97, 18,015-18,033.

Grooß, J.-U. ,G. Günther, R. Müller, P. Konopka, S. Bausch, H. Schlager, C. Voigt, C. M. Volk, G. C. Toon (2005), Simulation of denitrification and ozone loss for the Arctic winter 2002/2003, Atmos. Chem. Phys., 5, 1437-1448.

Hadjinicolaou, P., Jrrar, A., Pyle, J. A., and Bishop, L. (2002), The dynamically driven long-term trend in stratospheric ozone over northern mid-latitudes, Q. J. Roy. Met. Soc., 128, 1393-1412.

Hall, T.M., D.W. Waugh, K.A. Boering, and R.A. Plumb (1999), Evaluation of transport in atmospheric models, J. Geophys. Res., 104, 18815-18839.

Hanson, D., and K. Mauersberger (1988), Laboratory studies of the nitric acid tridydrate: Implications for the south polar stratosphere, Geophys. Res. Lett., 15, 855-858.

Hassinen, S., Kyrölä, E., Seppälä, A., Auvinen, H., Haley, C., Damski, J., Backman, L. (2004), Stratospheric ozone development as seen by assimilated OSIRIS and GOMOS data covering the year 2003, Proceedings of the XX Quadrennial Ozone Symposium 1-8 June 2004, Kos, Greece, Vol.I, pp. 348-349.

Harris, N. R. P., M. Rex, F. Goutail, B. M. Knudsen, G. L. Manney, R. Müller, and P. von der Gathen (2002), Comparison of empirically derived ozone losses in the Arctic vortex, J. Geophys. Res., 107(D20), 8264, doi: 10.1029/ 2001JD000482

Haynes, P. (2005), Stratospheric Dynamics, Annual Review of Fluid Mechanics Vol. 37: 263-293 (Volume publication date January 2005) (doi: 10.1146/ annurev.fluid.37.061903.175710).

Hein, R., Dameris, M., Schnadt, C., Land, C., Grewe, V., Kohler, L., Ponater, M., Sausen, R., Steil, B., Landgraf, L. and Bruhl, C. (2001), Results of an interactively coupled atmospheric chemistry-general circulation model: comparison with observations. Ann. Geophysicae, 19, 435-457.

Hintsa, E. J., et al. (1998), Dehydration and denitrification in the Arctic polar vortex during the 1995 - 1996 winter, Geophys. Res. Lett., 25, 501-504.

Horowitz, L. W., et al. (2003), A global simulation of tropospheric ozone and related tracers: Description and evaluation of MOZART, version 2, J. Geophys. Res., 108(D24), 4784, doi: 10.1029/ 2002JD002853.

Hu, R.-M., K. S. Carslaw, C. Hostetler, L. R. Poole, B. Luo, T. Peter, S. Füeglistaler, T. J. McGee, and J. F. Burris (2002), Microphysical properties of wave polar stratospheric clouds retrieved from lidar measurements during SOLVE/THESEO 2000, J. Geophys. Res., 107(D20), 8294, doi:10.1029/ 2001JD001125.

IPCC (1990), *Climate change–The IPCC Scientific Assessment*, edited by J. T. Houghton, G. J. Jenkins, and J. J. Ephraums, Cambridge University Press.

IPCC (1992), *Climate Change 1992–The Supplementary Report to the IPCC Scientific Assessment*, edited by J.T. Houghton, B.A. Callander, and S.K. Varney, Cambridge University Press.

IPCC (1996) , *Climate Change 1995–The Science of Climate Change*, edited by J.T. Houghton, L.G. Meira Filho, J. Bruce, H. Lee, B.A. Callander, E. Haites, N. Harris, and K. Maskell, Cambridge University Press.

IPCC (2001), *Climate Change 2001–The Scientific Basis. Contribution of Working Group I to the IPCC Third Assessment Report*, edited by Houghton, J.T., Ding, Y., Griggs, D.J., Noguer, M., van der Linden, P.J., Dai, X., Maskell, K. and Johnson, C.A., Cambridge University Press.

Jensen, E., O. B. Toon, K. Drdla, and A. Tabazadeh (2002), Impact of polar stratospheric cloud particle composition, number density, and lifetime on denitrification, J. Geophys. Res., 107(D20), 8284, doi: 10.1029/ 2001JD000440.

Jöckel, P., R. von Kuhlmann, M. G. Lawrence, B. Steil, C. A. M. Brenninkmeijer, P. J. Crutzen, P. J. Rasch, and B. Eaton (2001), On a fundamental problem in implementing flux-form advection schemes for tracer transport in 3-dimensional general circulation and chemistry transport models, Q. J. R. Meteorol. Soc., 127, 1035-1052.

Khosravi, R., G. Brasseur, A. Smith, D. Rusch, J. Waters and J. Russell III (1998), Significant reduction in the stratospheric ozone deficit using a three-dimensional model constrained with UARS data, J. Geophys. Res., 103, 16203-16219.

Kleinböhl, A., et al. (2002), Vortexwide denitrification of the Arctic polar stratosphere in winter 1999/2000 determined by remote observations, J. Geophys. Res., 108(D5), 8305, doi: 10.1029/ 2001JD001042

Knudsen, B. M., N. R. P. Harris, S. B. Andersen, B. Christiansen, N. Larsen, M. Rex, and B. Naujokat (2004), Extrapolating future Arctic ozone losses, Atmos. Chem. Phys., 4, 1849-1856. SRef-ID: 1680-7324/acp/2004-4-1849.

Kondo, Y., et al. (1999), NOy-N2O correlation observed inside the Arctic vortex in February 1997: Dynamical and chemical effects, J. Geophys. Res., 104, 8215-8224.

Kondo, Y., H. Irie, M. Koike, and G.E. Bodeker (2000), Denitrification and nitrification in the Arctic stratospheric during the winter of 1996-1997, Geophys. Res. Lett., 27, 337-340.

Krämer M., Müller R., Bovensmann H., Burrows J., Brinkmann J., Röth E.P., GrooßJ.-U., Müller R., Woyke T., Ruhnke R., Günther G., Hendricks J., Lippert E., Carslaw K.S., Peter T., Zieger A., Brühl C., Steil B., Lehmann R., McKenna D.S. (2003), Intercomparison of Stratospheric Chemistry Models under Polar Vortex Conditions, Journal of Atmospheric Chemistry, Volume 45, Number 1, 51-77(27).

Kylling, A. (1992), Radiation transport in cloudy and aerosol loaded atmosphere. Ph.D. thesis, University of Alaska.

Kylling, A., A. Albold, G. Seckmeyer (1997), Transmittance of a cloud is wavelength - dependent in the UV-range: Physical interpretation, Geophys. Res. Lett., 24(4), 397-400, 10.1029/ 97GL00111.

Langematz U., M. Kunze, K. Krüger, K. Labitzke, and G. L. Roff (2003), Thermal and dynamical changes of the stratosphere since 1979 and their link to ozone and CO2 changes, J. Geophys. Res., 108 (D1), 4027, doi: 10.1029/ 2002JD002069.

Lary, D.J., M.P. Chipperfield, J.A. Pyle, W.A. Norton, L.P. Rushojgaard (1995), Three-dimensional tracer initialization and general diagnostics using equivalent PV latitude-potential-temperature coordinates, Q. J. Roy. Met. Soc., vol. 121, no. 521, pp. 187-210(24).

Lefèvre, F., G. Brasseur, I. Folkins, and A. K. Smith (1994), Stratospheric chlorine monoxide and ozone: Three-dimensional model simulations, J. Geophys. Res., 99, 8183-8195.

Leggett, J., Pepper, W.J. and Swart, R.J. (1992), Emissions Scenarios for the IPCC: An Update. In: Climate Change 1992: The Supplementary Report to the IPCC Scientific Assessment (Eds. Houghton, J.T., Callander, B.A. and Varney, S.K.). Cambridge University Press, Cambridge, pp.69-95.

Levelt, P., B. Khattatov, J. Gille, G. Brasseur, X. Tie, and J. Waters (1998), Assimilation of MLS ozone measurements in the global three-dimensional chemistry transport model ROSE, Geophys. Res. Lett., 25, 4493-4496.

Lin, S.-J., and R. B. Rood (1996), Multidimensional flux-form semi-lagrangian transport schemes, Mon. Weather Rev., 124, 2046-2070.

Lin, S.-J., W. C. Chao, Y. C. Sud, and G. K. Walker (1994), A class of the van Leer-type transport schemes and its applications to the moisture transport in a General Circulation Model, Mon. Wea. Rev., 122, 1575-1593.

Mann, G. W., S. Davies, K. S. Carslaw, M. P. Chipperfield, and J. Kettleborough (2002a), Polar vortex concentricity as a controlling factor in Arctic denitrification, J. Geophys. Res., 107(D22), 4663, doi: 10.1029/ 2002JD002102.

Mann, G. W. ,S. Davies, K. S. Carslaw, and M. P. Chipperfield (2002b), Factors controlling Arctic denitrification in cold winters of the 1990s, Atmos. Chem. Phys. Discuss., 2, 2557-2586.

Mann, G. W., K. S. Carslaw, M. P. Chipperfield, S. Davies, and S. D. Eckermann (2005), Large nitric acid trihydrate particles and denitrification caused by mountain waves in the Arctic stratosphere, J. Geophys. Res., 110, D08202, doi: 10.1029/ 2004JD005271.

Manzini, E., B. Steil, C. Brühl, M. A. Giorgetta, and K. Krüger (2003), A new interactive chemistry-climate model: 2. Sensitivity of the middle atmosphere to ozone depletion and increase in greenhouse gases and implications for recent stratospheric cooling, J. Geophys. Res., 108(D14), 4429, doi: 10.1029/ 2002JD002977.

Marti, J. and K Mauersberger (1993), A survey and new measurements of ice vapor pressure at temperatures between 170 and 250 K, GRL 20, 363-366.

Massie, S. T., X.X. Tie, G. P. Brasseur, R. M. Bevilacqua, M. D. Fromm, and M. L. Santee (2000), Chlorine activation during the early 1995-1996 Arctic winter, J. Geophys. Res., 105, 7111-7131.

Mayer, B., A. Kylling, S. Madronich, G. Seckmeyer (1998), Enhanced absorption of UV radiation due to multiple scattering in clouds: Experimental evidence and theoretical explanation, J. Geophys. Res., 103(D23), 31241-31254, 10.1029/ 98JD02676.

Miles, G.M. , R.G. Grainger, E.J. Highwood (2004), The significance of volcanic eruption strength and frequency for climate, Q. J. Roy. Met. Soc., vol. 130, no. 602, pp. 2361-2376(16).

McLinden, C. A., S. C. Olsen, B. Hannegan, O. Wild, M. J. Prather, and J. Sundet (2000), Stratospheric ozone in 3-D models: A simple chemistry and the cross-tropopause flux, J. Geophys. Res., 105, 14653-14665.

Molina, M.J. and F.S. Rowland (1974), Stratospheric sink for chlorofluoromethanes-chlorine atom catalyzed destruction of ozone. Nature, 249, 810.

Nagashima, T., Takahashi, M., Takigawa, M. and Akiyoshi, H. (2002), Future development of the ozone layer calculated by a general circulation model with fully interactive chemistry. Geophys. Res. Lett., 29, doi: 10.1029/ 2001GL014026

NASA (2000), Studying Earth's Environment From Space – NASA-textbook, June 2000. (Materials accessed during April-August 2005),
http: //www.ccpo.odu.edu/SEES/index.html.

Newman, P. A., S. R. Kawa, and E. R. Nash (2004), On the size of the Antarctic ozone hole, Geophys. Res. Lett., 31, L21104, doi: 10.1029/ 2004GL020596.

Northway, M. J., et al. (2002), An analysis of large HNO3-containing particles sampled in the Arctic stratosphere during the winter of 1999 - 2000, J. Geophys. Res., 107(D20), 8298, doi: 10.1029/ 2001JD001079.

Pawson, S., et al. (2000), The GCM-reality intercomparison project for SPARC (GRIPS): Scientific issues and initial results. Bull. Am. Meteorol. Soc., 81, 781-796.

Plumb, R. A. (2002), Stratospheric Transport, J. Meteor. Soc. Japan,80, 793-809.

Post P., Backman, L., Van Roozendael, M., Damski, J., Fayt, C. and Taalas, P. (2004), Tropospheric BrO columns derived by use of ERS-2 GOME and 3D CTM FinROSE, Proceedings of the XX Quadrennial Ozone Symposium 1-8 June 2004, Kos, Greece, Vol.II, pp. 1024-1025.

Prather, M., M. McElroy, S. Wofsy, G. Russel, and D. Rind (1987), Chemistry of the Global Troposphere: Fluorocarbons as Tracers of Air Motion, J. Geophys. Res., vol. 92, No. D6, pp 6579 - 6613.

Ramaswamy, V., and M. D. Schwarzkopf (2002), Effects of ozone and well-mixed gases on annualmean stratospheric temperature trends, Geophys. Res. Lett., 29(22), 2064, doi: 10.1029/2002GL015141.

Randel, W.J., and P.A. Newman, 1999: The Stratosphere in the Southern Hemisphere. Chapter 6 of the AMS Monograph Meteorology of the Southern Hemisphere. Published by the American Meteorological Society, pp. 243-282.

Randel, W.J., and F. Wu (1999), A stratospheric ozone trends data set for global modeling studies. Geophys. Res. Lett., 26, 3089-3092.

Rasch, P. J., B. A. Boville, and G. P. Brasseur (1995), A three-dimensional general circulation model with coupled chemistry for the middle atmosphere, J. Geophys. Res., 100, 9041-9071.

Rex, M., et al. (1997), Prolonged stratospheric ozone loss in the 1995- 96 Arctic winter, Nature, 389, 835- 838.

Rex, M., R. J. Salawitch, P. von der Gathen, N. R. P. Harris, M. P. Chipperfield, and B. Naujokat (2004), Arctic ozone loss and climate change, Geophys. Res. Lett., 31, L04116, doi: 10.1029/ 2003GL018844

Riese, M., X. Tie, G. Brasseur and D. Offermann (1999), Three-dimensional simulation of stratospheric trace gas distributions measured by CRISTA, J. Geophys. Res., 104, 16419-16435.

Roscoe H.K., Fowler C.L., Shanklin J.D., Hill J.G.T. (2004), Possible long-term changes in stratospheric circulation: Evidence from total ozone measurements at the edge of the Antarctic vortex in early winter, Q. J. Roy. Met. Soc., vol. 130, no. 598, pp. 1123-1135(13).

Rosenfield, J. E., D. B. Considine, P. E. Meade, J. T. Bacmeister, C. H. Jackman, and M. R. Schoeberl (1997), Stratospheric effects of Mount Pinatubo aerosol studied with a coupled two-dimensional model, J. Geophys. Res., 102, 3649-3670.

Rosenfield, J.E., A.R. Douglass, and D.B. Considine (2002), The impact of increasing carbon dioxide on ozone recovery, J. Geophys. Res., 107 (D6), 4049, doi: 10.1029/ 2001JD000824.

Rose K., and G. Brasseur (1989), A three-dimensional model of chemically active trace species in the middle atmosphere during disturbed winter conditions, J. Geophys. Res., 94, D13, 16387-16403.

Rummukainen, M., Isaksen, I. S. A., Rognerud, B., and Stordal, F. (1999), A global model tool for three-dimensional multiyear stratospheric chemistry simulations: Model description and first results, J. Geophys. Res., 104, 26437-26456.

Sander, S. P., Friedl, R. R., DeMore, W. B., Ravishankara, A. R., Golden, D. M., Kolb, C. E., Kurylo, M. J., Hampson, R. F., Huie, R. E., Molina, M. J. and

Moortgat, G. K. (2000), Chemical Kinetics and Photochemical Data for Use in Stratospheric Modeling Supplement to Evaluation 12: Update of Key Reactions, Evaluation No 13, JPL Publ. 00-3.

Sander, S.P., A.R. Ravishankara, R.R Friedl, et al. (2003), Chemical Kinetics and Photochemical Data for Use in Atmospheric Studies, Evaluation Number 14, JPL Publ. 02-25.

Santer, B. D., et al. (2003), Behavior of tropopause height and atmospheric temperature in models, reanalyses, and observations: Decadal changes, J. Geophys. Res., 108(D1), 4002, doi: 10.1029/ 2002JD002258.

Santee, M.L., G.L. Manney, L. Froidevaux, W.G. Read, and J.W. Waters (1999), Six years of UARS microwave limb sounder HNO3 observations: Seasonal, interhemispheric, and interannual variations in the lower stratosphere, J. Geophys. Res., 104, 8225- 8246.

Santee, M.L., G.L. Manney, N.J. Livesey, and J.W. Waters (2000), UARS Microwave Limb Sounder observations of denitrification and ozone loss in the 2000 Arctic late winter, Geophys. Res. Lett., 27, 3213-3216.

Scaife, A. A., Butchart, N., Warner, C., Stainforth, D., Norton, W. and Austin, J. (2000), Realistic Quasi-Biennial Oscillations in a simulation of the global climate, Geophys. Res. Lett., 27, 3481-3484.

Schnadt, C., M. Dameris, M. Ponater, R. Hein, V. Grewe, and B. Steil (2002), Interaction of atmospheric chemistry and climate and its impact on stratospheric ozone, Clim. Dyn., 18, 501-517.

Seinfeld, J.H., and Pandis, S.M (1997), Atmospheric Chemistry and Physics, From Air Pollution to Climate Change, John Wiley & Sons, 1997.

Shindell, D.T., Rind, D. and Lonergan, P. (1998), Increased polar stratospheric ozone losses and delayed eventual recovery owing to increasing greenhouse-gas concentrations. Nature 392, 589 - 592 (09 April 1998); doi: 10.1038/ 33385.

Shepherd, Ted, Plumb, R. Alan, Wofsy, Steven C. (2005), PREFACE, Journal of the Atmospheric Sciences, 62: 565-566.

Shine, K. P., Bourqui, M. S., Forster, P. M. de F., Hare, S. H. E., Langematz, U., Braesicke, P., Grewe, V., Schnadt, C., Smith, C. A., Haigh, J. D., Austin, J., Butchart, N., Shindell, D., Randel, W. J., Nagashima, T., Portmann, R. W., Solomon, S., Seidel, D., Lanzante, J., Klein, S., Ramaswamy, V. and Schwarzkopf, M. D. (2003), A comparison of model-predicted trends in stratospheric temperatures. Q. J. Roy. Met. Soc., 129, 1565-1588.

Smith, A. K. (1995a), Numerical simulation of global variations of temperature, ozone, and trace species in the stratosphere, J. Geophys. Res., 100(D1), 1253-1270.

Smith, A. K. (1995b), Impact of averaged photolysis rates on stratospheric chemical models, J. Geophys. Res., 100(D6), 11,173-11,184.

Smolarkiewitz, P. K., and P. J. Rasch, (1991), Monotone advection on the sphere: An Eulerian versus semi-Lagrangian approach, J. Atmos. Sci., 48, 793–810.

Solomon, S. (1999), Stratospheric ozone depletion: A review of concepts and history, Rev. Geophys., 37, 275-316.

Solomon, S., R.R. Garcia, F.S. Rowland, and D.J. Wuebbles (1986), On the depletion of Antarctic ozone, Nature, 321, 755-758.

Steil, B., C. Brühl, E. Manzini, P. J. Crutzen, J. Lelieveld, P. J. Rasch, E. Roeckner, and K. Krüger (2003), A new interactive chemistry-climate model: 1. Present-day climatology and interannual variability of the middle atmosphere using the model and 9 years of HALOE/UARS data, J. Geophys. Res., 108(D9), 4290, doi: 10.1029/ 2002JD002971.

Stenke, A. and V. Grewe (2005), Simulation of stratospheric water vapor trends: impact on stratospheric ozone chemistry, Atmos. Chem. Phys., 5, 1257-1272, SRef-ID: 1680-7324/acp/ 2005-5-1257.

Stolarski, R. S., Cicerone, R. J. (1974), Stratospheric Chlorine: A Possible Sink for Ozone, Canadian Journal of Chemistry, 52, 1610-1615.

Tabazadeh, A., Drdla, K., Schoeberl, M. R., Hamill, P., and Toon, O. B. (2002), Arctic "ozone hole" in a cold volcanic stratosphere, Proc. Nat. Acad. Sci. USA, 99, 2609-2612.

Tabazadeh, A., E. J. Jensen, O. B. Toon, K. Drdla, and M. R. Schoeberl (2001), Role of the stratospheric polar freezing belt in denitrification, Science, 291, 2591-2594.

Tabazadeh, A., et al. (2000), Quantifying denitrification and its effect on ozone recovery, Science, 288, 1407-1411.

Tian, W., and M.P. Chipperfield (2005), A New coupled chemistry-climate model for the stratosphere: The importance of coupling for future O3-climate predictions, Q.J. Roy. Met. Soc., 131, 281-303.

Tie, X.X. and G. Brasseur, (1996), The importance of heterogeneous bromine chemistry in the lower stratosphere. Geophysical Research Letters, 23, 2505-2508.

Tie, X., G. Brasseur and C. Granier (1996), Model study of polar stratospheric clouds and their effect on stratospheric ozone. 2. Model results. Journal of Geophysical Research, 101, 12575-12584.

Tie, X.X., C. Granier, W. Randel and G. Brasseur (1997), Effects of interannual variation of temperature on heterogeneous reactions and stratospheric ozone. J. Geophys. Res., 102, 23519-23527.

Tilmes, S. , Müller, R., Grooß, J. -U. and Russell III, J. M. (2004), Ozone loss and chlorine activation in the Arctic winters 1991-2003 derived with the tracer-tracer correlations, Atmospheric Chemistry and Physics, Vol. 4, pp 2181-2213.

Toon, O. B., E. V. Browell, S. Kinne, and J. Jordan (1990), An analysis of lidar observations of polar stratospheric clouds, Geophys. Res. Lett., 17, 393-396.

Trenberth, K. E. (1992), *Climate system modeling*, Cambridge University Press, 788 pp.

UNEP (2000), "The Montreal Protocol on Substances that Deplete the Ozone Layer as adjusted and/or amended in in London 1990, Copenhagen 1992, Vienna 1995, Montreal 1997, Beijing 1999", Ozone Secretariat, United Nations Environment Programme,
http://www.unep.org/ozone.

Voigt, Ch., J. Schreiner, A. Kohlmann, P. Zink, K. Mauersberger, N. Larsen, T. Deshler, C. Kröger, J. Rosen, A. Adriani, F. Cairo, G. Di Donfrancesco, M. Viterbini, J. Ovarlez, H. Ovarlez, Ch. David, A. Dörnback (2000), Nitric Acid Trihydrate (NAT) in Polar Stratospheric Clouds, Science, 290, 1756-1758.

Waibel, A. E., et al. (1999), Arctic ozone loss due to denitrification, Science, 283, 2064- 2069.

Waugh, D., and T. Hall (2002), Age of stratospheric air: Theory, observations, and models, Rev. Geophys., 40(4), 1010, doi: 10.1029/ 2000RG000101.

Waugh, D.W., W.J. Randel, S. Pawson, P.A. Newman, and E.R. Nash (1999), Persistence of the lower stratospheric polar vortices, J. Geophys. Res., 104, 27191-27201.

Weatherhead, E. C., Reinsel, G. C., Tiao, G. C., Meng, X.-L., Choi, D., Cheang, W.-K., Keller, T., DeLuisi, J., Wuebbles, D. J., Kerr, J. B., Miller, A. J., Oltmans, S. J. and Frederick, J. E. (1998), Factors affecting the detection of trends: statistical considerations and applications to environmental data. J. Geophys. Res., 103, 17149-17161.

Weatherhead, E. C., Reinsel, G. C., Tiao, G. C., Jackman, C. H., Bishop, L., Hollandsworth Frith, S. M., DeLuisi, J., Keller, T., Oltmans, S. J., Fleming, E. L., Wuebbles, D. J., Kerr, J. B., Miller, A. J., Herman, J., McPeters, R., Nagatani, R. M. and Frederick, J. E. (2000), Detecting the recovery of total column ozone. J. Geophys. Res., 105, 22201-22210.

Wellemeyer, C.G., P.K. Bhartia, R.D. McPeters, S.L. Taylor, and Ch. Ahn (2004), A New Release of Data from the Total Ozone Mapping Spectrometer (TOMS), SPARC Newsletter, 22, 37-38, available at www.aero.jussieu.fr/˜sparc.

Williams, K. D., Senior, C. A. and Mitchell, J. F. B. (2001), Transient climate change in the Hadley Centre models: the role of physical processes. J. Climate, 14, 2659-2674.

WMO (1986), Atmospheric Ozone 1985, WMO Rep. 16, Global Ozone Res. and Monit. Proj., Geneva, Switzerland.

WMO (1992), Scientific Assessment of Ozone Depletion: 1991. *Global Ozone and Monitoring Project,* Report NO. 25, Geneva, Swizerland.

WMO (1994), Scientific Assessment of Ozone Depletion: 1994. *Global Ozone and Monitoring Project,* Report NO. 37, Geneva, Swizerland.

WMO (1999), Scientific Assessment of Ozone Depletion: 1998, Global Ozone Research and Monitoring Project, Report No. 44, Geneva.

WMO (2003), Scientific Assessment of Ozone Depletion: 2002, Global Ozone Research and Monitoring Project, Report No. 47, 498 pp., Geneva.

Wohltmann, I., M. Rex, D. Brunner, and J. Mäder (2005), Integrated equivalent latitude as a proxy for dynamical changes in ozone column, Geophys. Res. Lett., 32, L09811, doi: 10.1029/ 2005GL022497.

Zalesak, S. T. (1979), Fully multidimensional flux-corrected transport algorithms for fluid. J. Comput. Phys., 31, 335-362.

Appendix

Acronyms and Abbreviations

3-D	three-dimensional
CANDIDOZ	Chemical ANd Dynamical Influences on Decadal OZone changes
CFC	chlorofluorocarbon
CNRS	Centre National de la Recherche Scientifique (France)
CCM	chemistry-coupled general circulation model or chemistry climate model
CTM	chemical transport model or chemistry transport model
DJF	December-January-February
DLR	Deutschen Zentrum für Luft- und Raumfahrt (Germany)
DU	Dobson unit
EC	European Commission
ECMWF	European Centre for Medium-Range Weather Forecasts (UK)
EP	Earth Probe
EU	European Union
EuroSPICE	European project on Stratospheric Processes and their Impact on Climate and the Evironment
FAUVOR	Finnish Antarctic UV and Ozone Research
FIGARE	Finnish Global Change Research Programme
FSLT	flux-form semi-Lagrangian scheme
GCM	general circulation model
GHG	greenhouse gas
GOME	Global Ozone Monitoring Experiment
GWP	Global Warming Potential
HALOE	Halogen Occultation Experiment
HCFC	hydrochlorofluorocarbon
HFC	hydrofluorocarbon
hPa	hectoPascal
IS92a	"business-as-usual" type GHG emission scenario
IPCC	Intergovernmental Panel on Climate Change
IUPAC	International Union of Pure and Applied Chemistry
JJA	June-July-August
JPL	Jet Propulsion Laboratory (NASA)
LOUVRE	Long-term Ozone and UV Estimates
MAM	March-April-May
MOZART	Model for Ozone and Related Chemical Tracers, version 2
MPI-M	Max-Planck-Institut für Meterologie (Germany)

Appendix: Acronyms and Abbreviations

N7	Nimbus-7 (satellite)
NASA	National Aeronautics and Space Administration (USA)
NAT	nitric acid trihydrate
NCAR	National Center for Atmospheric Research (USA)
ODP	Ozone Depletion Potential
ODS	ozone-depleting substance
ppb	parts per billion
ppb_v	parts per billion by volume
ppm	parts per million
ppm_v	parts per million by volume
ppt	parts per trillion
ppt_v	parts per trillion by volume
PCE	photochemical equilibrium
PRT	photochemical replacement time
PSC	polar stratospheric cloud
PV	potential vorticity
PWD	planetary-wave drag
QBO	quasi-biennial oscillation
QUOBI	Quantitative Understanding of Ozone losses by Bipolar Investigations
RETRO	REanalysis of the TROpospheric chemical composition over the past 40 years
SBUV	solar backscatter UV instrument (on N7 satellite)
SON	September-October-November
SPARC	Stratospheric Processes and Their Role in Climate (WCRP)
STS	supercooled ternary solution
SZA	solar zenith angle
TOMS	Total Ozone Mapping Spectrometer
UARS	Upper Atmosphere Research Satellite
UKMO	United Kingdom Meteorological Office
UM	unified model
UMETRAC	Unified Model with Eulerian Transport and Chemistry
UNEP	United Nations Environment Programme
UV	ultraviolet
WMGHG	well-mixed greenhouse gas
WMO	World Meteorological Organization

Finnish Meteorological Institute Contributions

1. Joffre, Sylvain M., 1988. Parameterization and assessment of processes affecting the long-range transport of airborne pollutants over the sea. 49 p.

2. Solantie, Reijo, 1990. The climate of Finland in relation to its hydrology, ecology and culture. 130 p.

3. Joffre, Sylvain M. and Lindfors, Virpi, 1990. Observations of airborne pollutants over the Baltic Sea and assessment of their transport, chemistry and deposition. 41 p.

4. Lindfors, Virpi, Joffre, Sylvain M. and Damski, Juhani, 1991. Determination of the wet and dry deposition of sulphur and nitrogen compounds over the Baltic Sea using actual meteorological data. 111 p.

5. Pulkkinen, Tuija, 1992. Magnetic field modelling during dynamic magnetospheric processes. 150 p.

6. Lönnberg, Peter, 1992. Optimization of statistical interpolation. 157 p.

7. Viljanen, Ari, 1992. Geomagnetic induction in a one- or two-dimensional earth due to horizontal ionospheric currents. 136 p.

8. Taalas, Petteri, 1992. On the behaviour of tropospheric and stratospheric ozone in Northern Europe and in Antarctica 1987-90. 88 p.

9. Hongisto, Marke, 1992. A simulation model for the transport, transformation and deposition of oxidized nitrogen compounds in Finland — 1985 and 1988 simulation results. 114 p.

10. Taalas, Petteri, 1993. Factors affecting the behaviour of tropospheric and stratospheric ozone in the European Arctic and Antarctica. 138 s.

11. Mälkki, Anssi, 1993. Studies on linear and non-linear ion waves in the auroral acceleration region. 109 p.

12. Heino, Raino, 1994. Climate in Finland during the period of meteorological observations. 209 p.

13. Janhunen, Pekka, 1994. Numerical simulations of E-region irregularities and ionosphere-magnetosphere coupling. 122 p.

14. Hillamo, Risto E., 1994. Development of inertial impactor size spectroscopy for atmospheric aerosols. 148 p.

15. Pakkanen, Tuomo A., 1995. Size distribution measurements and chemical analysis of aerosol components. 157 p.

16. Kerminen, Veli-Matti, 1995. On the sulfuric acid-water particles via homogeneous nucleation in the lower troposphere. 101 p.

17. Kallio, Esa, 1996. Mars-solar wind interaction: Ion observations and their interpretation. 111 p.

18. Summanen, Tuula, 1996. Interplanetary Lyman alpha measurements as a tool to study solar wind properties. 114 p.

19. Rummukainen, Markku, 1996. Modeling stratospheric chemistry in a global three-dimensional chemical transport model, SCTM-1. Model development. 206 p.

20. Kauristie, Kirsti, 1997. Arc and oval scale studies of auroral precipitation and electrojets during magnetospheric substorms. 134 p.

21. Hongisto, Marke, 1998. Hilatar, A regional scale grid model for the transport of sulphur and nitrogen compounds. 152 p.

22. Lange, Antti A.I., 1999. Statistical calibration of observing systems. 134 p.

23. Pulkkinen, Pentti, 1998. Solar differential rotation and its generators: computational and statistical studies. 108 p.

24. Toivanen, Petri, 1998. Large-scale electromagnetic fields and particle drifts in time-dependent Earth's magnetosphere. 145 p.

25. Venäläinen, Ari, 1998. Aspects of the surface energy balance in the boreal zone. 111 p.

26. Virkkula, Aki, 1999. Field and laboratory studies on the physical and chemical properties of natural and anthropogenic tropospheric aerosol. 178 p.

27. Siili, Tero, 1999. Two-dimensional modelling of thermal terrain-induced mesoscale circulations in Mars' atmosphere. 160 p.

28. Paatero, Jussi, 2000. Deposition of Chernobyl-derived transuranium nuclides and short-lived radon-222 progeny in Finland. 128 p.

29. Jalkanen, Liisa, 2000. Atmospheric inorganic trace contaminants in Finland, especially in the Gulf of Finland area. 106 p.

30. Mäkinen, J. Teemu, T. 2001. SWAN Lyman alpha imager cometary hydrogen coma observations. 134 p.

31. Rinne, Janne, 2001. Application and development of surface layer flux techniques for measurements of volatile organic compound emissions from vegetation. 136 p.

32. Syrjäsuo, Mikko T., 2001. Auroral monitoring system: from all-sky camera system to automated image analysis. 155 p.

33. Karppinen, Ari, 2001. Meteorological pre-processing and atmospheric dispersion modelling of urban air quality and applications in the Helsinki metropolitan area. 94 p.

34. Hakola, Hannele, 2001. Biogenic volatile organic compound (VOC) emissions from boreal deciduous trees and their atmospheric chemistry. 125 p.

35. Merenti-Välimäki, Hanna-Leena, 2002. Study of automated present weather codes.153 p.

36. Tanskanen, Eija I., 2002. Terrestrial substorms as a part of global energy flow. 138 p.

37. Nousiainen, Timo, 2002. Light scattering by nonspherical atmospheric particles. 180 p.

38. Härkönen, Jari, 2002. Regulatory dispersion modelling of traffic-originated pollution. 103 p.

39. Oikarinen, Liisa, 2002. Modeling and data inversion of atmospheric limb scattering measurements. 111 p.

40. Hongisto, Marke, 2003. Modelling of the transport of nitrogen and sulphur contaminants to the Baltic Sea Region. 188 p.

41. Palmroth, Minna, 2003. Solar wind – magnetosphere interaction as determined by observations and a global MHD simulation. 147 p.

42. Pulkkinen, Antti, 2003. Geomagnetic induction during highly disturbed space weather conditions: Studies of ground effects 164 p.

43. Tuomenvirta, Heikki, 2004. Reliable estimation of climatic variations in Finland. 158 p.

44. Ruoho-Airola, Tuija, 2004. Temporal and regional patterns of atmospheric components affecting acidification in Finland. 115 p.

45. Partamies, Noora, 2004. Meso-scale auroral physics from groundbased observations. 122 p.

46. Teinilä, Kimmo, 2004. Size resolved chemistry of particulate ionic compounds at high latitudes. 138 p.

47. Tamminen, Johanna, 2004. Adaptive Markov chain Monte Carlo algorithms with geophysical applications. 156 p.

48. Huttunen, Emilia, 2005. Interplanetary shocks, magnetic clouds, and magnetospheric storms. 142 p.

49. Sofieva, Viktoria, 2005. Inverse problems in stellar occultation. 110 p.

50. Harri, Ari-Matti, 2005. In situ observations of the atmospheres of terrestrial planets. 246 p.

51. Aurela, Mika, 2005. Carbon dioxide exchange in subarctic ecosystems measured by a micrometeorological technique. 132 p.

52. Damski, Juhani, 2005. A Chemistry-transport model simulation of the stratospheric ozone for 1980 to 2019. 147 p.